COMPARISON OF RELATIVE DOSE FACTORS OF A 6 MV BEAM MEASURED WITH DIODE, RADIOCHROMIC FILM AND IONIZATION CHAMBERS IN DIFFERENT ORIENTATIONS

By

JOSEPH MAKURAZA
(ID: 10640193)

This Thesis is submitted to the Medical Physics Department, University of Ghana, Legon in Partial Fulfillment of the Requirement for the Award of the

MASTER OF PHILOSOPHY

in

MEDICAL PHYSICS

Accra - Ghana

October, 2019

DECLARATION

This thesis is the result of research work undertaken by **JOSEPH MAKURAZA** in the Department of Medical Physics, University of Ghana, under the supervision of Dr. Samuel N.A. Tagoe, Dr. Stephen Inkoom and Prof. A. W. K. Kyere. I hereby declare that this thesis is the results of my own original research and that no part of it has been presented for another degree in this university or elsewhere. Duly other works and/ or researches done by other researchers cited in this work have been acknowledged under references

Sign_____

JOSEPH MAKURAZA

(STUDENT)

Date:……

Sign_____

Dr. SAMUEL N. A. TAGOE

(PRINCIPAL SUPERVISOR)

Date:……

Sign_____

Dr. STEPHEN INKOOM

(CO-SUPERVISOR)

Date:……

Sign_____

Prof. A. W. K. KYERE

(CO-SUPERVISOR)

Date:……..

ABSTRACT

In this research study the output factors of a 6 MV beam were measured by using Razor diode, Gafchromic EBT-3 film and small volume ionization chambers 0.13 cc ionization chamber, 0.01 cc Razor ionization chamber from IBA – dosimetry, BahnhofstraBe, Germany. Both perpendicular and parallel orientations of ionization chambers relative to the propagation of radiation beam were considered. Varian Unique medical system Linac was used to deliver a 6 MV beam. Detectors were placed at the stage attached to the water phantom full of water. The measurements of output factor (OF) were conducted at different clinical set ups for source to surface distances of 100 and 90 cm at depths of d_{max} and 10 cm, respectively. From the results, relative errors (%) calculated on field size of 1 × 1 cm^2 between output factors of 0.13 cc chamber and EBT-3 film when the chamber was positioned parallelly with respect to the beam central axis were -2.23 and 0.57%, and -19.68 and -9.40% at SSD = 90 cm and SSD = 100 cm respectively when the chamber was set perpendicularly relative to the beam central axis. Relative errors (%) calculated on field size of 1 × 1 cm^2 between OFs of Razor chamber and EBT-3 film when the chamber was positioned parallel with respect to the beam central axis were 8.45 and 12.53%, and -3.29 and 4.12% at SSD = 90 cm and at SSD = 100 cm respectively when the chamber was set perpendicularly relative to the beam central axis. Relative errors (%) were also calculated between 0.13cc chamber and Razor diode, of which the findings were -7.75 and -9.97% at SSD = 90 cm and at SSD = 100 cm when the chamber was set parallel to the central beam axis. The study has shown that 0.13 cc ionization chamber could be a good choice for measurement of output factor from small to large field sizes when the chamber was positioned parallel with respect to the beam central axis.

DEDICATION

I dedicate this work to my wife Delphine MUKAWERA, my son SHAMI Dylan Josephson, my family and friends.

ACKNOWLEDGEMENTS

I would like to thank my supervisors Dr. Samuel N. A. Tagoe, Dr. Stephen Inkoom and Prof. A. W. K. Kyere for their unlimited support. I like to convey my deepest gratitude to my lovely wife Delphine MUKAWERA for her love, limitless passion, and reinforcement during the study.

My special thanks go to my dear parents, relatives and others who laid the foundation of my pedagogy, though it was hard, but they never give up to take this heavy weighted burden.

I am thankful to Dr. Theresa B. Dery for providing EBT-3 films which were used in this research work.

I am also grateful to the academic mentors and my classmates from Department of Medical Physics for their supports and advices which were really encouraging and full of knowledge.

TABLE OF CONTENTS

LIST OF TABLES

LIST OF FIGURES

LIST OF ABBREVIATIONS

AAPM	American Association of Physicists in Medicine
ABS	Acrylonitrile butadiene styrene
AHARA	As high as reasonably achievable
ALARA	As low as reasonably achievable
BST	Back scatter factor
CPE	Charge-particle equilibrium
CT	Computed tomography
EBT	Electron beam texturing
ESTRO	European society for radiotherapy and Oncology
GM	Geiger – Muller
HVL	Half-value layer
IAEA	International atomic energy agency
IC	Ionization chamber
IMRT	Intensity modulated radiation therapy
ISP	International specialty products
LINAC	Linear accelerator
MLC	Multi-leaf collimator
MU	Monitor unit
OAR	Off-axis ratio
OD	Optical density
PDD	Percentage depth dose
PMT	Photomultiplier tube

POAR	Primary off-axis ratio
PSF	Peak scatter factor
PTFE	Polytetrafluoroethylene
PTV	Planning target volume
QA	Quality assurance
RDF	Relative dose factor
ROI	Region of interest
SAD	Source to axial distance
SD	Small field detector
SPD	Source - point distance
SSD	Source to surface distance
SSD_o	Standard source-surface distance
TF	Tray factor
TLD	Thermoluminescent dosimeters
TPR	Tissue phantom ratio
TPS	Treatment planning system
VMAT	Volumetric modulated arc therapy

LIST OF SYMBOLS

AgH	Silver halide
Al	Aluminium
Ba	Barium
Bi	Bismuth
C	Carbon
Cl	Chloride
D_o	Normalization depth for photon and electron for dose measurement
H	Hydrogen
I	Transmitted optical intensity
I_0	Incident optical intensity
K_{air}	Air kerma in air
$K_{T,P}$	Temperature and pressure factor
Li	Lithium
N	Nitrogen
Na	Sodium
O	Oxygen
S	Sulfur
S_c	Collimator scatter factor
$S_{c,p}$	Total scatter factor
S_p	Phantom scatter factor
TI	Thallium
Z_{eff}	Effective atomic number

CHAPTER ONE

1.0 INTRODUCTION

1.1 Background

Radiation dosimetry plays a significant role in most fields of radiation medicine and in radiation protection for dose optimization. In radiotherapy dose escalation requires optimization of the dose delivered so that the highest levels can be attained with minimal complications known as, as high as reasonably achievable (AHARA). On the other hand, in radio-diagnostics, there is also a demand for optimizing patient dose delivery to the lowest point which allows the production of a quality image for diagnostic purposes known as, as low as reasonably achievable (ALARA). These optimization techniques form part of the quality management process which sets up a high standard level of patient improved care [1].

In radiation dosimetry, the use of traditional dosimetric systems such as radiographic films , thermo luminescent dosimeters (TLDs), semiconductors, and ionization chambers have demonstrated several problems related to the isodose curves measurement and depth-dose distribution in high gradient regions of beams [2]. It has been observed that ionization chambers and semiconductors do not present appropriate spatial resolution for many treatment planning needs. Dosimetric data from TLDs cannot be stored for future use and each dose is single use readout. Silver-halide radiographic films have also faced difficulties in the evaluation of an ionizing photon beam due to the large variation in sensitivity to photon energies. It is also very challenging to treat and analyze data from radiographic films because of its sensitivity to room light and require chemical handling.

From these limitations, scientists have begun to search for measuring radiation systems which possess high spatial resolution and gives comfort of data analysis and manipulation. The introduction of radiochromic films has solved some of these limitations stated. Radiochromic films possess a very high spatial resolution and the films are not sensitive to visible light which gives them the ability to be handled comfortably in room light. Furthermore, the films have relatively low spectral sensitivity variation. Radiochromic films change color directly when exposed to radiation exposure. Image formation occurs as a polymerization process, in which energy is transferred from an energetic photon or particle to the receptive part of the colorless photomonomer molecule, initiating color formation through chemical changes [2].

The output factor is one of the factors influencing the calculation of monitor unit or treatment time. The output factor is the change in dose rate that occurs with different field sizes. Large field would usually have a higher output factor, leading to increased dose rates for the same number of monitor units [3]. In radiotherapy, the computation of the monitor unit (MU) is necessary to deliver a prescribed absorbed dose for the planning target volume (PTV). It is well known in external beam radiotherapy (EBT) that all treatment machines that are used to transmit the radiation dose to patients are designed and configured such that radiation dose received by a patient is quantified in terms of treatment time or monitor unit (MU). It is very crucial to know machine output at any level inside the patient for any irradiation field size. The machine output factor is also called total scatter factor $S_{c,p}$ or relative dose factor (RDF). The photon beam treatment planning systems (TPSs) split $S_{c,p}$ into two components namely collimator scatter factor (S_c) and phantom scatter factor (S_p). It is very important to split $S_{c,p}$ into the two

components S_c and S_p for dose and monitor unit calculation to avoid unnecessary errors. Up to now many TPS require entry of $S_{c,p}$, S_c, and S_p data at the depth of maximum dose ($d_{\max}$). Moreover, both hand calculation and in-house developed computer programs also use these data at $d_{\max}$. Failure to split $S_{c,p}$ into its S_c and S_p components by using hand calculations or computer programs may cause errors up to 3% in dose calculations for highly blocked fields [4]. The S_c is commonly called the output factor or head scatter factor, and may be defined as the ratio of the output in the air for a given field size for that output in the air for a reference field size (10 cm × 10 cm). The $S_{c,p}$ is defined as the ratio of the absorbed dose at d_{max} in a water phantom for specific field to the absorbed dose in a reference field size (10 cm × 10 cm). Unlike S_p which is very difficult to measure, $S_{c,p}$ and S_c can be measured directly. The S_p can be calculated by using analytical method as the ratio between measured total scatter factor ($S_{c,p}$) and collimator scatter factor (S_c). From literature reviews, in measuring total scatter and collimator scatter factors in air build-up caps made of aluminum, copper and polytetrafluoroethylene (PTFE) have been employed to achieve electron equilibrium and to prevent electron contamination to the detector [5].

The objective of this research work is to compare the relative dose factors of a 6 MV beam measured with a diode detector, radiochromic film and ionization chambers in different orientations.

1.2 Problem statement and research justification

Treatment machines that are used in external beam radiation therapy to deliver radiation to patients are designed and configured such that the radiation dose received by a patient

is quantified in terms of treatment time (duration of the beam-on) or monitor unit. It is, therefore, imperative to know accurately the output of a treatment machine at any point within the patient for any irradiation geometry used to deliver the radiation, for the purpose of being able to convert the prescribed radiation dose into treatment time or monitor unit. Obtaining treatment machine output for all irradiation geometries to be used clinically is very cumbersome. With reference to this, the treatment machine output is determined or measured for a set of reference treatment conditions; and dosimetric functions are derived to be used to convert the machine output for the reference conditions to those of non-reference treatment conditions likely to be used clinically. The treatment conditions are: field size, treatment depth and treatment technique. The process of determining or measuring the output of a treatment machine is referred to as treatment machine output calibration or beam calibration. The recommended field size of beam calibration is 10×10 cm^2. How this field size relates to other field sizes used clinically is defined by the relative dose factor (or total output factor). When beam modifiers are placed in the path of the beams, the various components of $S_{c,p}$ are influenced differently, hence the need to treat them separately. In clinical practice phantom scatter factor is not measurable and is often derived from $S_{c,p}$ and S_c. In the measurement of $S_{c,p}$ and S_c with ionization chamber there is the need to establish at all times charge-particle equilibrium (CPE) and reduce volume averaging effects. The size of the sensitive volume of an ionization chamber relative to the radiation field size is very crucial in achieving CPE as well as reduction of volume averaging effects associated with the detector. Ignoring these influences would create uncertainties in the measured output factors leading to large discrepancies in the dose delivered to a patient. Choice of detector to use for the

measurement of an output factor is therefore very crucial, and need special considerations. The outcome of this research would predict which radiation detector between ionization chamber, diode and radiochromic film is more suitable for radiotherapy of 6 MV photon beam for a particular field size. Furthermore, it would increase opportunities for further research in dosimetry of megavoltage energy beam.

1.3 Objectives

1.3.1 General objective

The general objective of this research study is to measure relative dose factors per the requirements of treatment planning systems with 0.13 cc (CC13) ionization chamber, 0.01 cc Razor ionization chamber, Razor diode and EBT-3 Gafchromic film.

1.3.2 Specific objectives

i. To assess which orientation relative to the beam central axis will a detector produce accurate and precise measurements of output factor.

ii. To compare the obtained relative dose factors with those found in literature.

iii. To ascertain which detector would be more suitable and appropriate for the measurement of a particular output factor, and the conditions under which a particular detector gives the most optimal and accurate output factor.

1.4 Research questions

i. Which orientation relative to the beam central axis a detector may produce

accurate and precise measurements of output factor?

ii. What are the relative dose factors measured with different types of ionization chambers and Gafchromic EBT-3 model film?

iii. Which detector would be more suitable and appropriate for the measurement of output factors?

1.5 Scope and delimitation

In this research work the measurement of output factors were measured by using diode, ionization chambers and Gafchromic EBT-3 model film, after which the findings from both detectors were compared. The outcome of this study was also compared to the data available in literature. The measurements were conducted at National Centre for Radiotherapy and Nuclear Medicine at Korle-Bu Teaching Hospital, Accra, Ghana.

1.6 Dissertation organization

This research document is sequentially ordered in five chapters. Background and introduction to the research work are summarized in chapter one. The literature reviews on this topic are included in chapter two. Chapter three focuses on materials and methodology used in this research study. Results and discussion are found in chapter four. Conclusion and recommendations are found in chapter five.

CHAPTER TWO

2.0 LITERATURE REVIEW

In this section the theoretical background that underlies the work are presented. A short description overview on relative dose factor (RDF), phantom scatter factor, and collimator scatter factor, ionization chambers, and radiochromic films are presented. The summary of overviews of what have been done relating to this research topic is also introduced in this part.

2.1 Overviews of works that have been done on the measurement of output factors

Studies based on the dosimetry of output factors by using various ionization chambers have been done by several researches. Iftikhar, 2012 [3] used X-ray beam from 6 and 15 MV produced by a Varian Clinac 2100C Linac to investigate the head output factor (OF). The measurements were conducted by using farmer type and compact cylindrical ionization chambers. The dosimeters were placed along the beam central axis at the reference depth of d_{max} in acrylic and brass build up caps. The reference depths of 1.5 cm and 2.9 cm for 6 and 15 MV beams respectively were used. The measurement of head scatter factor was taken by increasing the field from 3 × 3 cm^2 to 35 × 35 cm^2. The findings showed that the increase of field size resulted in the increase of output factors for both 6 and 15 MV beams. The difference of 1.53% and 0.97% were noted between both energies for acrylic and brass build up caps, while there was no significant difference found for both ionization chambers. Figure 2. 1 illustrates the variations of output factors with field size: (a) measured with Farmer type ionization chamber fitted with acrylic build up cap, (b) measured with Compact cylindrical ionization chamber

fitted with acrylic build up cap, (c) measured with Compact cylindrical ionization chamber fitted with brass build up cap.

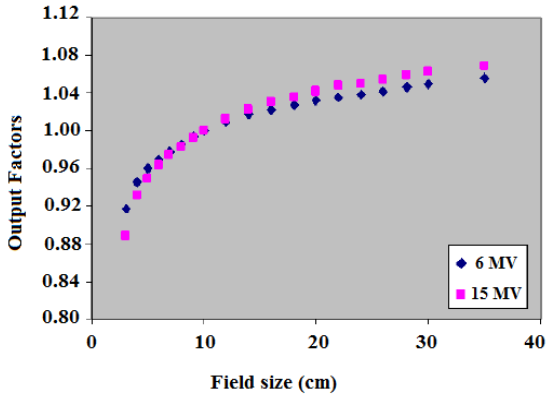

(a)

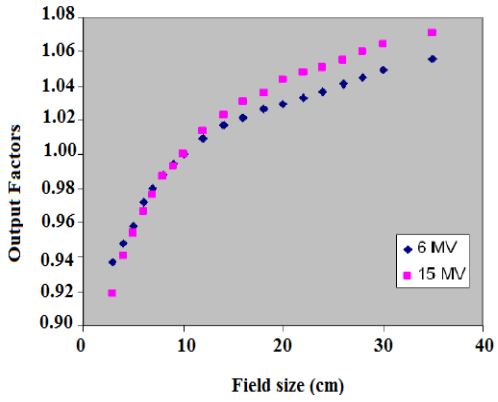

(b)

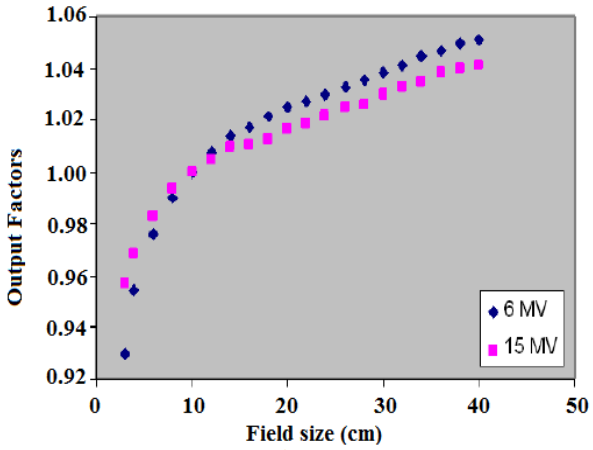

(c)

Figure 2. 2: Variations of output factors with field size: (a) measured with Farmer type ionization chamber fitted with acrylic build up cap, (b) measured with Compact cylindrical ionization chamber fitted with acrylic build up cap, (c) measured with Compact cylindrical ionization chamber fitted with brass build up cap [3]

It is clearly seen from Figure 2.1a that the output factors measured with Farmer type ionization chamber and acrylic build up cap increases with field size. Output factors for 6

MV photon beams are bigger than its corresponding values for 15 MV photons for field size smaller than reference field size. Experiment shows inverse results at field size bigger than reference field size where the output factors for 15 MV become bigger than its corresponding value for 6 MV photon beams. Nevertheless, the difference in OFs for 6 and 15 MV beams is more noticeable for compact cylindrical ionization chamber than that for Farmer type ionization chamber (Figure 2.1a). Hence, the output factors also depend on the radiation detector used in the measurement [3]. When comparing the results obtained with Compact cylindrical ionization chamber fitted with brass and acrylic build up caps (Figures 2.1b and 2.1c), the following was observed. Unlike the results with acrylic build up cap; the output factors for 15 MV photons with brass build up cap is larger than its corresponding value for 6 MV photons for smaller field sizes. Analogous controversy also exits between brass and acrylic build up caps for field sizes bigger than the reference field size; it was observed that the output factor for 6 MV photons was larger than its corresponding value for 15 MV photon beam. Therefore, the output factor also depends on density of construction material of the buildup cap employed [3]. There was no significant difference found in both ionization chambers fitted with acrylic build up cap. For Farmer type ionization chamber, the deviation in output factor for acrylic and brass build up caps decreases with increasing field size for 6 MV. Yet, for 15 MV photon energy, this deviation decreases to the reference field size and increases up to the maximum field size [3]. Shamsi *et al.,(*2017) [6] investigated a dosimetric comparison of total scatter factor for small fields in radiotherapy. In their study total scatter factors were measured by using CCO1 and CCO4 ionization chamber detectors for 6 and 18 MV beams delivered from a Linac. All data were taken in water

phantom. The small fields were created by collimator jaws and multi-leaf collimators separately, the field sizes ranging from 0.6 cm × 0.6 cm to 10 cm × 10 cm and 0.5 cm × 0.5 cm to 20 cm × 20 cm respectively. It was observed that CCO1 detector could measure total scatter factor at all the given field sizes for both the energy beams whereas CCO4 could not measure total scatter factor for the field sizes less than one centimeter square (< 1 cm^2) due to the volume averaging and perturbation effects. CCO1 has been shown to be effective for measurement of total scatter factor in sub-centimeter field sizes and also CCO1 can be used to measure other dosimetric quantities in small fields by using different energy beams [6].

2.2 Relative dose factor (RDF)

For a given photon beam with energy ($h\nu$) at a given SSD, the dose at point P (at depth d_{max}) depends on field size A. The larger the field size, the larger is the dose. The relative dose factor $S_{c,p}$ is defined as the ratio of the dose in phantom at a point P for a given field size to the dose at the same point P for the reference field size. Relative dose factor is commonly known as total scatter factor S_T or $S_{c,p}$ or machine output factor (OF): Equation 2.1 below is the mathematical expression of $S_{c,p}$ and arrangement illustrates how to measure relative dose factor (Figure 2.2).

$$RDF(A, h\nu) = S_{c,p}(A, \mathrm{h}\nu) = \frac{D(d, A, f, h\nu)}{D(d, 10, f, h\nu)} \qquad (2.1)$$

- For A > 10 × 10 cm^2; RDF(A, hν) < 1
- For A = 10 × 10 cm^2; RDF(A, hν) = 1
- For A > 10 × 10 cm^2; RDF (A, hν) > 1

Where $D(d,A,f,h\nu)$: is the dose measured at d (depth) on beam central axis within a tissue-equivalent phantom for an arbitrary field size of A, and beam energy of $h\nu$.

$D(d,10,f,h\nu)$: is the dose measured at at d (depth) on beam central axis within a tissue-equivalent phantom for reference field size of 10 cm × 10 cm , and beam energy of $h\nu$.

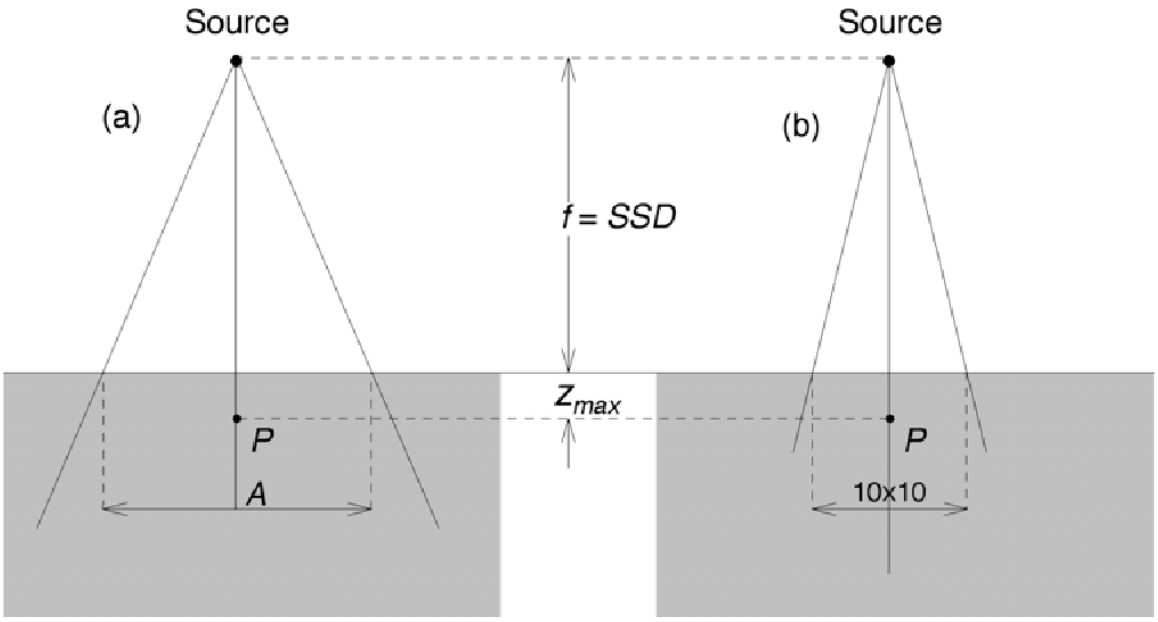

Figure 2. 3: Arrangement illustrates how to measure relative dose factor

The relative dose factor can be broken up into two parts namely phantom scatter factor (S_p) and collimator scatter factor (S_c) [7].

2.2.1 Collimator scatter factor

The collimator scatter factor (S_c) is also called relative exposure factor or in-air output factor. It measures the dose variation produced from the head of the Linac in the different range of field sizes. The measurement of S_c is the necessity of the most dose calculation

algorithms used in the clinical TPSs for a precise monitor unit (MU) calculation. Note that (S_c) is a function of the field size defined in the treatment head, not the final field size that reaches the patient. Collimator scatter factor is defined as the ratio of output in air for a given field size to that of the reference field size (10 cm × 10 cm). Equation 2.1 is the mathematical expression of collimator scatter factor, S_c.

$$S_c(A, h\nu) = \frac{X(A, h\nu)}{X(10, h\nu)} = \frac{(K_{air}(A, h\nu)_{air})}{(K_{air}(10, h\nu)_{air})} = \frac{D'(A, h\nu)}{D'(10, h\nu)} \qquad (2.2)$$

Collimator scatter factor, S_c, become one when it is normalized to the reference field size of 10 cm × 10 cm at the reference conditions of the treatment machine [8].

• S_c > 1; for fields A exceeding 10 × 10 cm^2

• S_c = 1; for 10 × 10 cm^2 field

• S_c < 1; for fields A smaller than 10 × 10 cm^2

Where X_{air}: exposure in air,

$(K_{air})_{air}$: air kerma in air,

$\acute{D}(A, h\nu)$: is the dose measured at a depth of d in air for an arbitrary field size of A and beam energy of hU.

$\acute{D}(10, h\nu)$: is the dose measured at the same depth obtained with reference field size of 10 x 10 cm^2 and beam energy of hU.

The big task in assessing the influence of the linear accelerator head to the dose measurement and its uncertainties is the probability of conducting measurements in conditions of electronic equilibrium and prevention of electron contamination, while excluding the phantom influence, which is accountable of the electronic equilibrium achievement. The electronic equilibrium can be achieved by applying a suitable build-up cap added to detectors in use. The build-up cap should have a sufficient thickness to give

an assurance of the electronic equilibrium, and it must be totally covered by the irradiation field size. That is why the high Z - materials build-up caps have been chosen for small field dosimetry. The theory of the mini-phantom was endorsed and introduced in 1991 by the European Society for Radiotherapy and Oncology ESTRO [9]. This mini-phantom was designed and given a cylindrical shape so that it could hold a detector at its central axis where the detector axis coincides with beam central axis. The dimensions of the mini-phantom were thought to be broad enough to provide lateral electron equilibrium and to permit the output factors measurement at various depths. Li et al. (1995) [9,10] assessed the smallest radial thickness of a mini-phantom with Monte Carlo simulations to achieve the lateral electron equilibrium with the $TPR_{20,10}$. The investigation has shown that the lateral electronic equilibrium could be attained when the radius of the mini-phantom is equal or greater than 13 mm water equivalent thickness or 1.3 g/cm^2 for a 6 MV beam of $TPR_{20,10} = 0.670$.

2.2.2 Phantom scatter factor

Phantom scatter factor (S_p) quantifies the relationship between the field size on the patient surface and the dose resulting from scatter within the patient or phantom. Note that (S_p) is a function of the field size as defined on the patient, not the field size as defined in the treatment head. S_p is defined as the ratio of the absorbed dose at the depth of maximum dose (d_{max}) for a given field to that in the reference field (10 × 10 cm^2) at the same depth with the same collimator opening. The photon beams for which backscatter factors can be precisely measured (e.g., up to ^{60}Co), S_p factor at the reference depth of maximum dose can be defined simply as the ratio of backscatter factor (BSF) which is also called peak scatter factor (PSF) for the given field to that in the reference

field (10 cm × 10 cm). The following equation 2.3 is the mathematical expression of phantom scatter factor, for such beams:

$$S_p(A) = \frac{BSF(A)}{BSF(A_o)} \tag{2.3}$$

Where A is the side of the equivalent square field and A_o is the side of the reference field (10 cm x 10 cm). The S_p becomes difficult to measure in practice [3]. There are many methods to determine S_p including Monte Carlo simulation and analytical method, but the most practical method for determining S_p is to measure S_c and $S_{c,p}$ for symmetric fields and then divide the measured $S_{c,p}$ by S_c. The most practical method of calculating phantom scatter factor comprises of indirect determination from equation (2.4).

$$S_p(A) = \frac{S_{c,p}(A)}{S_c(A)} \tag{2.4}$$

Where $S_{c,p}(A)$ is the relative dose factor defined as the dose rate at a reference depth for a given field size A divided by the dose rate at the same point and depth for the reference field (10 cm × 10 cm) (Fig. 2.2). Hence, $S_{c,p}(A)$ comprises both the collimator and phantom scatter factors and when divided by $S_c(A)$ provides $S_p(A)$[7].

2.3 Radiation monitoring instruments

The theory of radiation detection and an overview of the design and detection principles of detectors are described in this section. Neither can radiation be smelt nor tasted. That is why instruments are needed to indicate the presence of ionizing radiation. Radiation is energy travelling in the form of particles or waves in bundles of energy called photons. Radiation detector is a device designed to detect or identify ionizing radiation, such as those produced by particle accelerators, emitted by radioactive materials or observed in

cosmic rays. Such radiation includes alpha radiation, beta radiation and gamma radiation with matters which create electrons and positively charged ions. Radiation monitoring devices are classified into two types of radiation instruments which could be used as survey monitors, namely solid state and gas filled detectors.

2.3.1 Gas filled detectors

All gas filled detectors have the same basic design of two electrodes (anode and cathode) separated by air volume or a special fill gas but differs in the methods used to measure the total number of ion-pairs that are collected. The detector's response to ionizing radiation depends on type and pressure of the filled gas and the strength of the electric field applied between the electrodes. Figure 2.3 illustrates the operation principle of gas filled detectors.

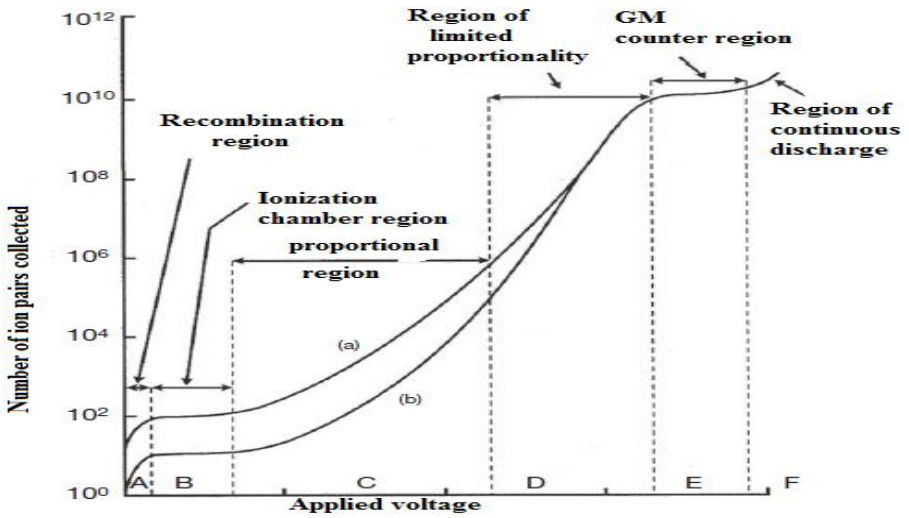

Figure 2. 4: Various operation regions of a gas filled detector [8]

Depending on the design of the gas filled detector and applied voltage between electrodes, gas filled detector can operate in one of three regions, namely, the ionization chamber region B, proportional region C or Geiger-Müller (GM) region E.

Recombination region A and limited proportional region D are out of use for survey meters. The characteristics of different operation regions of gas filled detector shown in Fig.3 are discussed below:

Recombination region A. From diagram above Fig. 2.3 when the applied voltage is too low, it gives low electric field strength. The charges collected from gas to electrodes become small due to low electric field strength, hence resulting in considerable ions recombination.

Ionization chamber region B. This region is also called saturation region. The applied voltage in this region is high enough to prevent recombination and low enough to prevent secondary ionization. The output current remains constant (saturation current) as the applied voltage increases while incident radiation level remains constant.

Proportional region C. Gas amplification takes place in this region due to the increase of primary ion energy level which is caused by increase of voltage. The secondary ionization occurs in this region and adds to total collected charge on electrodes. The number of primary ionizations is proportional related to the increase of output current via the proportionality constant. This region is so called proportional region because there is direct proportionality between number of ions pairs collected and number of ion pairs initially produced in the detector by radiation if the voltage remain constant.

Limited proportional region D. In this region, collected charge becomes independent of number of primary ionizations and secondary ionization evolutions to photoionization (photoelectric effect). Contrary to the proportional region the proportionality constant is no longer accurate in this region. Hence this region is not a very useful range for radiation detection.

Geiger-Müller (GM) region E. In the GM region any radiation event is strong enough to produce primary ions results in a complete ionization of gas. The detector becomes insensitive after an initial ionizing event for a period of time called dead time and within this period of time no radiation event can be detected. It is well known that negative ions (mostly electrons) reach anode faster than heavy positive ion can reach cathode. Photoelectric effect causes the anode to be completely surrounded by a cloud of secondary positive ions. The anode is shielded and surrounded by cloud of secondary positive ions so that no secondary negative ions can be collected and in this case detector is effectively "shut off". Detector recovers from shut off mode after positive ions migrate to cathode. The detector is off in dead time period usually 100 to 500 μs, hence limits the number of radiation events that can be detected.

Continuous discharge region F. Electric field is very high and intense in this region hence no initial radiation event is required to completely ionize the gas, the field itself propagates secondary ionization and there is a complete avalanching. Radiation detection in this region is impossible. There are three principal types of gas filled detectors, namely, 1) ionization chambers, 2) proportional counters, 3) Geiger-Müller tubes [8].

2.3.2. Ionization chamber

Ionization chamber belongs to gas-filled radiation detectors, and is the most widely used types of dosimeter for the detection and measurement of certain types of ionizing radiation such as X-rays, gamma rays and beta particles. Ionization chambers have a wider range of applications depending on varying geometries, different shapes and sizes. Ion chambers can be used as survey devices, depending on what is being monitored;

chambers can be large or small in volume. The large volume ion chambers are often positioned around nuclear reactor installation facilities and outside medical radiation rooms such as nuclear medicine clinics and radiotherapy to alert medical clinicians of improper storage of radioactive sources for the occupational safety purpose, while small volume ion chambers are often used by medical physicists as portable radiation survey meters for environmental monitoring. The ionization chambers with very big volumes are also employed in the calibration of radioactive isotopes. In this case, the radiation source is positioned directly inside of the ion chamber volume and then the activity of the source can be measured. The large volume will increase the chance that radiation is going to be detected and reduces the time needed to get statistically important data. Ionization chambers have also significant applications in clinical settings; they can be used for automatic beam monitoring and also for QA test of diagnostic and radiotherapy machines. In line with beam monitoring ion chambers are aiming to switch off the radiotherapy machine when prescribed dose is met or exceeded.

2.3.2.1 Operation principles of ionization chamber

An ionization chamber is a gas-filled chamber consisting of two electrodes, namely, anode and cathode. Electrodes may have various designs which can be in the form of parallel plates known as parallel plate ionization chambers or may be a cylindrical arrangement with a coaxially located internal anode wire. The electric field is created when the potential difference is applied between the two electrodes. The gas inside the chamber (i.e between the electrodes) becomes ionized by incident ionizing radiation then ion-pairs are produced. Under the influence of electric field, positive ions and electrons

move to the electrodes of opposite polarity; positive ion goes to anode while dissociate electron goes to cathode. This movement of electrons creates ionization current which is measured with electrometer connected to the circuit. Depending on the chamber design, radiation dose and applied voltage of most electrometers are designed to measure very small output current which is in the region of femtoamperes to picoamperes. The illustration diagram (Fig. 2.4) of parallel plate ion chamber shows drift of ions due to electric field.

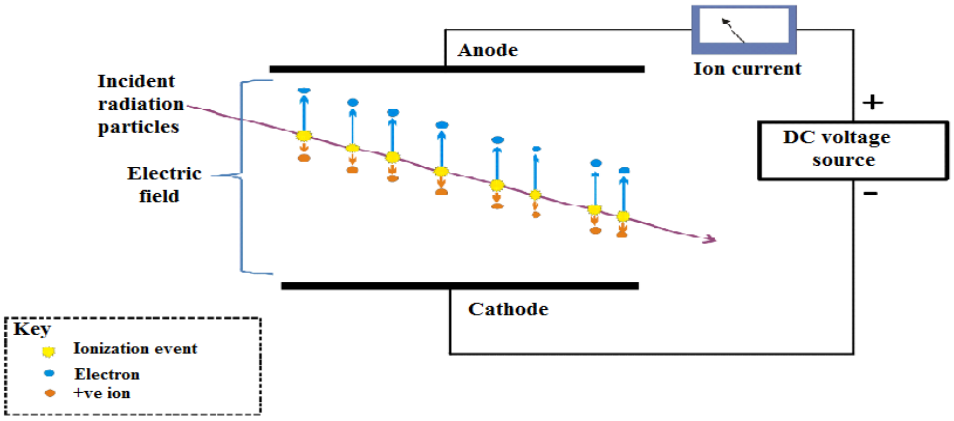

Figure 2. 5: Block of parallel plate ionization chamber illustrates movement of ions cause by electric field [41].

2.3.3 Main type of ionization chambers

2.3.3.1 Free air ionization chamber

The theory and working principle of this chamber is explained by using Fig. 2.5. The chamber is freely opened to the atmosphere. The photon beams are collimated and focused to the diaphragm on left-hand side and then exit to the opposite side. This chamber has two parallel plate electrodes mount with guard wires and a concentric guard ring. These two parallel plate electrodes envelop the volume of air from which secondary

charged particles are collected [11].

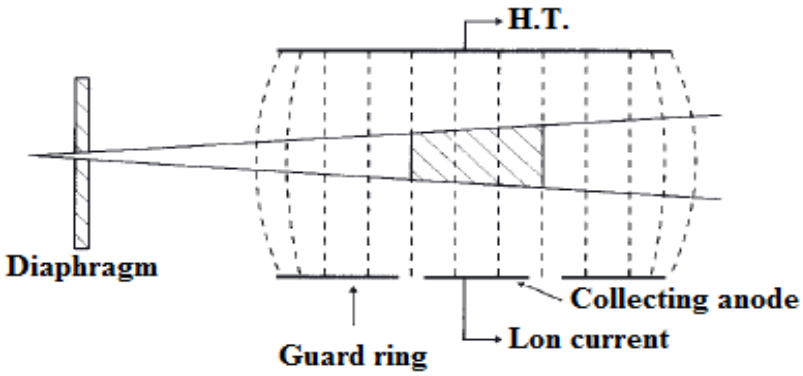

Figure 2. 6: Illustration of free-air ionization chamber [11].

A potential difference is applied between the two electrodes to collect ion pairs which are created by incident ionizing radiation. The free air ionization chamber accurately detects radiation exposure for energies up to 300 kV.

2.3.3.2 Cavity ionization chambers

A cavity ionization chamber is made up of an envelope surrounding air volume between external wall and central electrode with an applied high voltage of several hundred volts. The applied voltage creates electric field that collects the ion-pairs resulting from the ionization of the air inside the cavity. The cavity chambers are not suitable equipment for everyday clinical use due to large size and chambers are not portable. Reference ionization chambers are usually made by graphite material which is a conductive material of low Z and close to human tissue with wall thickness of 3 mm, this thickness is enough to achieve electronic equilibrium in a Co-60 photon beam [11]. The structure of the thimble chamber ionization chamber is represented in Fig. 2.6.

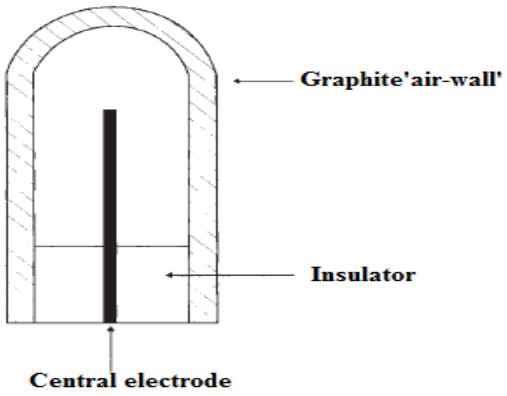

Figure 2. 7: Structure of the thimble chamber [11]

2.3.3.3 Plane-Parallel ionisation chamber

The chamber is made by two parallel plates of plastic materials separated by a small gap, typically 2 mm or less. This plastic material is coated with a conducting layer that makes the positive and negative electrodes. The secondary charged particles are enclosed in air cavity and trapped between two electrodes. The air gap between electrodes is very small leading to very little perturbation. The parallel plate chambers can only be used when the mean electron energy is ranged from 5 up to 50 MeV at any depth [11]. The illustration of parallel plate ionization chamber is represented in Fig. 2.7.

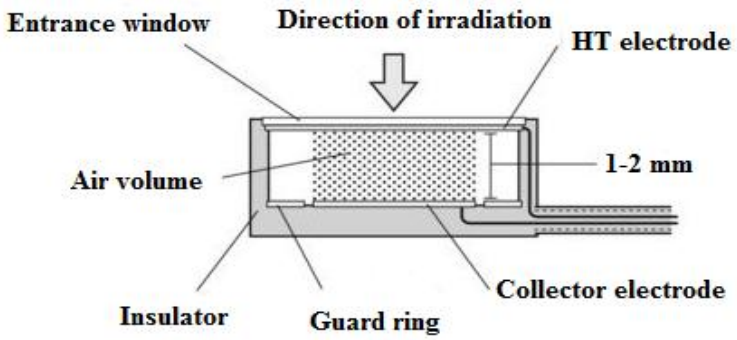

Figure 2. 8: Structure of a parallel plate ionization chamber [11]

2.3.4. Solid state detectors

Solid state detectors play an important role in medical physics providing precision detection of ionizing radiations. The solid state detector's sensitivity is about 10^4 times higher than that of gas filled detectors. Unlike a gas filled detector, a semiconductor detector's response does not depend on temperature and pressure i.e temperature and pressure correction formalism K_{TP} is not applied. There are also two common basic types of solid state detectors, namely, 1) scintillator detectors and 2) semiconductor detectors.

2.3.4.1. Scintillation detector

This detector belongs to the class of solid state detectors, it consists with a scintillator material which is made of inorganic crystals e.g thallium activated inorganic phosphors such as NaI(TI) or CsI(TI) or organic crystals such as antracene, stilbene and plastic scintillator. The scintillator emits light on absorption of incident photons. A photomultiplier tube (PMT) is one of electronic device which is directly in connection with a scintillator detector to transform the energy photons to electric charges; also photodiodes can be used in place of PMTs for some detectors [8]. The diagram (Fig 2.8) below represents a scintillation detector's components and its operation principle.

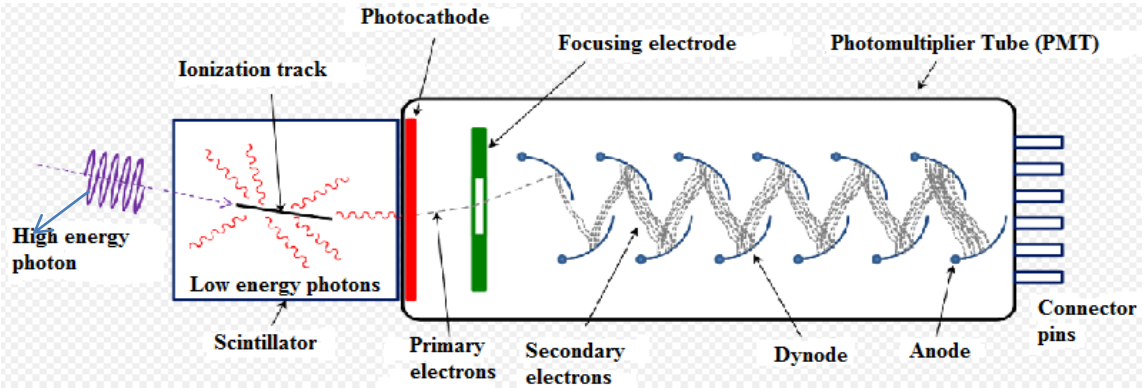

Figure 2. 9: Block diagram represents scintillation detector's components and its operational principle [42].

2.3.4.2. Semiconductor detector

The type of this detector also belongs in the class of solid state detectors. Semiconductors detectors are made from intrinsic semiconductor elements such as silicon or germanium doped with impurities such as phosphorus or lithium to form junction detectors. Semiconductor detectors have a couple of advantages in radiotherapy such as relative dosimetry of photon and electron beam, in vivo dosimetry of photon and electron beams and quality assurance measurement [8].

2.3.5. Radiographic and radiochromic films

Radiographic film has been used in radiation therapy physics for dose measurements for long time. The film has been utilized mostly for electron beam measurements and quality control. Though, the chemical composition of this film is not a tissue equivalent material and therefore it is difficult for its use in measurement of photon beam. Hence, radiochromic film is more suitable for photon beam dosimetry due to its composition of being more tissue equivalent than radiographic film [8].

2.3.5.1 Radiographic film

Silver halide (AgH) emulsion radiographic films are commonly used for relative dose measurement of external radiation treatment beams in the megavoltage photon beam. Dose distribution on film can encompass a range of doses from few cGy up to several Gy. Radiographic film has an extensive scope of advantages in dosimetry such as broad availability, low cost, high spatial resolution and ability to be localized deep down a range of phantoms without perturbing CPE. Film dosimetry is more accurate for

measuring the large dose differences than other techniques (e.g ionization measurements or thermoluminescent dosimetry) [12].

2.3.5.2 Radiochromic film

Radiochromic film is a type of self-developing film used in the testing and characterisation of radiographic equipment such as computed tomography (CT) scanners and radiotherapy linacs. Radiochromic dosimeters are solid state detectors and contain a dye which changes colour when exposed to irradiation, allowing the level of exposure and beam profile to be characterized. Unlike X-ray film, there is no chemical developing process needed and results can be obtained almost instantly, while it is insensitive to visible light. Radiochromic dosimeters are commercially available in numerous phases such as gels, pellets, liquids, and films. The films are more suitable in radiotherapy centers for the measurement of 2-D dose distributions; this is due to several advantages such as being handled in light, can be cut to size, bend to shape, immerse in water, wide dynamic range and high spatial resolution.

2.3.5.3 Historical background of radiochromic dosimeters

In 1826, Joseph Niepce was the first scientist to release a document of radiochromic film processes. It was observed that molecule underwent a radio-synthesis to produce dyes. In 1986, the International Specialty Products Incs (ISP) technology a division of the General Aniline and Film (GAF) chemical corporation produced a new radiochromic film medium known as Gafchromic [13]. International Specialty Products Incs produces various films under the product name Gafchromic. In the middle of 2000's ISP released a new film called Gafchromic EBT. This film had the sensitive layer with a variety of the

monomer used in the previous films. The new sensitive layer was also found to be more sensitive with a dose range of 0.01 – 8 Gy [12]. In 2009, the production of EBT was closed and switched to EBT-2. The active component of EBT-2 film was the same as EBT but with a yellow dye added to the active layer. The EBT-2 film was also constructed as a single layer instead of double and a slightly narrower active layer than EBT. The film also has a little different overall chemical composition (Table 2.1). The effective atomic number (Z_{eff}) of EBT-2 is 6.84 compared to 6.98 for EBT, and close to Z_{eff} of water (7.3) [13]. Figure 2.9 is an illustration diagram of the physical structure of Gafchromic EBT compared to EBT-2. In 2011, a new generation of films called Gafchromic EBT-3 was released by the ISP. Both EBT-2 and EBT-3 films have similar properties. The structure of EBT-3 film is symmetrical, which prevents probable errors in measurement of optical density and also prohibits the fringe artifact formation.

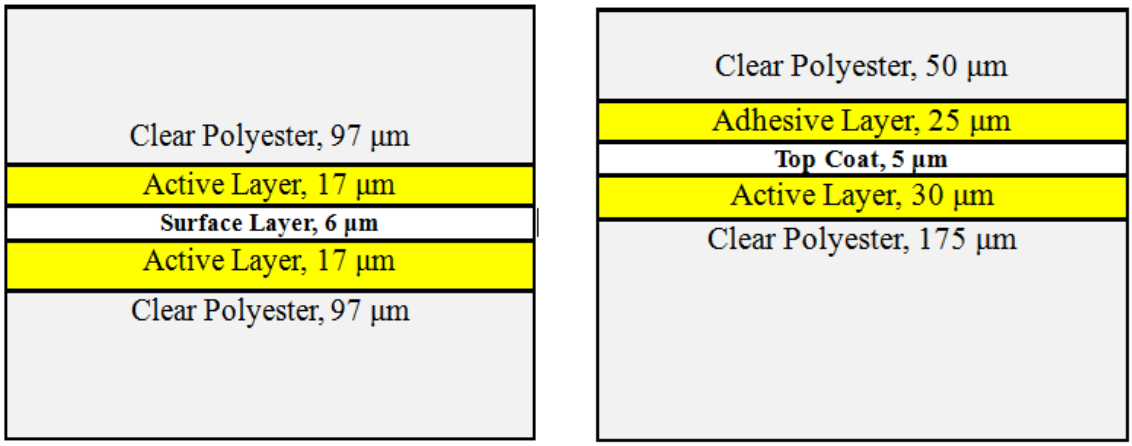

(a) (b)

Figure 2. 10: Structure diagram illustrates the design of Gafchromic films: (a) EBT model compared to (b) EBT-2 model [13].

Figure 2.10a and 2.10b illustrates the schematic structure of Gafchromic film EBT-3 model and EBT-XD model respectively; EBT-3 film is made of a 30 micrometer active

layer in the center and two 125 micrometer polyester layers on the sides of the active layer.

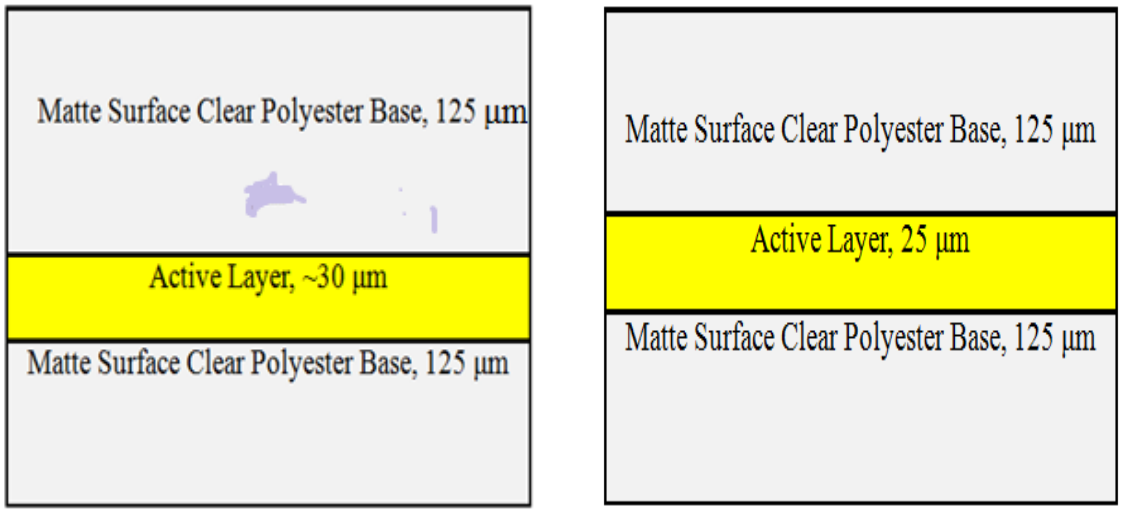

(a) (b)

Figure 2. 11: Schematic structure of Gafchromic film: (a) EBT-3 film, (b) EBT-XD film [14]

From Fig. 2.10a both sides of this film are the same, the film scanning light conditions are the same either on its front side or back side because of its symmetrical structure [15]. The EBT-3 films have shown a couple of advantages compared to the previous films. Besides, the film is designed to measure doses lower than 1000 cGy. Therefore, the evaluation and quality assurance of high-dose prescription was not possible. In 2015, the ISP produced the latest Gafchromic EBT-XD film models. This film is the most suitable for measurement and evaluation of dose in some fields of radiation therapy namely, stereotactic body radiation therapy (SBRT) and stereotactic radiation surgery due to its best performance in a dose range of 40 up to 4 x 10^3 cGy [14, 16]. The structure of EBT-XD model (Fig.10b) and EBT-3 film are almost the same, but the dynamic layer of EBT-XD is a slight bit thinner and the chemical components of the active layer are slightly dissimilar.

2.3.5.4 Physical-chemical characteristics of radiochromic dosimeters

All radiochromic film models discussed in this section are only used for medical dose measurement. However, ISP produced other films models used for industrial purposes. The chemical composition of sensitive layer and dose ranges of Gafchromic films used in medical dosimetry are listed in Table 2.1.

Table 2. 1: Chemical composition of sensitive layers and corresponding dose ranges of Gafchromic films used in radiotherapy and diagnostic radiology for dose measurement [16]

Film model	Elemental composition of active layer by atomic percentage (%)										Dose range in [Gy]	Z_{eff}
	Li	H	C	O	N	Na	Al	S	Cl	Bi		
XR-QA2	1.0	56.20	27.6	11.7	1.6	-	-	-	0.1	1.7	0.0001–0.02	55.2
HD-V2	0.6	58.20	27.7	11.7	0.4	0.5	0.3	0.1	0.6	-	10–100	7.63
MD-V3	0.6	58.20	27.7	11.7	0.4	0.5	0.3	0.1	0.6	-	1–100	7.63
EBT-XD	0.6	57.00	28.5	11.7	0.4	0.1	1.5	0.1	0.1	-	0.04–40	7.46
EBT	0.3	39.79	42.3	16.2	1.1				0.3		0.01-8	
EBT-2	0.6	56.50	27.4	13.3	0.3	0.1	1.6	0.1	0.1	-	0.01–30	7.46
EBT-3	1.0	56.20	27.6	11.7	1.6	-	-	-	0.1	-	0.01–30	7.46

Note: H - Hydrogen, Li – Lithium, C – Carbon, N – Nitrogen, O – Oxygen, Na – Sodium, Al – Aluminium, S – Sulfur, Cl – Clorine, and Bi – Bismuth

XR-QA model was first designed by ISP to measure very small doses. This film was utilized in diagnostic imaging tests of low energy photon. Later on the film was replaced by XR-QA2 Gafchromic film model which can measure the exposure in dose range of 0.1-20 mGy or 0.0001-0.02 Gy. The radiation active layer with thickness of 25 μm is attached to opaque white polyester with thickness of 97 μm at the bottom, and adhesive layers of 20 μm thick pressure is attached at the top of the active layer and, is over-coated with a 97 μm protective yellow polyester. From Table 2.1 it could be seen that the

chemical compositions of sensitive layers of HD-V2 and MD-V3 film models are the same. The film models slightly differ in dose range where HD-V2 and MD-V3 model are ranged 10-100 Gy and 1-100 Gy respectively. Elemental compositions of layers excluding active layers for various Gafchromic film models are listed in Table 2.2. The effective atomic number ($Z_{eff} = 7.46$) and dose range 0.01-30 Gy of EBT-2 and EBT-3 models are both the same. The effective atomic number of these films is approximately close to Z_{eff} of water (7.3).

Table 2. 2: Elemental compositions of layers excluding active layers for different Gafchromic films found in Fig 2.9a and 2.9b; and 2.10a and 2.10b

Layer	Elemental composition of layer by atomic percentage (%)							
	C	Li	H	N	O	S	Ba	Z_{eff}
Clear Polyester	45.4	-	36.4	-	18.2	-	-	6.64
Matte Polyester	45.4	-	36.4	-	18.2	-	-	6.64
Adhesive (EBT-2)	33.3	-	57.1	-	9.5	-	-	6.26
Adhesive (XR-QA2)	33.2	0.48	56.9	-	9.4	-	-	6.25
Transparent Yellow Polyester	45.4	-	36.4	-	18.2	-	-	6.64
White Polyester Film Base	42.3	-	33.8	-	21.6	1.18	1.18	27.5

Note: H - Hydrogen, Li – Lithium, C – Carbon, N – Nitrogen, O – Oxygen, S – Sulfur, Cl – Clorine, and Ba – Barium

The overall chemical composition of sensitive layers of EBT-2 and EBT-3 models is different in terms of atomic number percentages and elemental composition. It is seen from Table 2.1 that almost elemental composition found in EBT-2 sensitive layer also can be found in EBT-3 except some elements such as Na, Al and S.

2.3.5.5 Response of radiochromic film to light

It has proven that once a portion of radiochromic film is exposed to ionizing radiation,

the sensitive part of the film absorbs energy of charged particles which is able to cause a polymerization process [16]. This polymerization process will take place within the sensitive layer of the film and the portion of the film will immediately modify its coloration. Figure 2.11 shows the absorption spectra of the unexposed portion of the radiochromic film EBT-3 model and irradiated with a dose of 500 cGy (to water). Absorption spectrum of irradiated EBT-3 film has shown the highest absorption peak at the wavelength of 633 nm which is found in the range of the red portion of the optical spectrum [16]. The previous research works conducted on dose response of EBT film models have shown the energy- dose response dependence of the particular film model [16-18].

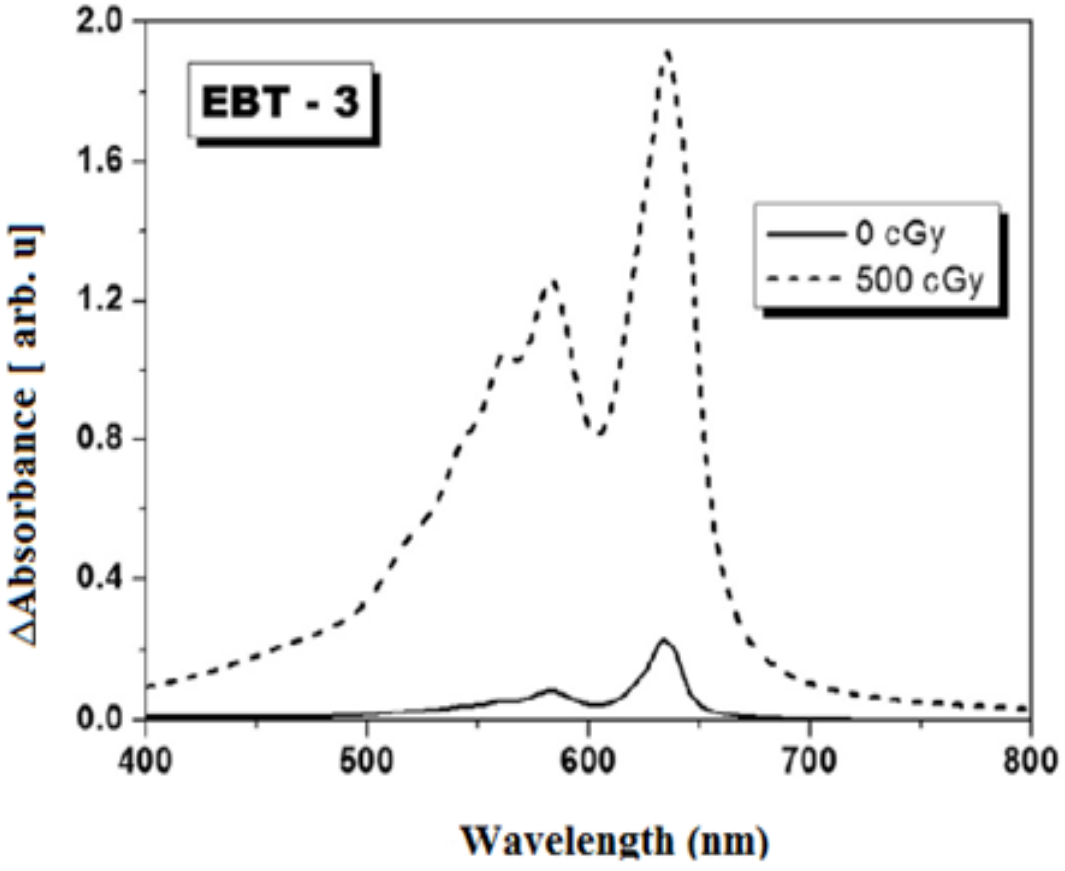

Figure 2. 12: Absorption spectra of the unexposed EBT-3 film portion show by solid line

and exposed at a dose of 5 Gy show by dotted line [16]

Figure 2.12 shows the energy dependent response of the EBT-3 film model. As it is understood from the Figure 2.12, the Gafchromic EBT-3 film is proven that the energy response is independently from megavoltage energies of 400 keV (measurements with ^{192}Ir [17]).

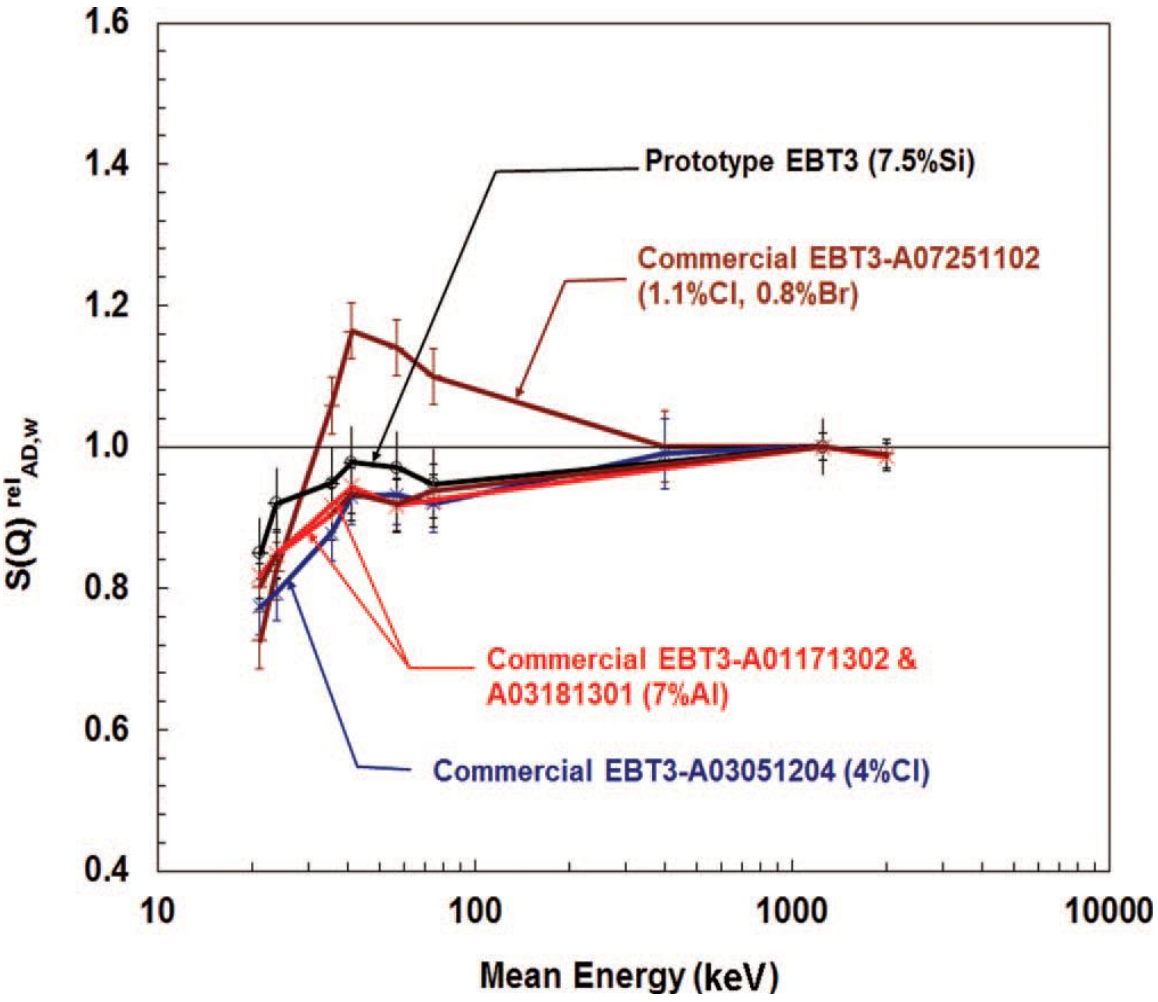

Figure 2. 13: Energy dependent response of the Gafchromic EBT-3 film model [27]

The recent publications have indicated that "when the alumina is added inside the sensitive layer it further enhances the energy response of the Gafchromic EBT-3 film displaying under response of 5% at 50 keV effective photon energy" [18] (Fig. 2.12).

2.3.5.6 Calibration irradiations of radiochromic film

When the suitable film model and densitometer are chosen, it is necessary to find the protocol and the sensitometric curve which would be utilized later for measurement of the unknown doses. It is important to note that calibration curve would depend on the beam quality, on film model and also on scanning processes and data collection protocol used. The beam output measurements are normally conducted by referring to one of appropriate reference dose measurement protocols such as TRS-398 for all ranges of electrons, energy photons and protons [19], AAPM TG-51 and AAPM TG-61 could also be used for electrons and high energy photons [20], and for low energy photons, respectively [21]. Figure 2.13 represents the process of delivering a known dose which is called the reference irradiations to Gafchromic films EBT based models.

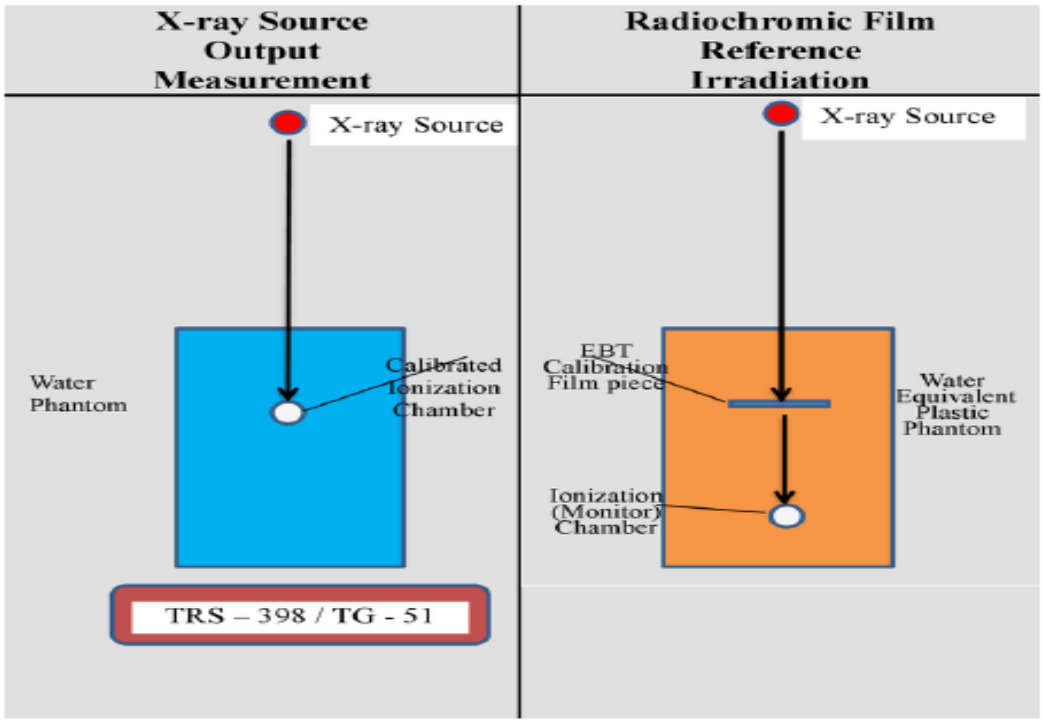

Figure 2. 14: Illustration of calibration process for Gafchromic films EBT models for megavoltage beam energies [16]

Due to the fact that the reference output is usually expressed in function of dose to water; it is endorsed to irradiate calibration strips in any checked water equivalent material. It is very crucial and advisable to use the reference depth (usually 10 cm) as stipulated in protocols. At this depth beam profiles are quantified and have the appropriate flatness. The monitor chamber is highly endorsed to be used during Gafchromic film reference irradiations due to the fact that there is quite significant uncertainty in delivering a dose at low doses. This monitor ionization chamber should be positioned away (10 cm) from the film position so that it cannot disturb the backscatter signal towards the calibration film strip.

2.3.5.7 Cutting and scanning Gafchromic film pieces

When sensitive layer of the film receives radiation exposure it changes colour because of polymerization processes. The needlelike polymers produced in this process are developed in one orientation (Fig. 2. 2). As a consequence, it has been understood that the film itself behave like a polarizer during the measurement of light absorption. When the film portion which is on the bed of a scanner is rotated it could yield a different response results over the same region of interest (ROI). Devic et al., (2016) and Aldelaijan et al., (2010) reported that the different response values over the same ROI for EBT-2 film model was found to be of the order of 8%. Besides, this film model presented the rather small dependence of the top - bottom film orientation attributed to its asymmetric design [16, 22]. This dependence of top-bottom film direction is not seen on the newest EBT film models such as EBT-3 (Fig. 2. 10a) and EBT-XD (Fig. 2. 10b) due to their symmetric structure. Figure 2.14 shows how to place the film piece on flatbed scanner: A. cutting the small film pieces from the original sheet; B. position and direction

of film strips during the scanning procedure.

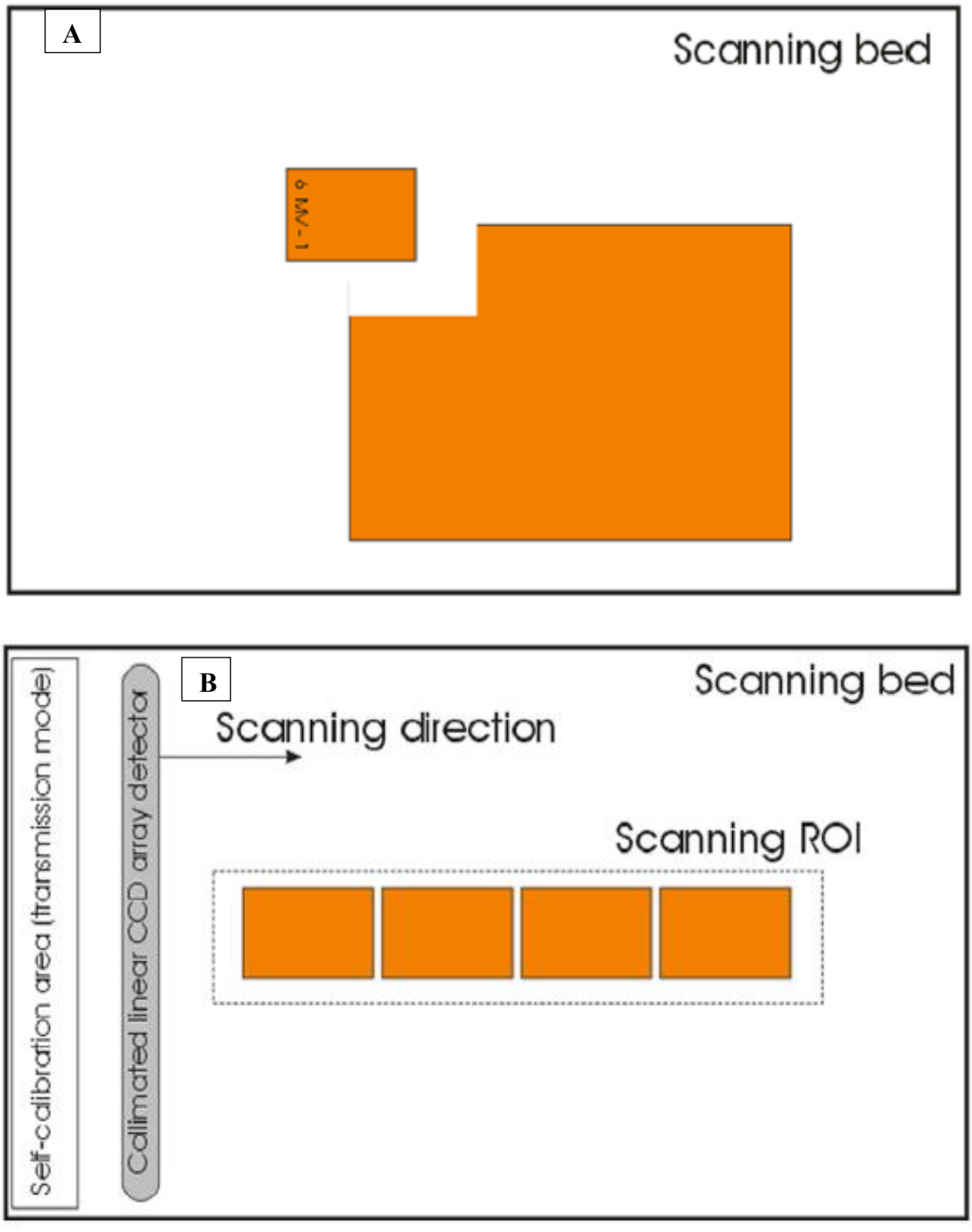

Figure 2. 15: Position of the film pieces on flatbed scanner: A. cutting the film pieces from the original sheet; B. position and direction of film strips during the scanning procedure

Care should only be taken on the film piece rotational dependence which is placed on a scanning bed, whereas the direction of the film strips cutting and locating on the scanner bed could be subjective. In order to follow the direction of the film relative to the scanner bed, it is recommended to keep the elongated edge side of the film piece along the long edge of the scanner bed (Fig.2.14B). Furthermore, the rectangular film piece has one more advantage because it permits for partitioning the film piece into the measuring section and labeling section which could be utilized to display important information on every film portion. It is recommended that films should be getting cut by using the paper trimmer together a ruler to make sure that film piece strips have a perfect straight cut.

2.4 Monitor unit (MU)

International Commission on Radiation Units and Measurement (ICRU) recommends that dose measurement systems should be able to deliver a dose with a precision of 5% for clinical dose [24]. Moreover, it is very important to enhance the accuracy of the monitor unit (MU) calculations which are necessary to improve the modeling and prediction of dose-volume effects of radiotherapy [23, 24]. The great contributors of random and systematic errors in radiotherapy come from target delineation, daily patient set up, and dose calculation. Hence, there is a need of accurate determination of dose per monitor unit (MU) at a single calculation point is an important part of this process. Monitor unit calculations for photon beams may be implemented using either a tissue phantom ratio (TPR) (isocentric) or percentage depth dose (PDD) (nonisocentric) formalism.

2.4.1 Monitor unit equations

The equations (2.5) and (2.6) represent monitor unit calculations for photon using tissue phantom ratio (TPR) [23].

$$MU = \frac{D}{D_o' \times S_c(r_c) \times S_p(r_d) \times TPR(d, r_d) \times WF(d, r_d, x) \times TF \times OAR(d, x) \times \left(\frac{SSD_o + d_0}{SPD}\right)^2} \quad (2.5)$$

When the dose is determined at the isocenter point, the equation (2.5) reduces to equation (2.6)

$$MU = \frac{D}{D_o' \times S_c(r_c) \times S_p(r_d) \times TPR(d, r_d) \times WF(d, r_d) \times TF \times \left(\frac{SSD_o + d_0}{SPD}\right)^2} \quad (2.6)$$

Where D_o' is the dose rate of the beam used under normalization conditions. $S_c(r_c)$ is the collimator scatter factor or simply in-air output ratio. $S_p(r_d)$ is the phantom scatter factor. The parameters S_c and S_p denote collimator and phantom scatter factors respectively. TTF is the total transmission factor for physical attenuators such as compensators, wedges and trays, and virtual such as dynamic or virtual wedges attenuators, and OAR is the off-axis ratio. $TPR(d, r_d)$ is the tissue phantom ratio. $WF(d, r_d, x)$ is the wedge factor. TF: Tray factor. $OAR(d, x)$ is the ratio of the open field dose rate at an Off-axis ratio point to that for the same field shifted such that the point of calculation lies on the central axis. SSD_o is the standard source - surface distance. d_0 is the normalization depth for photon and electron dose measurement which is field-size dependent. SPD is the source - point distance. Beam outputs from teletherapy machines are generally expressed in cGy/min at d_{max} in tissue equivalent phantom. Unlike linear accelerators machine's outputs are generally expressed in cGy/MU at d_{max} in tissue equivalent phantom. Equations 2.7 and 2.8 represent dose rate at d_{max} for reference field size (10×10 cm^2) at

SSD of 100.0 cm and dose rate at d_{max} for 100.0 cm of SSD and for any given field size *A,* respectively. The monitoring ionisation chambers in linear accelerators are frequently calibrated in the way that machine output matches to:

- 1 cGy/MU
- At d_{max} in phantom (point *A*)
- For a 10 × 10 cm^2 field size
- At SSD of 100 cm

$$\dot{D}_p(d_{max}, 10{,}100, h\nu) = {}^{1cGy}/_{MU} \tag{2.7}$$

The dose rate at point *A*, $\dot{D}_p(d_{max}, A, 100, h\nu)$ at arbitrary field *A,* SSD of 100 cm could be found by multiplying $\dot{D}_p(d_{max}, 10{,}100, h\nu) = {}^{1cGy}/_{MU}$ with the relative dose factor RDF (A, hν).

$$\dot{D}_p(d_{max}, A, 100, hV) = \dot{D}_p(d_{max}, 10{,}100, h\nu) \times S_{c,p}(\mathrm{A}, \mathrm{h}\nu) \tag{2.8}$$

From the monitor unit equations and dose rate (2.5), (2.6) and equation (2.7) respectively above, it is clearly seen that MU is inversely proportional to both collimator and phantom scatter factors. These mathematical relationships explains well the dependence of monitor units calculation on output factors [23].

2.5 Volume averaging effect

Various types of ionization chamber have been used in small field radiation therapy dosimetry. In radiotherapy, it is well known that all the fields smaller than 4 cm × 4 cm

are taken as small radiation fields. There are a couple of advantages associated with small field radiotherapy techniques such as stereotactic or intensity modulated radiation therapy (IMRT). The small radiation fields produce a beam that conforms to the tumor target and thus spare the normal tissues. Besides, the advantages of using small field techniques, there are also some limitations associated with radiotherapy techniques. The output factor from linear accelerator will reduce as the irradiation field is becoming smaller. The fluence of photon beam will be perturbed as the detector dimensions are becoming larger. This perturbation effect of detector is caused by the presence of gas-filled cavity inside the detector thereby resulting to the volume averaging effect [25]. The volume averaging effect is the case where dosimeter measures the dose by averaging the dose over the entire volume of dosimeter. It has been observed that the variation in the signal for small fields is not linear, especially in the region of steep dose gradients. It implies that the dose average value for larger detectors cannot provide good results as the smaller can [26]. Therefore detector dimension and its special resolution play an important role in the measurement of standard dosimetric parameters. The ion chamber to be used needs to be sufficiently smaller than the beam itself. The existing different rules of thumb indicate that the dimension of the detector needs to be less than 25% of the field width [27]. It is recommended to use a very small volume ion chamber in order to minimize the impact of the volume averaging effect.

CHAPTER THREE

3.0 MATERIALS AND METHODS

3.1 Introduction

In this research work, different equipment were used such as: diode, Gafchromic EBT3 films and two types of vented cylindrical ionization chambers having sensitive volumes of 0.01 cc and 0.13 cc. The data were collected in full scatter motorized water phantom with 6 MV beams from Varian Unique Performance linear accelerator. For the measurements with the ionization chambers and the diode, each detector was connected to PTW UNIDOS electrometer. A digital thermometer and digital barometer were employed to measure treatment room temperature and pressure respectively to facilitate correction of readings of the ionization chambers for influencing factors such as temperature and pressure. Relative dose factor measurements were performed with each of the detectors and the film at depths of 10.0 cm and d_{max} (1.45 cm) for source-to-surface distances (SSDs) of 90 cm and 100 cm, respectively. The measurements were taken with square field sizes ranging from 1×1 to 40×40 cm^2. Specifications of equipment used in this research work are provided in section 3.2 of this chapter.

3.2 Materials

3.2.1 Varian Unique Performance medical system linear accelerator

The Varian Unique Performance medical Linac (Varian Medical System, Palo Alto, CA,

USA) which was used in this research work is a 6 MV medical system Linac with intensity modulated radiotherapy (IMRT) and volumetric arc therapy (RapidArc) capabilities. The medical linear accelerator (Linac) was manufactured in June, 2014, and installed at the National Centre for Radiotherapy and Nuclear Medicine of the Korle Bu Teaching Hospital, Accra, Ghana in August, 2016. The Linac was commissioned for clinical use in April, 2019, but the first patient was treated with the Linac at the later days of the succeeding month of the same year. Physical specifications of the Linac (gantry, gantry stand and treatment couch) and its collimator system are depicted in Fig. 3.1 and Fig. 3.2, respectively. Dosimetric characteristics of beam from the Linac are listed in Table 3.1.

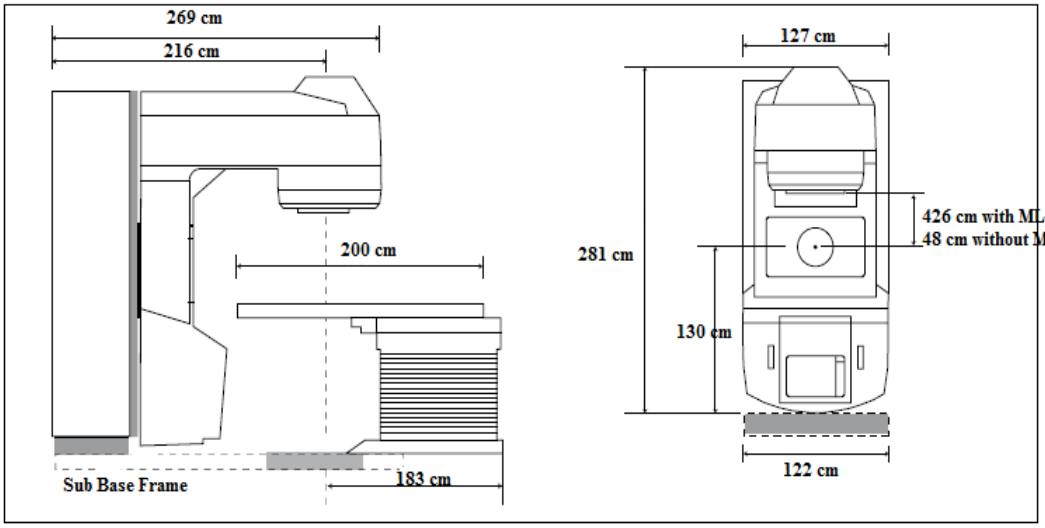

Figure 3. 1: Physical dimensions of the Varian Unique Performance linear accelerator

The Linac is equipped with asymmetric secondary collimator jaws and 120-millenium multileaf collimator system. The field sizes that can be obtained with the secondary collimator jaws ranges from 0.5 × 0.5 to 40 × 40 cm^2 (defined at the isocenter). The gantry of the Linac is mounted isocentrically with source-axial distance (SAD) of 100.0 cm. The beam forming components within the collimator system (or the treatment head)

of the Linac are made up of: an electron gun, a standing wave accelerating waveguide, multileaf collimator system, variable secondary collimator jaws, a fixed primary collimator, Tungsten target, transmission ionization chamber, and a flattening filter. The electron gun and the target are respectively attached to each end of the waveguide as depicted in Figure 3.2. A magnetron is used as the microwave power source to generate the radiofrequency (RF) power required to accelerate electrons produced by the electron gun in the waveguide. The waveguide assembly is pressurized with a dielectric gas (Sulphur hexafluoride). The beam forming components are arranged and aligned in the direction of propagation of the photon beam (X-rays), making it unnecessary to incorporate a beam transport system. Owing to this arrangement, the back of the treatment head protrudes outwards, and the top of the turntable of the sub base frame has to submerge when the gantry is approaching 180 degrees to accommodate the gantry. The transmission ionization chamber placed close to the flattening filter is used to monitor the beam output (dose, symmetry, flatness, and dose rate).

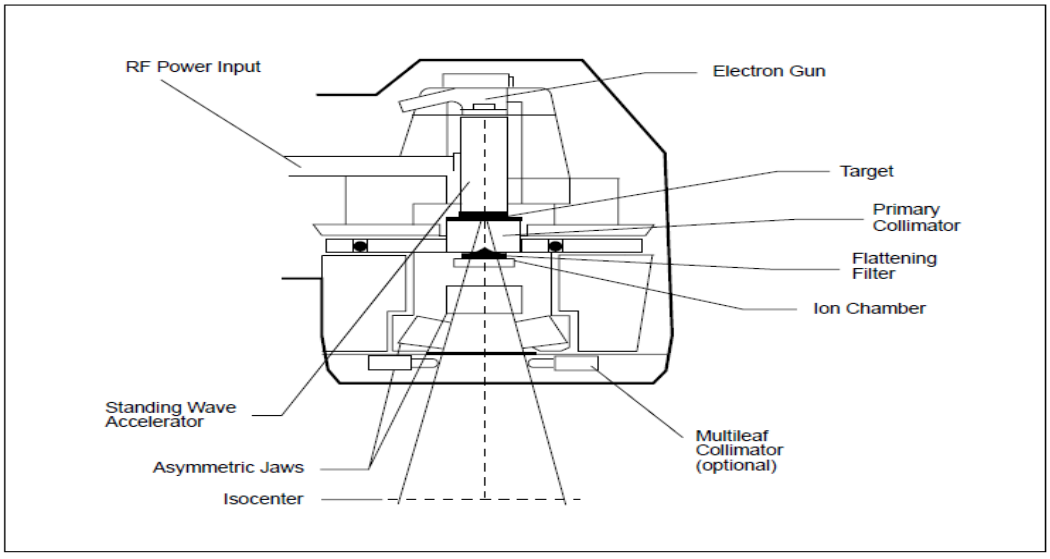

Figure 3. 2: Schematic diagram of the collimator system of the Linac, showing beam forming component and other subsystems

The machine was manufactured by a Switzerland company, Varian Medical Systems International AG. It was installed in 2016 at Korle-Bu Teaching Hospital-Accra, Ghana. The X-ray performance of the Varian unique linear accelerator machine is represented in Table 3.1.

Table 3. 1: Dosimetric characteristics of beam from the Varian Unique Performance linear accelerator

Dosimetric Parameter	**Specification**	**Measured value (%)**
Percentage Depth Dose at depth of 10cm (D10)	10 cm × 10 cm field size	66.8
Maximum Field intensity at d_{max} for 40 × 40 cm^2 field size	Diagonal plane (D + +/- -)	106.9
	Diagonal plane (D + +/ - -)	107.0
Photon field flatness at depth of 10 cm for 40 x 40 cm^2 field size	In-plane	± 2.2
	Cross-plane	±2.0
Photon field flatness for 10 × 10 cm^2 field size at depth of 10 cm	In-plane	1.4
	Cross-plane	0.8
Photon field symmetry for 40 × 40 cm^2 field size at depth of 10 cm	In-plane	1.4
	Cross-plane	0.6

The flattening filter is a metallic cone placed in the path of the beam to attenuate the beam more at the central part than at the periphery such that uniform beam intensity is achieved within the radiation field. The front portion of the bottom part (shoe) of the treatment couch is firmly mounted and secured on a graduated turntable within the sub base frame (which is buried into the floor of the treatment room) of the Linac, which makes the treatment couch capable of rotating 180 degrees in a plane perpendicular to that of the direction of rotation of the gantry. In addition to this movement, the top of treatment couch (or couch top) has three degrees of freedom associated with it. It can move in the vertical, horizontal and lateral directions. The position of the couch top is noted or marked with a well-defined coordinate system using the patient as the reference,

and it is indicated by digital or mechanical display indexer systems attached to the treatment couch. These are used to enhance reproducibility of patient setup between inter-fractions during treatment delivery. The top of the treatment couch (or patient support system) is made from carbon fibre.

At a depth of 10 cm, the Linac has a beam output of 0.800 Gy/100 MU for the reference field size of 10 × 10 cm^2. Beam dose rate ranges from 100 to 600 MU/min (increments of 100 MU/min). Collimator system of the Linac has at its end an accessory holder for mounting of blocks, physical wedges and other treatment accessories. The Linac also comes with dynamic wedge system and the modulation of beam intensity to produce the impression of the wedge can be implemented along the y-jaw direction. Attached to gantry at the opposite end of the collimator systems is a flat panel electronic portal imaging device (EPID) mounted on robotic arm, which is used with the megavoltage (MV) beam for treatment verification purposes. The EPID is always tacked away from the path of the beam when not in use. A picture of the Linac with the motorized water phantom used to acquire beam data in this research work is shown in Figure 3.3.

Figure 3. 3: Varian Unique Performance medical system linear accelerator with motorized water phantom set up for beam data acquisition.

3.2.2. 0.01 cc Razor ionization chamber

The 0.01 cc cylindrical ionization chamber that was employed in this research study is a Razor ion chamber (IBA Dosimetry, BahnhofstraBe, Germany). The Razor chamber is a

waterproof pinpoint ionization chamber and specifically designed for photon and electron relative dosimetry in radiotherapy. The Razor chamber is recommended for small field dosimetry and measurements in regions with high dose gradients such as stereotactic radiotherapy. Its sensitive volume has an air cavity volume of 0.01 cc (cavity radius of 1.0 mm) and the covering wall with thickness of 0.088 g/cm^3 is made from a material called shonka [28]. The covering of the sensitive volume serves as the outer electrode for the chamber, and central electrode material is graphite. The various parts of the Razor ionization chamber and their compositions are listed in Table 3.2. Technical specifications and performance characteristics of the Razor chamber detector are provided in Tables 3.3 and 3.4, respectively. A picture of the Razor ionization chamber in its containing box is represented in Figure 3.4.

Table 3. 2: Parts of the Razor ionization chamber

Part	**Material**	**Characteristics** [g/cm^3]
Outer electrode	Shonka (C-552)	ρ = 1.76
Inner electrode	Graphite	ρ = 1.60
Chamber stem	PEEK	ρ = 1.32
Waterproof sleeve	Silicone	

Table 3. 3: Technical specifications of the Razor ionization chamber

Part	**Dimension** [mm]
Total active length	3.60
Cylinder length	2.60
Inner diameter of outer electrode	2.00
Wall thickness	0.50
Inner diameter of an electrode	0.55
Inner length of an electrode	2.80
Active volume	0.01cm^3

Table 3. 4: Performance characteristics of the Razor ionization chamber

Influence	Rated Range	Limit
Post-irradiation leakage	5 s after irradiation	$\pm$ 0.5%
Minimum dose rate	0.2 Gy/min	
Maximum absorbed dose per pulse	0.2 cGy	> 99%
Stray radiation effect	Parts within 50 cm cable length	$< \pm 2\%$
Polarity	Co-60 – 15 MV	$< \pm 1.3\%\ at + 300\ V\ and - 300\ V$
Orientation-rotation	$0°\ to\ 360°$	$< \pm 0.3\%$
Field size	2×2 to 20×20 cm^2	$< \pm 2.0\%$

Figure 3. 4: Razor ionization chamber in its storage box

3.2.3. 0.13 cc (CC13) cylindrical ionization chamber

The 0.13 cc cylindrical ionization chamber that was used in the research work was a CC13 cylindrical ionization chamber (SN 16115) designed and manufactured by IBA Dosimetry, BahnhofstraBe, Germany. The ionization chamber is recommended for relative dose measurement of proton, photon, and electron beams in external beam radiotherapy. The CC13 is the most preferred chamber to be used in conjunction with the Blue phantom^2 (motorized water phantoms from IBA Dosimetry) for depth dose, beam profile, transmission factor and output factor measurements for clinical applications. It can also be used for absolute dosimetry once it is calibrated by an accreditable dosimetry laboratory. The chamber has a short stem for mounting and a flexible connecting cable. A mark is placed on the stem of the chamber to ensure proper alignment of the chamber within the radiation beam for absolute dosimetry. The chamber is designed to be water-resistant, though it is vented to the environment through its flexible connecting cable [28]. A picture of the CC13 ionisation chamber in its storage box is shown in Fig. 3.5. The various parts of the CC13 ionization chamber and their compositions are listed in Table 3.5. Technical specifications and operational characteristics of the CC13 ionisation chamber are provided in Table 3.6 and Table 3.7, respectively. Since the ionization chamber can be used for absolute dosimetry, Table 3.8 provides beam quality factors appropriate for various beam energies to be used for the chamber to account for variations in chamber response to different beam qualities.

Table 3. 5: Parts of the CC13 ionization chamber

Part	Material	Characteristic [g/cm^3]
Outer electrode	Shonka (C-552)	ρ = 1.76
Inner electrode	Shonka (C-552)	ρ = 1.76
Chamber stem	PEEK	ρ = 1.32
Waterproof sleeve	Silicone	

Table 3. 6: Technical specification of the CC13 ionization chamber

Part	Dimension [mm]
Total active length	5.80
Cylinder length	2.80
Inner diameter of outer electrode	6.00
Wall thickness	0.40
Inner diameter of an electrode	1.00
Inner length of an electrode	3.30
Active volume	0.13 cm^3

Table 3. 7: Operational characteristics of the CC13 ionization chamber

Item	Characteristics
Polarizing voltage	$\pm 300\ V\ (max. \pm 500\ V)$
Typical leakage current	3.0 fA
Recommended pre-irradiation	5.0 Gy
Typical sensitivity	3.60 nC/Gy
Guard potential	$\pm 300\ V\ (max. \pm 500\ V)$
Temperature range	$15℃ - 35℃$
Relative humidity range	$20\% - 80\%$

Table 3. 8: Beam quality factors of the CC13 ionization chamber

Beam quality	Nominal range	Rated range according to reference	Limit of variation (K_Q)	Reference [19]
X-ray (air kerma)	70 kV – C_o-60	HVL 0.06 mm Cu –C_o-60	0.98 – 1.00	
X-ray (absorbed dose to water)	140 kV – C_o-60	HVL 0.42 mm Cu –C_o-60	0.93 – 1.00	
Photons	Co-60 – 25 MV	$TPR_{20,10}$ 0.50 – 0.84	1.001 – 0.943	TRS 398
Electrons	10 – 50 MeV	R_{50} 4.0 – 20.0 cm	0.920 – 0.877	TRS 398
Protons	40 – 230 MeV	R_{res} 0.5 – 30.0 cm	1.041 – 1.037	TRS 398

The nominal useful energy range for the CC13 chamber is from 70 kV to 25 MV for photons, 10 MeV to 50 MeV for electrons and 40 to 230 MeV for protons [28]. The chamber uses male Threaded Neill–Concelman (TNC) connector to connect to an electrometer. The chamber has a guard ring (or guard electrode) which covers the entire measuring volume. The measuring volume (or the sensitive volume) covers a length of 5.8 mm and has an outer electrode with inner diameter of 6.0 mm; giving the chamber a nominal sensitive volume of 0.13 cc [28]. A picture of the CC13 ionization chamber in its storage box is displayed in Fig. 3.5.

Figure 3. 5: CC13 ionization chamber in its storage box

3.2.4 Razor diode detector

The diode that was used in the research work was a Razor detector (IBA Dosimetry, BahnhofstraBe, Germany). The diode is designed for dosimetry in small photon beam field sizes namely those ones met in stereotactic radiotherapy, volumetric arc radiation therapy (VMART) and intensity modulated radiation therapy (IMRT), and regions with high dose gradients. This diode detector is appropriate for relative dose measurements of electron fields and photon in radiation therapy. It is suitable for profile and depth dose measurements in air, solid and water phantoms. It can also be used for the output factor measurement of small to medium field sizes. It is suitable for the measurement in beam qualities ranging from ^{60}Co to 15 MV for photon beams, and 6 to 15 MeV for electron beams. The Razor diode is a p-type diode which is designed to be rigid and long-lasting [29]. The stem and enclosure materials are made with stainless steel, acrylonitrile butadiene styrene plastic (ABS) and epoxy, respectively. The position of measurement point is indicated by a cross-hair marked on top of the detector. The effective point of measurement is located 0.8 ± 0.2 mm from the surface. The active diameter of the Razor diode is 0.6 mm, the active thickness is 0.02 mm, the head diameter 4.0 mm, head length 15.0 mm, stem diameter 4.0 mm and total length of the diode is 60.0 mm [29]. It is made by infusing n-type semiconductor into p-type semiconductor such that the resultant p-n junction can function in photovoltaic mode without any bias voltage. With reference to this, external stimuli such as an ionizing effect of radiation can be used to generate electron–hole pairs within the diode. The signal of the diode is obtained by electrons diffusing freely through the crystal, and electrons are able to cross the p-n junction region with the aid of the built-in electric field of the depleted region. Electron-hole pairs that

are produced directly in the depleted region contribute marginally to the signal of the diode [30]. The diode is a shielded diode and therefore requires to be used with its long-axis parallel to the direction of propagation of the beam in which the diode is placed (as shown in Figure 3.6.B). Pictures of the diode are shown in Figure 3.6.

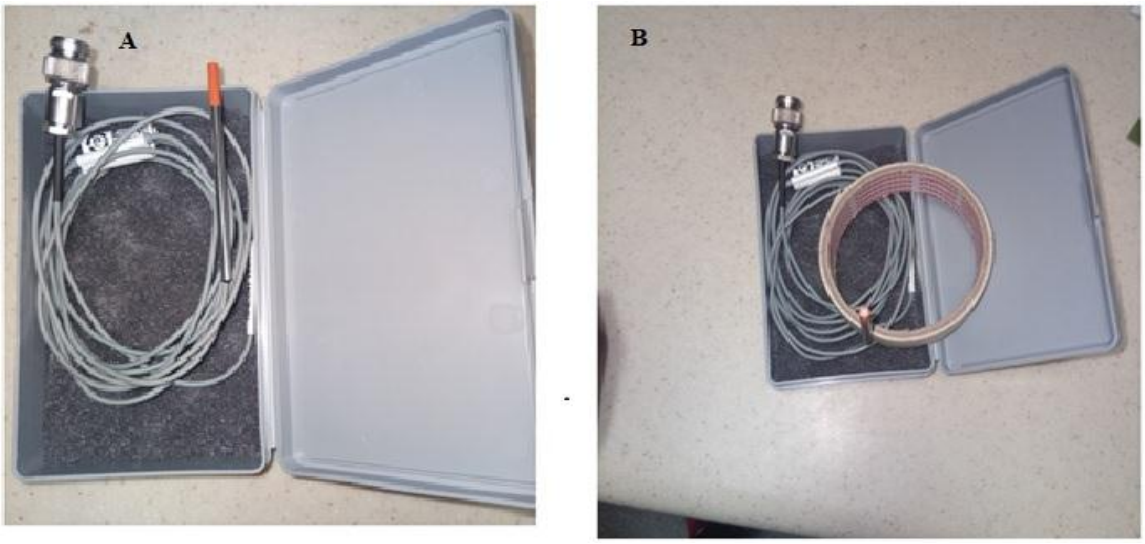

Figure 3. 6: Razor diode detector in it storage box; A. placed horizontally to show its metallic stem and enclosure material (orange portion), and B. in vertical orientation to show its surface (top) and the cross-hair marked on the surface of the diode.

3.2.5 Gafchromic film EBT-3 model

The radiochromic film that was utilized in this research study was Gafchromic EBT-3 film (Ashland Specialty Ingredients, NJ, USA). The sensitive layer of the film is made up of a thin layer material impregnated with a special dye. This layer is sandwiched between two layers of thin clear polyester materials which are tissue-equivalent. The dye gives the film its yellowish characteristic colour. Schematic diagram showing the composition of the film is depicted in Figure 3.8. The film does not react to light and does not need to be processed after exposure to ionizing radiation. Exposing the film to direct sunlight and

extreme temperature conditions could impact the functionality of the film. The film can be marked, immersed directly in water and cut into any shape (or smaller pieces) without affecting its response. When the film is exposed to ionizing radiation, the special dye undergoes polymerization and changes colour from yellow to blue and then black depending on the amount of radiation received by the film. The optical density of the exposed film can be read with a densitometer or an ordinary document scanner. Correlating the film optical densities with their corresponding known radiation doses may be used to obtain a sensitometric curve (or calibration curve) for the film making it possible to use the film as a dosimeter. The film can be used to measure doses in the range of 0.2 to 10 Gy. The film is used for dose measurement in radiotherapy techniques and brachtherapy where doses in two-dimension come in handy [31, 32]. A film is identified by a unique lot number and the lot numbers of films from the same pack (or box) are the same. The film comes in two different sizes of: 12.70 × 20.32 c and 33.02 × 43.18 cm^2. The latter size was used for this research work and the lot number of the films was 03211601. A schematic of Gafchromic film EBT-3 model is shown in Fig. 3.7.

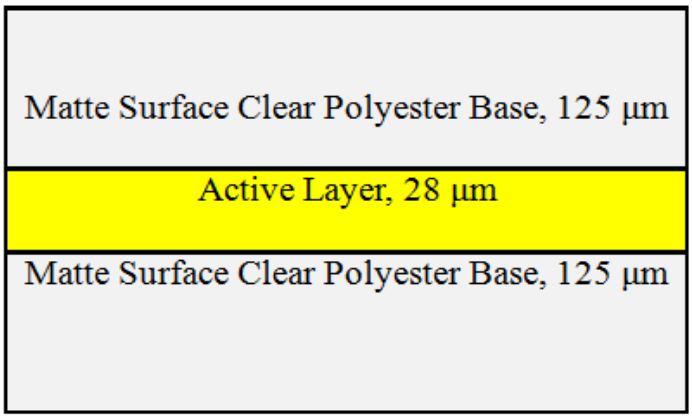

Figure 3. 7: Schematic of Gafchromic film EBT-3 model

3.2.6 Blue Phantom^2 motorized water phantom

The Blue Phantom^2 motorised water phantom is the latest model of IBA Dosimetry, three-dimensional motorised water phantoms, which is designed specifically for commissioning, quality assurance (QA) and acceptance testing requirements of linear accelerators. It is a replacement for the existing Blue Phantom and RFA-300 water phantoms (IBA Dosimetry, Germany). The Blue Phantom^2 motorised water phantom consists of a 48 × 48 × 41 cm^3 water tank, a lifter table, a water reservoir and a central control unit (CCU). On top of the water tank is an automated detector holder mechanism capable of moving a detector in the longitudinal, vertical and lateral directions. The water phantom detector holder mechanism is furnished with magnetostrictive technology to ensure high accurateness and precision in positioning a detector during measurements. The detector holder mechanism also comes with leveling knobs for fine leveling of a detector. The water tank is mounted on the lifter table during measurements. The top of the lifter table is able to move up and down using a telescopic mechanism. The water reservoir is used to hold all the water required for the water tank when not needed. The water reservoir has a bi-directional pump for pumping water in and out of the water tank. The CCU is used to control movements of the detector holder. It also contains an electrometer for receiving signals from connected detectors. The water phantom has temperature and pressure sensors which are linked to the CCU such that ionization chamber readings can be corrected automatically for temperature and pressure influencing factors. For more efficiency, hand pendants are used to allow easy and intuitive control of the water tank, lifter table and the water reservoir. The CCU is usually connected to a laptop computer with windows operating system (windows 10) via

Ethernet (RJ-45) connection and with the manufacturer of the water tank myQA Accept software, facilitate fast and automatic beam data acquisition, data handling, analysis and processing [33]. Picture of the water phantom is shown in Figure 3.8.

Figure 3. 8: Blue Phantom^2 motorized water Phantom

3.3 Experimental

3.3.1 Measurement with ionization chambers

Outputs of the Linac were measured in the Blue Phantom^2 motorized water phantom by using the 0.13 cc ion chamber for numerous open square field sizes (ranging from 1 × 1 to 40 × 40 cm^2) defined by collimator jaws. The ion chamber during the measurements was connected the UNIDOS electrometer. The radiation dose measurements were done at a depth of 1.45 cm (depth of maximum dose) for SSD of 100 cm with the ionization chamber in different orientations relative to the orientation of propagation of the beam for

each set of measurements with the open field sizes. The measurements were done with ionization chamber aligned such that its long-axis is parallel and perpendicular relative to the propagation of radiation beam, respectively. The two orientations of the ionization chamber are depicted in Figure 3.9. For each field size measurement, the initial and final temperatures of the phantom and the pressure within the treatment room were measured with thermometer and the barometer, respectively. Temperature and pressure factor ($K_{T,P}$) were multiplied to the electrometer readings for correction. The corrected electrometer readings for the various field sizes were normalized to that of their respective 10 × 10 cm^2 field size to obtain relative dose factor (RDF) for each of the field sizes for the various set of measurements. The above measurements were repeated with the ionisation chamber positioned at a depth of 10.0 cm but the SSD was set to 90.0 cm. Relative dose factors for the various field sizes per set of measurements for this depth were obtained.

The measurements were also repeated with the Razor ionization chamber to obtain RDFs for the various field sizes per each set of measurements with this chamber. The Razor ionization chamber was also coupled to the UNIDOS electrometer. For the measurements with the ionization chambers, the electrometer was set to measure charges in integral mode with a bias voltage of +300 V. Electrometer readings were acquired for 100 MU using dose rate of 400 cGy/MU for each measurement with a particular field size. The electrometer readings were corrected for pressure and temperature factor ($K_{T,P}$) given in the equation (3.1)(IAEA TRS 398, 2000) [19]:

$$K_{T,P} = \frac{(273.15 + T)}{(273.15 + T_o)} \times \frac{P_o}{P} \tag{3.1}$$

where P and T are the cavity air pressure and temperature at the time of the measurements, and P_o and T_o are the reference values (generally 101.325 kPa and 20°C), respectively.

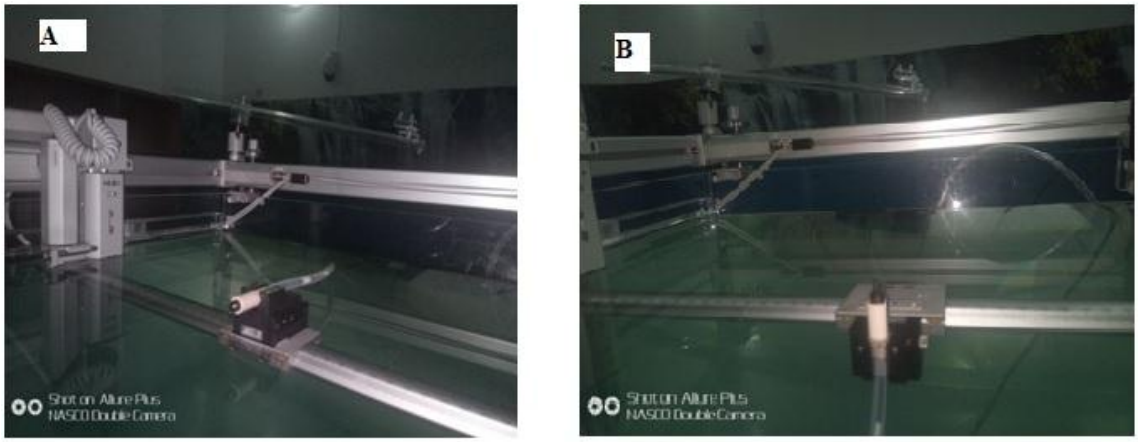

Figure 3. 9: Ionization chamber in different orientations positioned at the required depth of measurement; A. perpendicular direction and B. parallel direction.

3.3.2 Measurements with diode

The measurements in section 3.3.1 of this chapter were repeated with the Razor diode. The diode was connected to the same electrometer, but the bias voltage was set to 0 V. A single alignment of the diode was used in these measurements. The diode was aligned such that its long-axis is parallel relative to the orientation of propagation of the photon beam. The readings of the electrometer in this case were not corrected for the influences of temperature and pressure as with the ionization chambers. The electrometer readings obtained for the diode for the various field sizes were normalized to that of their respective 10 × 10 cm^2 reference field size to obtain RDF for each of the field sizes for the various set of measurements at the two depths.

3.3.3 Measurements with Gafchromic films

Prior to the measurements with the film, a holder to hold film strips within the motorized water phantom was locally designed and constructed from Perspex (PMMA). The holder at one end, has slits at the sides where film strips having dimensions of 2.1 × 1.3 cm^2 can be pushed through. Orthogonal to the slits are flat surfaces either side of a slit. These flat surfaces have a circular hole through them which covers about 80% of the total film area. This was done to ensure that the water gets in contact with a film placed in the holder, and also the beam is not attenuated by the Perspex material with density (1.18 g/cm^3) slightly higher than that of water. The other end of the holder is shaped into a rod to facilitate easy mounting on the available detector holder of the motorized water phantom. A picture of the constructed film holder is displayed in Fig. 3.10.

Figure 3. 10: Picture of constructed film holder

At the beginning of the measurements, beam calibration was done for the Linac based on the IAEA-TRS 398 protocol [19] using a calibrated 0.6 cc PTW Farmer type ionization chamber (TW 30013) which was connected to the same electrometer used for ionometric measurements in the previous section. The measured beam output (dose per MU) for the

10×10 cm^2 (reference field size) obtained during the calibration process was used to compute monitor units (MUs) of prescribed doses ranging from 0.5 to 6.0 Gy (increments of 0.5 Gy) for the reference field size and SSD irradiation technique (SSD=100.0 cm). The doses were prescribed to a depth of 5.0 cm along the beam central axis. Film strips having dimensions of 2.1×1.3 cm^2 were cut from the large film such that the longer side of a film strip corresponded to that of the large film. This was done to ensure that the film strips after exposure are scanned in the same direction. Samples of the film strips are represented in Fig. 3.11.

Figure 3. 11: Gafchromic EBT-3 films used for the measurements

The irradiation geometry which was utilized to compute the monitor units was replicated on the treatment machine (Linac), and film strips were placed in turns into the constructed film holder which had been mounted on the detector holder of the motorized water phantom. With the calculated MUs the films strips were irradiated with a range of

selected radiation doses. After the film irradiations, a post-irradiation period of two days was allowed before the exposed films were scanned with Epson flatbed document scanner (Epson, USA). Picture of the scanner which was used to scan exposed films is displayed in Fig. 3.12. The exposed films were scanned in a batch such that their longer sides were perpendicular to the scan direction. After scanning the films, the scan image was saved in tagged image file format (TIFF) and imported into an ImageJ software (National Institute of health, USA) installed on a laptop for analyses. A rectangular region of interest (ROI) having an area of one-fourth the surface area of a film strip was used to obtain pixel values at the central portion of a film strip per each colour channel (RBG). The mean pixel value was determined for each ROI and converted to film net optical density (OD) using equation 3.2:

$$Net\ (OD) = -log_{10} \times \left(\frac{P_{ex.}}{P_{unex.}}\right) \tag{3.2}$$

Where OD - optical density

$P_{ex.}$ and $P_{unex.}$ are the ROI mean pixel values for exposed and unexposed films, respectively.

A correlation between net OD and radiation dose was established for the film using graphical approach. From this a sensitometric curve (calibration curve) for converting film OD into radiation dose was obtained. Determination of RDFs for the Linac as obtained with the diode in section 3.3.2 of this chapter was repeated with the Gafchromic EBT-3 films. During the measuring process the film strips were inserted into the constructed film holder which was mounted on the detector holder of the Blue Phantom^2 motorized water phantom similar to that of the film calibration process.

Figure 3. 12: Epson stylus CX5900 scanner

Using the same dose rate as that used for the previous measurements and for each field size setting, a film inserted into the constructed film holder was irradiated for 400 MU. For the various field sizes, the exposed films were taken through the same processes as that of the film calibration procedure to obtain their net ODs. These ODs were converted to radiation doses using the calibration curve equation ($y = 5965x^3 + 1679.3x^2 + 1210.9x + 0.807$); this polynomial equation was obtained from the dose response of calibration curve for green channel. For each depth of measurement, the film dose obtained at each particular field was normalized by the film dose obtained at 10×10 cm^2 field size to determine the film measured RDF for the field size.

3.4 Data Analyses

Each detector measured RDFs for the various field sizes were compared to one another. To appreciate the differences Microsoft Excel spreadsheet (Microsoft Corporation, USA) was used to provide graphical representations of the RDFs. Graphs of RDF were plotted against one side of a square field size using the same axes for the different detectors.

Tabular forms of the RDFs were also produced to show discrepancies between RDF values of the various detectors. Ratios of RDF values obtained with the different detectors were also determined and provided in the form of tables. The electrometer readings corrected for temperature and pressure are given in Appendix.

CHAPTER FOUR

4.0 RESULTS AND DISCUSSIONS

4.1 Relative dose factors measured by using CC13 ionization chamber

The percentage relative errors were calculated from equation (4.1) where perpendicular and parallel orientations of ionization chamber with respect to the beam central axis were taken as usual and unusual orientation, respectively. Relative errors (%) calculated and the relative dose factors measured by CC13 chamber are summarized in Table 4.1. Figure 4.1a and Figure 4.1b illustrate relative dose factors against one side of a square field measured with CC13 ionization chamber at SSDs of 90 cm and 100 cm at depths of 10 cm and at d_{max}, respectively.

$$Percentage\ relative\ error = \frac{RDF_{CC13perp} - RDF_{CC13parallel}}{RDF_{CC13perpendicular}} \times 100 \quad (4.1)$$

Table 4. 1: Measured relative dose factor by using CC13 chamber for 6 MV beam

4.1a. SSD = 90.0 cm at d = 10.0 cm				4.1b. SSD = 100.0 cm at d_{max}		
Field (cm)	RDF, CC13 (Perpendicular)	RDF, CC13 (Parallel)	Relative error (%)	RDF, CC13 (Perpendicular)	RDF, CC13 (Parallel)	Relative error (%)
1	0.498	0.583	-17.102	0.638	0.702	-10.060
2	0.783	0.787	-0.454	0.890	0.893	-0.318
3	0.835	0.836	-0.146	0.920	0.921	-0.114
4	0.870	0.871	-0.073	0.937	0.939	-0.119
5	0.893	0.901	-0.813	0.953	0.953	0.019
7	0.949	0.948	0.079	0.975	0.975	-0.046
10	1.000	1.000	0.000	1.000	1.000	0.000
15	1.058	1.059	-0.077	1.027	1.027	-0.036
20	1.095	1.097	-0.133	1.046	1.045	0.061
30	1.145	1.148	-0.280	1.070	1.069	0.076
40	1.171	1.174	-0.292	1.080	1.080	-0.003

From Table 4.1a, it was observed that the relative dose factors measured increased with an increase of the field sizes as expected in both sets up and orientations.

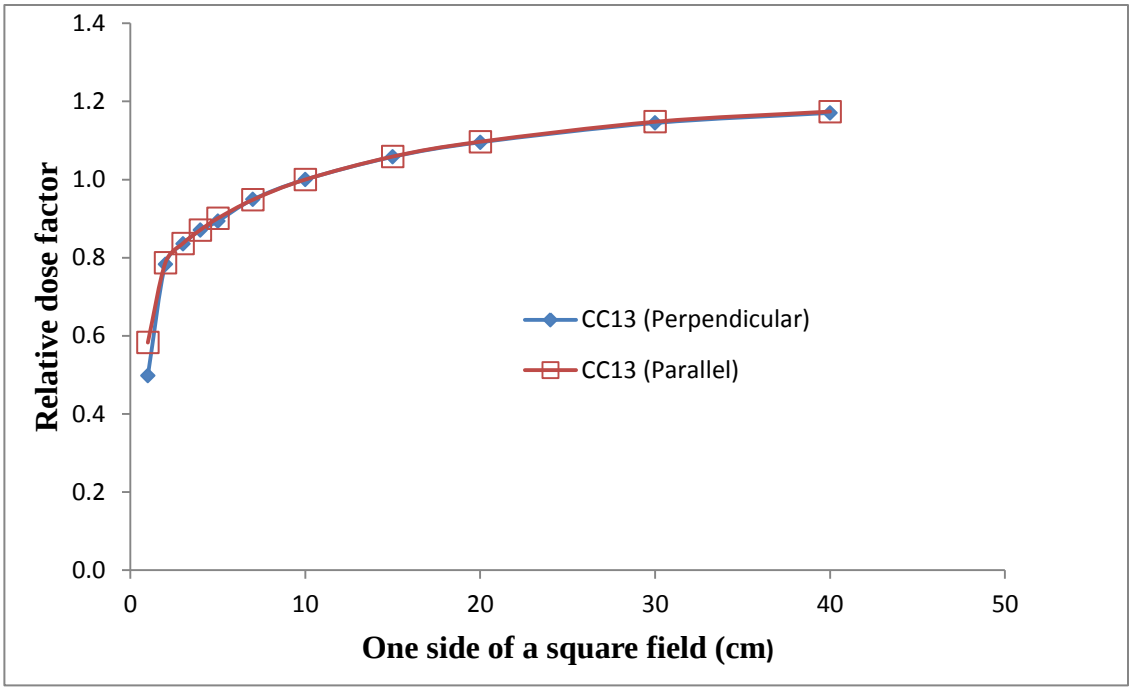

(a)

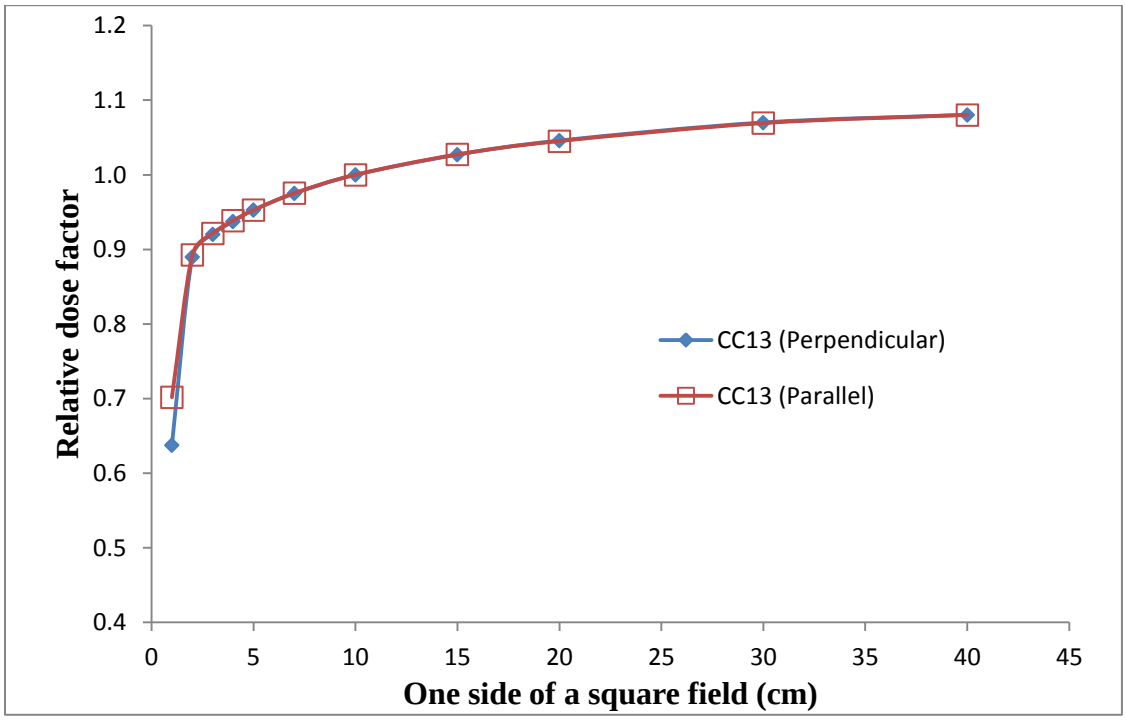

(b)

Figure 4. 1: Relative dose factor against one side of a square field measured with CC13 chamber: (a) at depth of 10 cm for SSD = 90 cm and (b) at d_{max} for SSD = 100 cm

Relative dose factors measured at depth of 10.0 cm for SSD = 90.0 cm, when the ionization chamber was placed parallel with respect to the beam central axis were all higher than relative dose factors measured when the chamber was positioned perpendicular relative to the beam central axis for all field sizes except at 10 cm × 10 cm and 7 cm × 7 cm. The percentage relative errors were less than 1% for all field sizes which agrees with the AAPM TG-142 report [34] except at field size of 1 cm × 1 cm where relative error was seen to be high 17.1% and 10.1% at SSDs of 90 cm and 100 cm, respectively. The sensitive volume of a CC13 detector was not comparable to 1 cm × 1 cm field size. As a consequence, the percentage relative error at this field size was big due to volume averaging effect and lack of electronic equilibrium. From Fig. 4.1, the relative dose factors measured for both perpendicular and parallel orientations from field size of 2 cm × 2 cm up to 40 cm × 40 cm field size were in full accordance with each other; the relative errors (%) found in this range of field size varies from 0 to 0.81%, which is < 1% and agrees with the AAPM TG-142 report [34]. It was also observed that CC13 chamber readings were slightly higher when chamber positioned parallel to the beam central axis. At this orientation CC13 ionization chamber showed high detection ability for measurement of relative dose factor at 1 cm × 1 cm field size both at SSDs of 90.0 cm and 100.0 cm at depths of 10.0 cm and at d_{max} as it shown from Figure 4.2. At d_{max} for SSD of 100.0 cm, the chamber readings were higher than chamber readings at depth of 10 cm for SSD = 90.0 cm from 1 × 1 to 7 × 7 cm^2 field size. The increase in relative dose factor was due to the fact that the absorbed dose depends on depth and distance from the radiation source to the detector. The non-linear behavior of relative dose factor for smaller fields found both in Fig. 4.1a and Fig. 4.1b strongly agrees with

the further classification of smaller fields [26].

4.2 Relative dose factors measured with the Razor ionization chamber

Relative dose factors measured and percentage relative errors calculated are summarized in Table 4.2. The percentage relative errors were calculated by using equation (4.2). Figures 4.3 and 4.4 illustrate relative dose factors against one side of a square field measured with Razor ionization chamber at SSDs of 90 cm and 100 cm at depths of 10 cm and at d_{max}, respectively.

$$Percentage\ relative\ error = \frac{RDF_{Razor\ Ic\ perp} - RDF_{Razor\ Ic\ parallel}}{RDF_{Razor\ Ic\ perpendicular}} \times 100 \qquad (4.2)$$

Table 4. 2: Measured relative dose factors by using Razor ionisation chamber for 6 MV beam through the jaws

4.2a.				**4.2b.**		
SSD = 90.0 cm, d = 10.0 cm				**SSD = 100.0 cm at d_{max}**		
Field (cm)	RDF, Razor chamber (Perpendicular)	RDF, Razor chamber (Parallel)	Relative error (%)	RDF, Razor chamber (Perpendicular)	RDF, Razor chamber (Parallel)	Relative error (%)
1	0.577	0.651	-12.907	0.728	0.798	-9.716
2	0.786	0.784	0.321	0.900	0.897	0.383
3	0.829	0.827	0.307	0.921	0.921	0.000
4	0.863	0.852	1.287	0.941	0.938	0.366
5	0.889	0.891	-0.191	0.955	0.953	0.181
7	0.944	0.931	1.406	0.979	0.969	1.056
10	1.000	1.000	0.000	1.000	1.000	0.000
15	1.064	1.060	0.402	1.031	1.038	-0.669
20	1.103	1.103	0.000	1.062	1.062	0.000
30	1.179	1.162	1.449	1.100	1.095	0.470
40	1.222	1.200	1.797	1.131	1.114	1.524

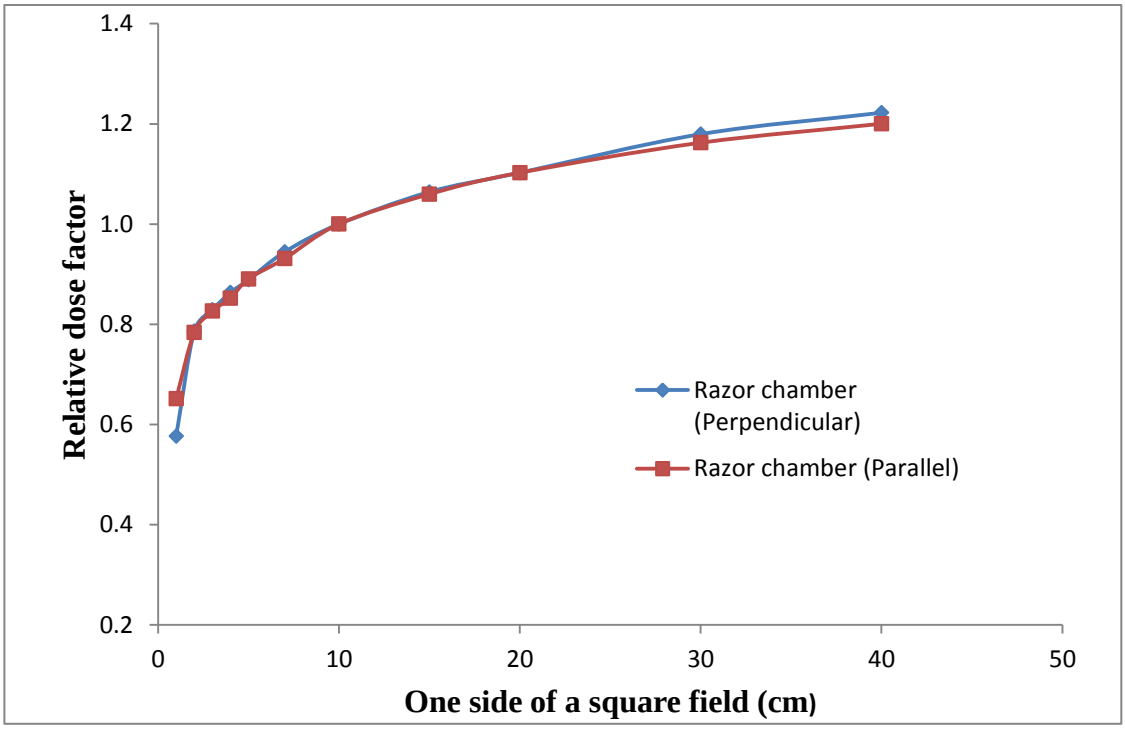

(a)

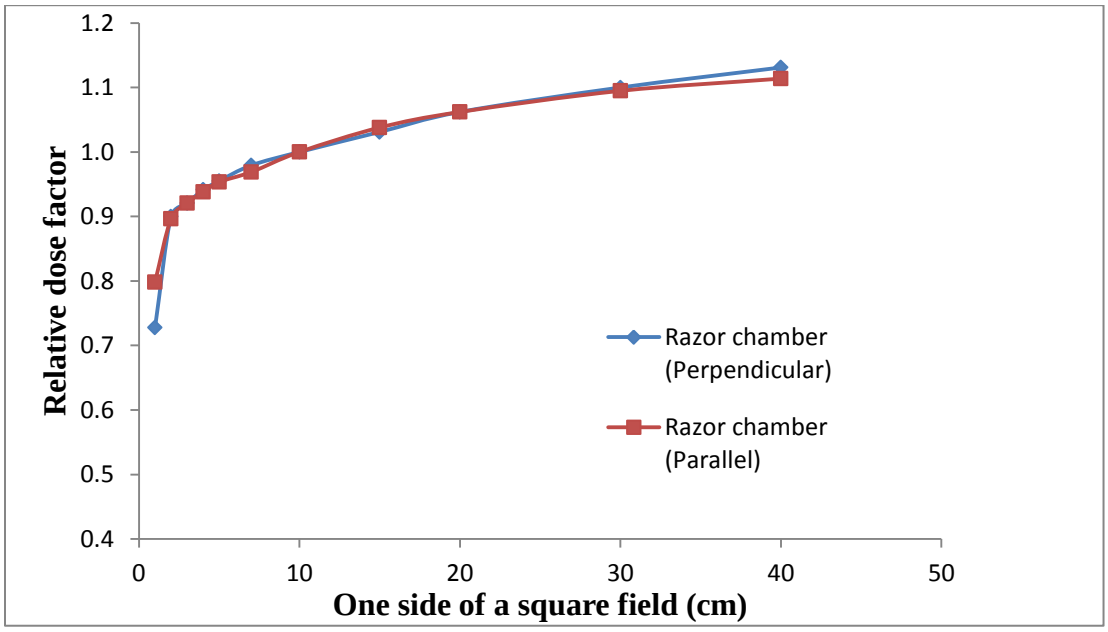

(b)

Figure 4. 2: Relative dose factors against one side of a square field measured with a Razor chamber: (a) at depth of 10.0 cm for SSD = 90.0 cm and (b) at d_{max} for SSD = 100.0 cm

From Table 4.2, the relative dose factors measured using Razor chamber were increasing with field sizes for both set up and orientations as expected. Razor chamber has also

shown high detection ability at smaller field size 1 × 1 cm^2 when it is positioned parallel relative to the radiation beam propagation. Comparing relative dose factors of CC13 chamber and Razor chamber at 1 × 1 cm^2 field size are 0.498, 0.583 and 0.577, 0.651 for both perpendicular and parallel orientations respectively at SSD of 90.0 cm. It is seen that relative dose factors measured by Razor chamber were higher than those ones measured by CC13 chamber. This was due to the fact that the volume averaging effect is minimized and electronic equilibrium is established for the Razor chamber at smaller field size. The sensitive volume of CC13 is thirteen times bigger than the sensitive volume of Razor chamber. Relative dose factors measured by the Razor chamber in both orientations at depth of 10.0 cm for SSD of 90.0 cm (Fig.4.2a) have shown a good agreement in the range of field size from 2 × 2 to 20 × 20 cm^2; In this range of field sizes the orientation of the chamber did not affect the readings except at 4 × 4 and 7 × 7 cm^2 where the relative errors were slightly higher 1.28% and 1.40% respectively. Disagreement was found at 30 × 30 cm^2 and 40 × 40 cm^2 field sizes where the percentage relative errors were higher by1.45% and 1.80%, respectively. At this field sizes Razor chamber showed high detection ability when it was set perpendicularly with respect to the propagation of radiation beam. The same observation of high percentage relative errors of RDFs was found at d_{max} for SSD of 100.0 cm, (Fig. 4.2b) from 30 × 30 cm^2 to 40 × 40 cm^2 field sizes. The Razor ionization chamber showed high detection ability at large field sizes when it was positioned perpendicular to the beam central axis. It can be understood that the sensitive volume of Razor chamber was bigger and more comparable to the large field sizes under investigation when it was set perpendicularly relative to the beam central axis.

4.3 Comparison of relative dose factors measured by using Razor ion chamber and Razor diode

Relative errors calculated by using equation (4.3) between RDFs measured by Razor chamber and Razor diode are summarized in Table 4.3. Figure 4.3a and Figure 4.3b illustrate relative dose factors against one side of a square field measured by Razor chamber and Razor diode at SSDs of 90 cm and 100 cm at depths of 10 cm and at d_{max}, respectively.

$$Relative\ error\ (\%) = \left(\frac{RDF_{Razor\ IC} - RDF_{Razor\ diode}}{RDF_{Razor\ IC}}\right) \times 100 \qquad (4.3)$$

Table 4. 3: Measured relative dose factors by using Razor ionization chamber and a Razor diode for 6 MV beam through the jaws

4.3a.				**4.3b.**		
SSD = 90.0 cm, d = 10.0 cm				**SSD = 100.0 cm at d_{max}**		
Field (cm)	RDF, Razor chamber (Parallel)	RDF, Razor diode (Parallel)	Relative error (%)	RDF, Razor chamber (Parallel)	RDF, Razor diode (Parallel)	Relative error (%)
1	0.651	0.632	2.919	0.798	0.772	3.258
2	0.784	0.748	4.592	0.897	0.884	1.449
3	0.827	0.812	1.814	0.921	0.901	2.172
4	0.852	0.848	0.469	0.938	0.930	0.853
5	0.891	0.881	1.122	0.953	0.946	0.735
7	0.931	0.937	-0.644	0.969	0.971	-0.206
10	1.000	1.000	0.000	1.000	1.000	0.000
15	1.060	1.078	-1.698	1.038	1.033	0.482
20	1.103	1.136	-2.992	1.062	1.058	0.377
30	1.162	1.225	-5.422	1.095	1.094	0.091
40	1.200	1.284	-7.000	1.114	1.115	-0.090

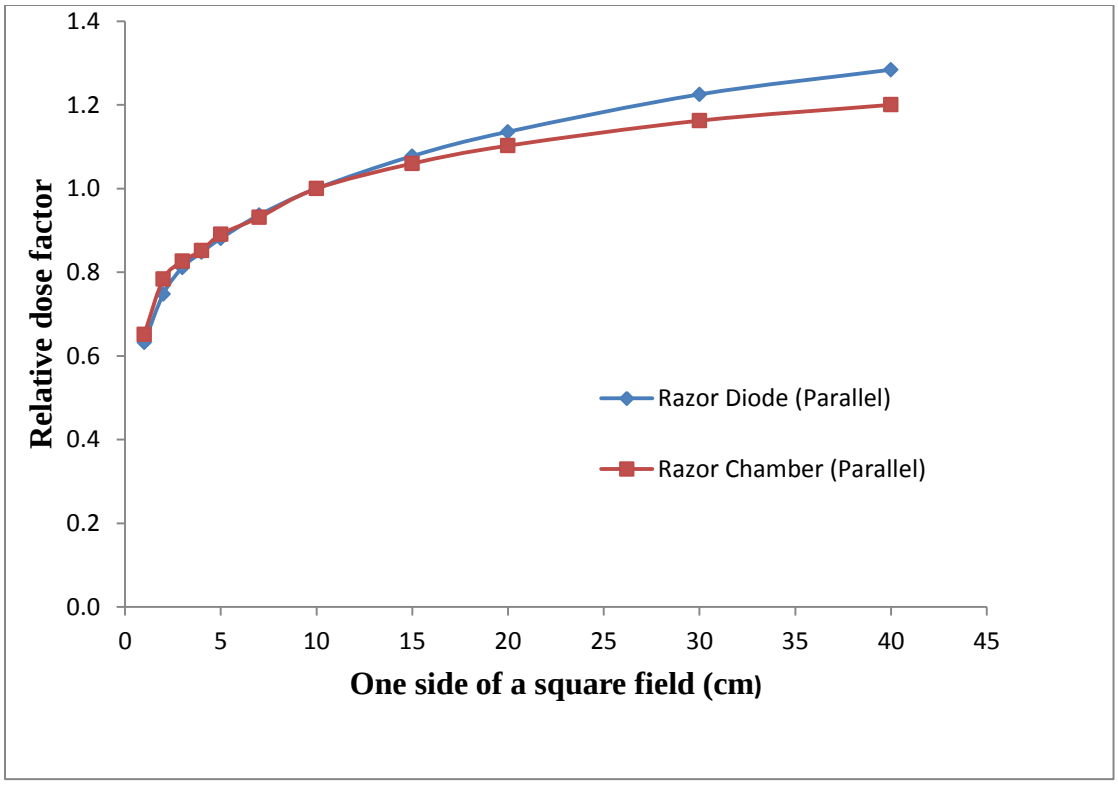

(a)

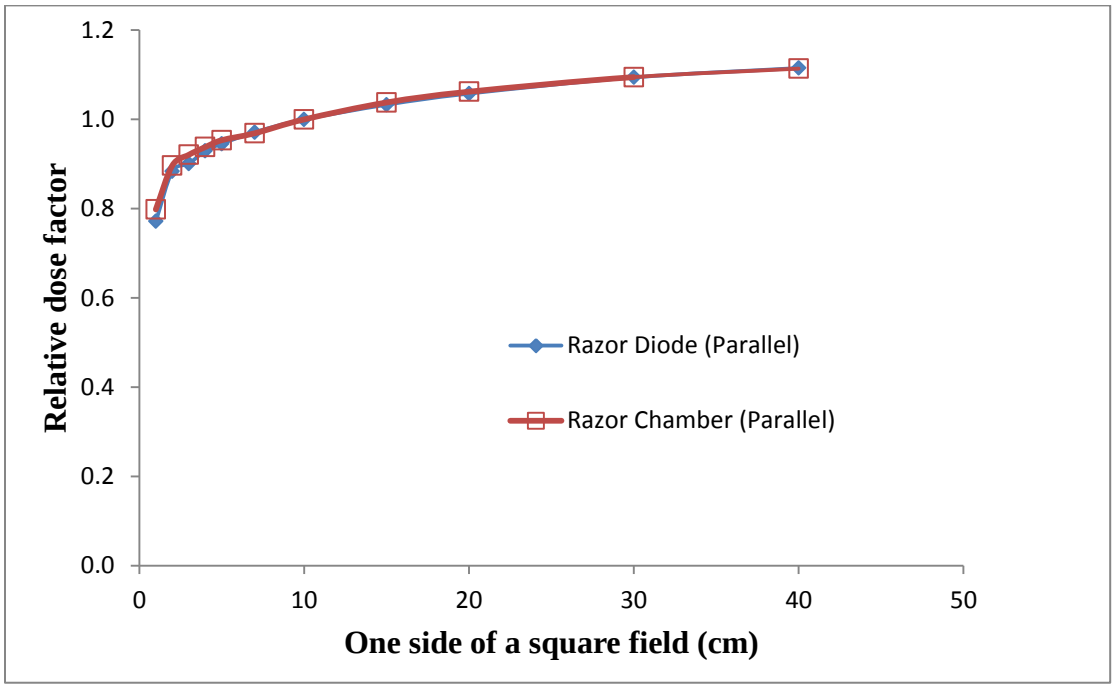

(b)

Figure 4. 3: Relative dose factors against one side of a square field measured by Razor chamber and Razor diode: (a) at depth of 10.0 cm for SSD = 90.0 cm and (b) at d_{max} for SSD = 100.0 cm

Table 4.3b and Fig. 4.3b show that relative dose factors measured by Razor chamber which was positioned in parallel orientation relative to the beam central axis are in good agreement with the relative dose factors measured by Razor diode at d_{max} for SSD of 100.0 cm; the relative errors calculated from field size of 4 × 4 to 40 × 40 cm^2 are less than 1% which is in good accordance with AAPM TG-142 [34] except at 1 cm × 1 cm field size where percentage relative error was little bit higher 3.25% at d_{max} for SSD = 100.0 cm.

4.4 Comparison between relative dose factors measured with CC13 ionisation chamber and Razor diode

Relative errors calculated by using equation (4.4) between RDFs measured by CC13 chamber and Razor diode are demonstrated in Table 4.4. Figure 4.4a and Figure 4.4b illustrate relative dose factors against one side of a square field measured with CC13 chamber and Razor diode at SSDs of 90 cm and 100 cm at depths of 10 cm and at $d_{max,}$ respectively.

$$Relative\ error\ (\%) = \left(\frac{RDF_{CC13\ Ic} - RDF_{Razor\ diode}}{RDF_{CC13\ Ic}}\right) \times 100 \qquad (4.4)$$

Table 4. 4: Measured relative dose factors by using CC13 ionization chamber and Razor diode for 6 MV beam

4.4a.				4.4b.		
SSD = 90.0 cm at d = 10.0 cm				**SSD = 100.0 cm at d_{max}**		
Field (cm)	RDF, CC13 chamber (Parallel)	RDF, Razor diode (Parallel)	Relative error (%)	RDF, CC13 chamber (Parallel)	RDF, Razor diode (Parallel)	Relative error (%)
1	0.583	0.632	-7.753	0.702	0.772	-9.972
2	0.787	0.748	5.214	0.893	0.884	1.008
3	0.836	0.812	2.956	0.921	0.901	2.172
4	0.871	0.848	2.712	0.939	0.930	0.958
5	0.901	0.881	2.270	0.953	0.946	0.735
7	0.948	0.937	1.174	0.975	0.971	0.410
10	1.000	1.000	0.000	1.000	1.000	0.000
15	1.059	1.078	-1.763	1.027	1.033	-0.584
20	1.097	1.136	-3.433	1.045	1.058	-1.244
30	1.148	1.225	-6.286	1.069	1.094	-2.339
40	1.174	1.284	-8.567	1.080	1.115	-3.241

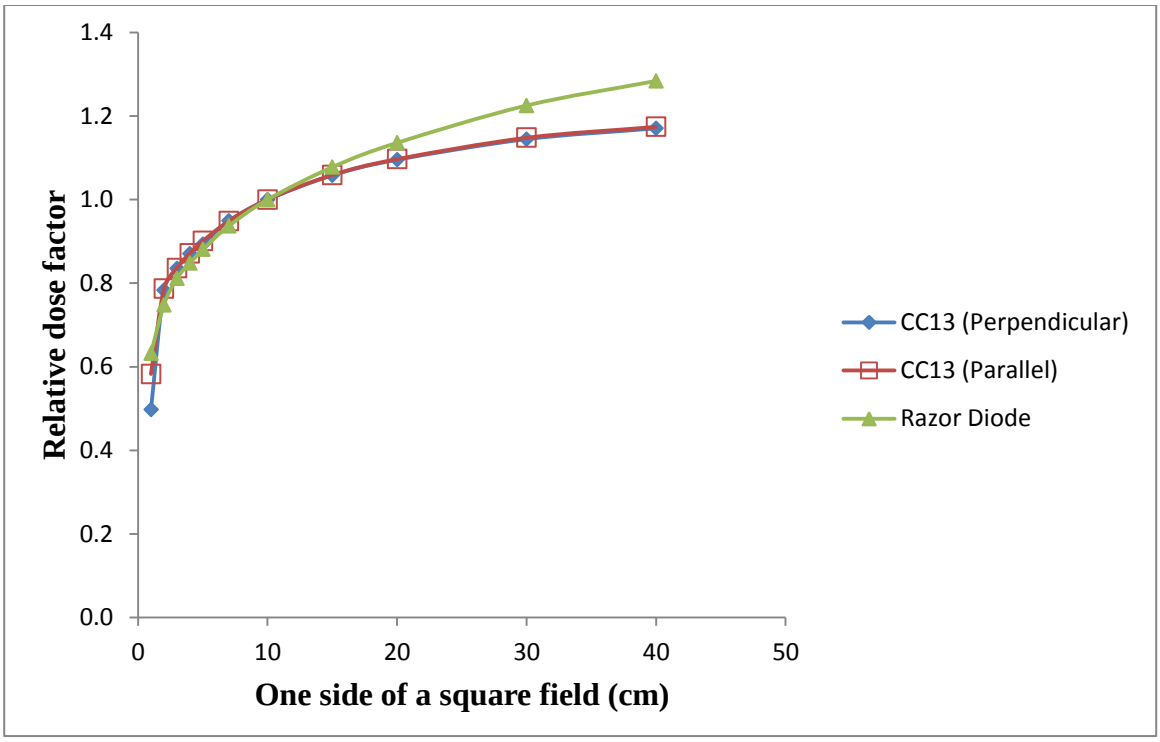

(a)

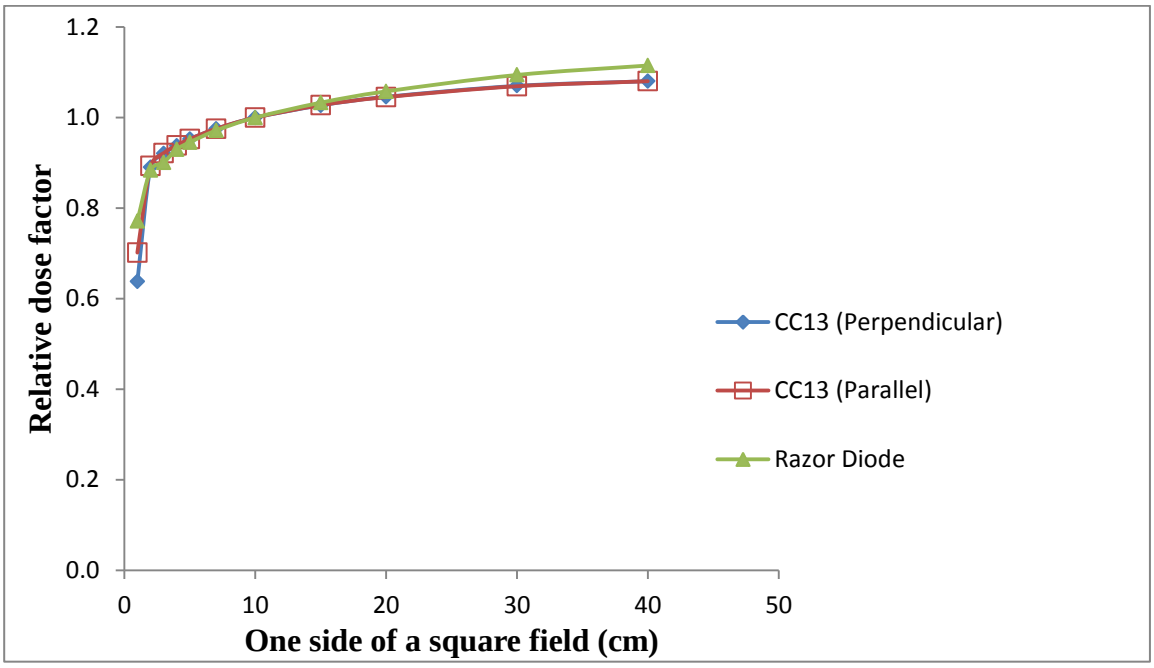

(b)

Figure 4. 4: Relative dose factors against one side of a square field measured by CC13 chamber and Razor diode: (a) at depth of 10.0 cm for SSD = 90.0 cm and (b) at d_{max} for SSD = 100.0 cm

It was observed from Fig.4.4a that Razor diode started to overestimate the dose from a field size of 15 × 15 to 40 × 40 cm^2 at depth of 10.0 cm for SSD of 90.0 cm. Razor diode readings were also found to be overestimated (Fig. 4.4b) compared to CC13 ionization chamber from 20 × 20 cm^2 to 40 × 40 cm^2 field sizes at d_{max} for SSD of 100.0 cm. The overestimation of the dose of large field size by Razor diode was due to the fact that Razor diode was designed for small field dosimetry.

Relative errors (%) calculated between measured RDFs of the CC13 chamber and the Razor diode at smaller field size 1 × 1 cm^2 were 7.75% and 9.97% at SSD of 90.0 cm and 100.0 cm respectively.

4.5 Assessment of relative dose factors measured by CC13 and Razor ionisation chamber

Percentage relative errors were calculated between the RDFs measured by CC13 and Razor chamber from the equation (4.4) and summarized in Table 4.5. Figure 4.5a and Figure 4.5b represent relative dose factors against one side of a square field measured with CC13 chamber and Razor chamber both at SSDs of 100 cm and 90 cm, at depths of d_{max} and 10 cm, respectively.

$$Relative\ error\ (\%) = \left(\frac{RDF_{CC13\ IC} - RDF_{Razor\ IC}}{RDF_{CC13\ IC}}\right) \times 100 \qquad (4.4)$$

Table 4. 5: Measured relative dose factor using CC13 and Razor ionization chamber for 6 MV beam

4.5a.				**4.5b.**		
SSD = 90.0 cm, d = 10.0 cm				**SSD = 100.0 cm at d_{max}**		
Field (cm)	RDF, CC13 chamber (Perpendicular)	RDF, Razor chamber (Perpendicular)	Relative error (%)	RDF, CC13 chamber (Perpendicular)	RDF, Razor chamber (Parallel)	Relative error (%)
1	0.498	0.577	-15.863	0.638	0.728	-14.107
2	0.783	0.786	-0.383	0.890	0.900	-1.124
3	0.835	0.829	0.719	0.920	0.921	-0.109
4	0.870	0.863	0.805	0.937	0.941	-0.427
5	0.893	0.889	0.448	0.953	0.955	-0.210
7	0.949	0.944	0.527	0.975	0.979	-0.410
10	1.000	1.000	0.000	1.000	1.000	0.000
15	1.058	1.064	-0.567	1.027	1.031	-0.389
20	1.095	1.103	-0.731	1.046	1.062	-1.530
30	1.145	1.179	-2.969	1.070	1.100	-2.804
40	1.171	1.222	-4.355	1.080	1.131	-4.722

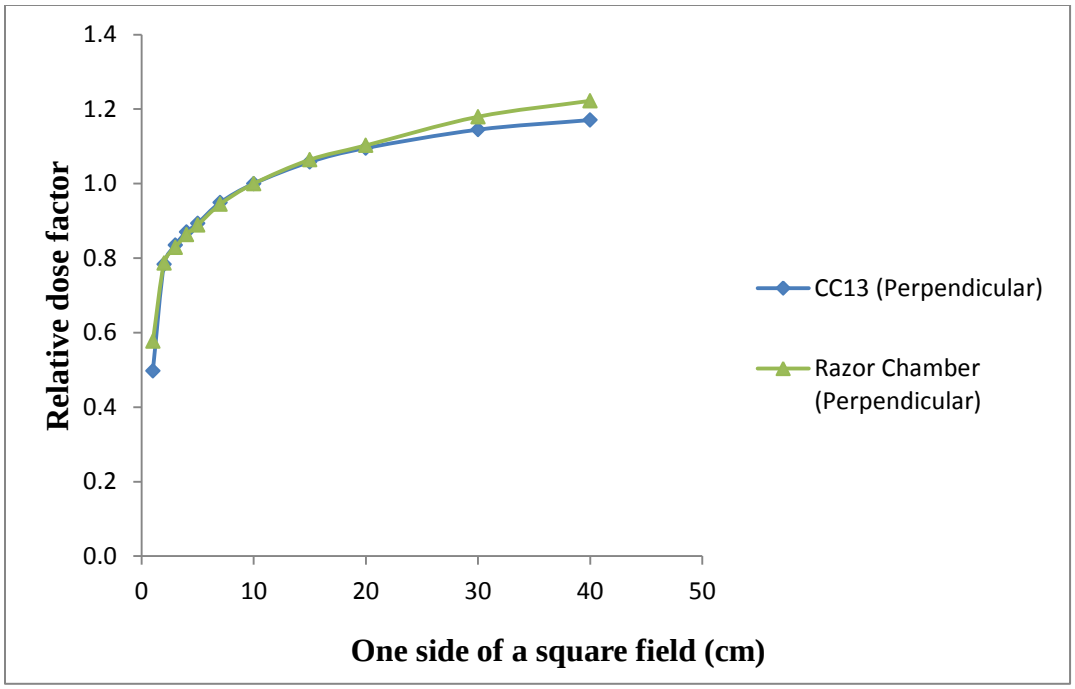

(a)

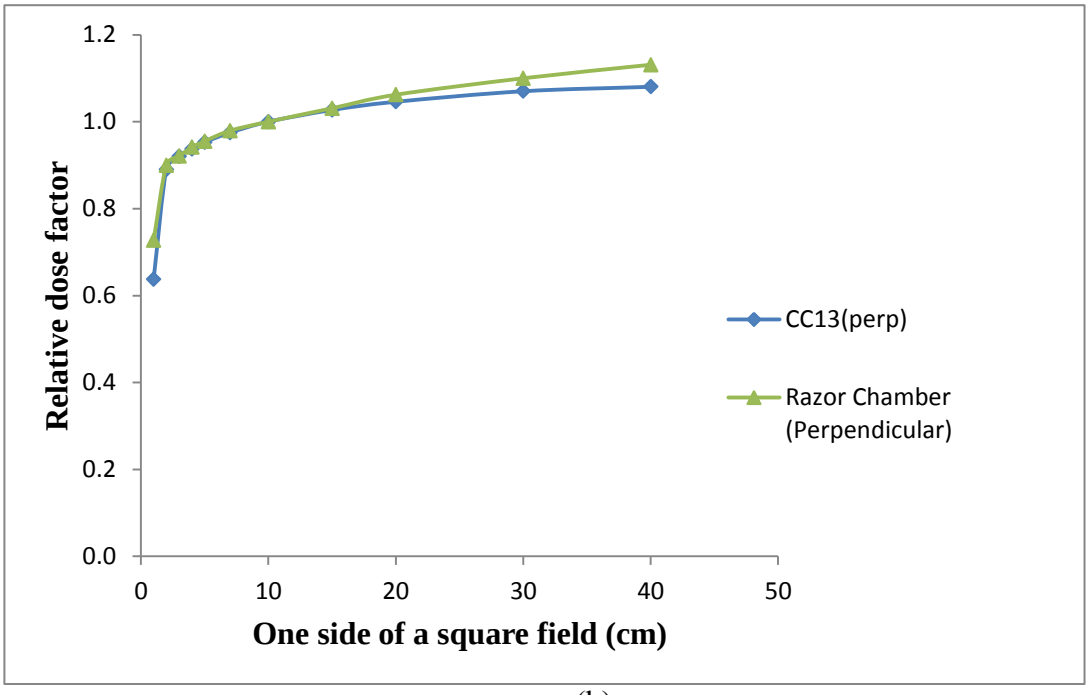

(b)

Figure 4. 5: Relative dose factors against one side of a square field measured by CC13 chamber and the Razor chamber: (a) at depth of 10.0 cm for SSD = 90.0 cm and (b) at d_{max} for SSD = 100.0 cm

It was observed from Tables 4.5a and 4.5b that percentage relative errors calculated

between RDFs measured by CC13 chamber and the Razor chamber at smaller field size 1 cm × 1 cm were bigger than other relative errors. It could be understood that this big deviation in relative error was caused by different factors such as the volume averaging effect (i.e. lack of electronic equilibrium) and expansion of the penumbra of the dose profile (i.e. the central part of the beam was not uniform over the spatial extent of the radiation detector used) [36, 37]. On the other hand, relative errors were smaller than 1% from 2 × 2 cm^2 to 20 × 20 cm^2 field size, which were in agreement with the AAPM TG-142 report [34], which indicates that reproducibility of X-ray output factors should not be greater than 1%. From Fig. 4.5a and 4.5b it could be seen that Razor chamber overestimateed the output factors for large field sizes such as 20 × 20, 30 × 30, and 40 × 40 cm^2 by up to 0.73%, 2.97%, and 4.35% at depth of 10.0 cm for SSD = 90.0 cm and 1.53%, 2.80%, and 4.72% at at d_{max} for SSD = 100.0 cm respectively due to the high content of low-energy photons.

4.6 Calibration curve

Determining the dose response of the Gafchromic EBT-3 film is an important step in utilizing these films in dose determination. A calibration curve was plotted by applying third-order polynomial fit to the data. Dose response curves of Gafchromic EBT-3 film for multichannel color from RGB is illustrated in Figure 4.6.

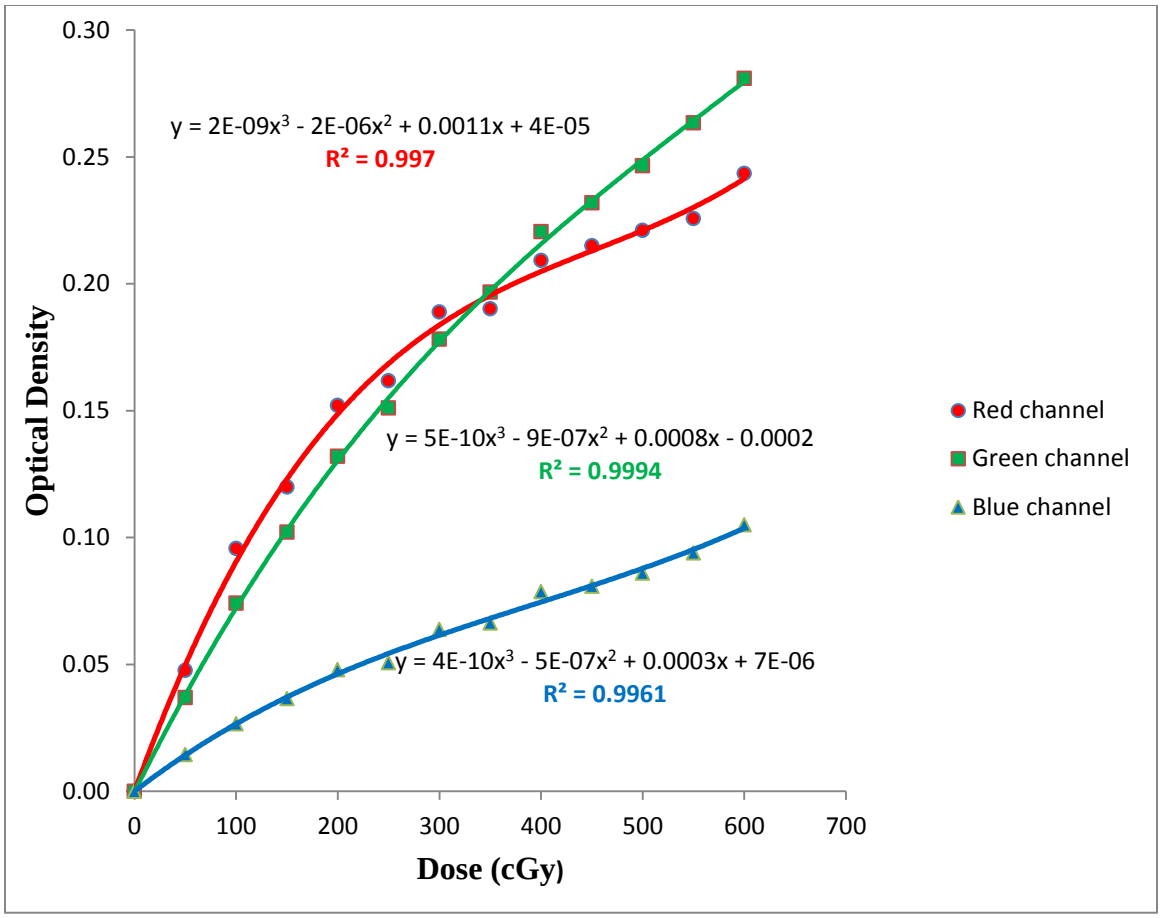

Figure 4. 6: Gafchromic EBT-3 film multichannel calibration curves up to 6 Gy

Figure 4.6 illustrates the dose response curves (Net optical densities vs doses) of the EBT-3 Gafchromic film model for multichannel color from RGB scanned images. Doses are ranged from 0 to 6 Gy and net optical density ranged from 0 to 0.280. From Figure 4.6, the response of EBT-3 film scanned in the red and green channels is above the ones scanned in the blue channels. It could also be concluded that the signal weakly depends on the dose and strongly depends on the thickness of the active layer in the blue channel, it agrees with previous researches on characteristics of calibration curves of EBT-3 films [38, 39]. It is also clearly seen that the net optical density versus dose curves for the red and green channel display an intersection at 3.5 Gy. This strange behaviour of red

channel of being saturated at low dose might be induced by many factors, including degradation of the active layer of the film, systematic error during irradiation and scanning process of the films. It has also been reported that dose response for red channel of the EBT-3 film become more affected when film expires [40]. The green channel has shown a higher sensitivity to third order polynomial fit of $R^2 = 0.9994$ than the red channel with a polynomial fit of $R^2 = 0.997$. Therefore, the green channel was used for the further image analysis. Figure 4.7a and 4.7b represent dose response sensitometric curves of Gafchromic EBT-3 film for red and green channel, respectively.

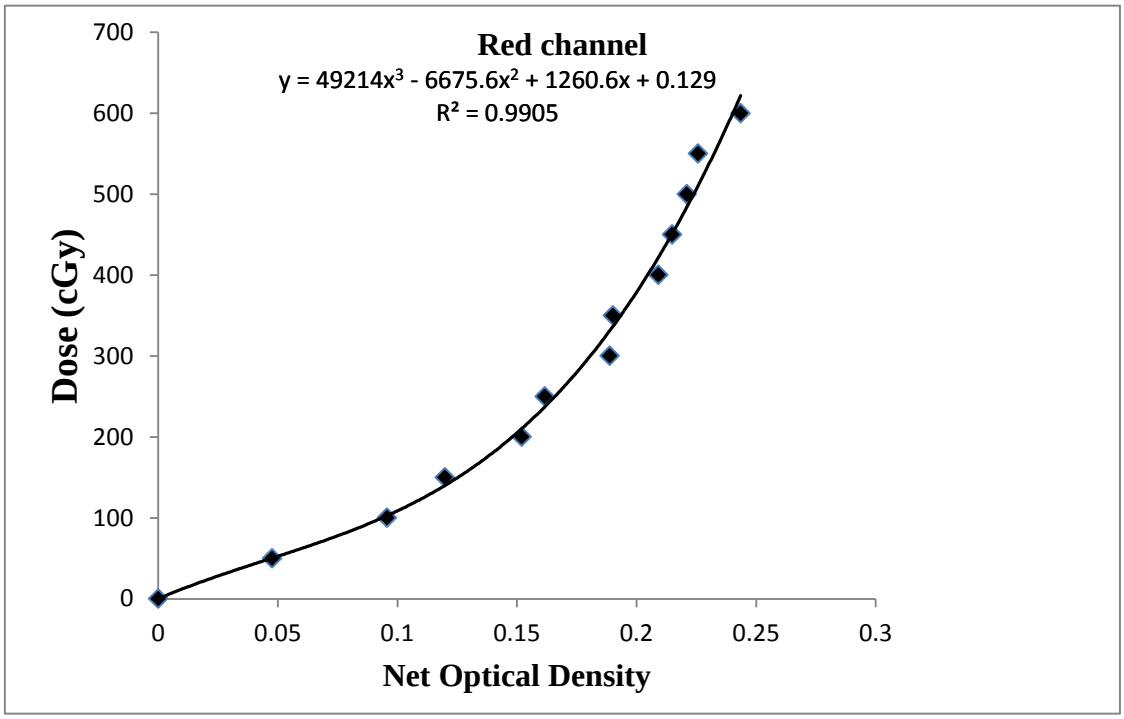

(a)

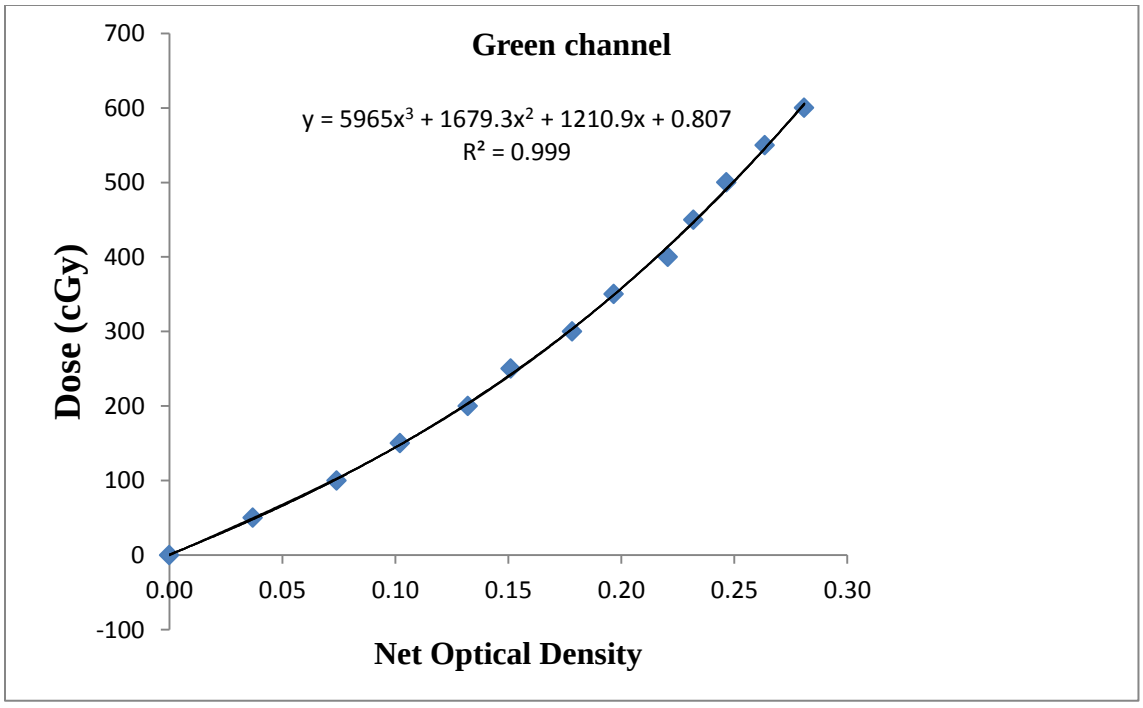

(b)

Figure 4. 7: Dose response calibration curve of Gafchromic EBT-3 film: (a) red channel and (b) green channel

A third order polynomial equation ($y = 5965x^3 + 1679.3x^2 + 1210.9x + 0.807$) obtained from the dose response of calibration curve for green channel was used to calculate unknown doses for other EBT-3 films. Calibration curve for green channel was used because the channel was stable and the most linear. Both dose and relative dose factors calculated are presented in Table 4.6. Figure 4.8a and 4.8b represent relative dose factors against one side of a square field measured with Gafchromic EBT-3 film both at SSDs of 100 cm and 90 cm, at depths of d_{max} and 10 cm, respectively.

Table 4. 6: Dose and relative dose factors measured with EBT-3 film

4.6a.			**4.6b.**	
SSD = 90.0 cm, d = 10.0 cm			**SSD = 100.0 cm at d_{max}**	
Field (cm)	Dose (cGy), EBT-3 film	Relative dose factor, EBT-3 film	Dose (cGy), EBT-3 film	Relative dose factor, EBT-3 film
1	137.194	0.596	200.890	0.698
2	170.371	0.740	243.149	0.845
3	191.693	0.832	254.034	0.883
4	212.692	0.924	260.458	0.905
5	213.697	0.928	262.158	0.911
7	217.748	0.946	276.746	0.961
10	230.281	1.000	287.842	1.000
15	235.746	1.024	289.517	1.006
20	250.381	1.087	298.957	1.039
30	273.362	1.187	302.643	1.051
40	261.453	1.135	314.509	1.093

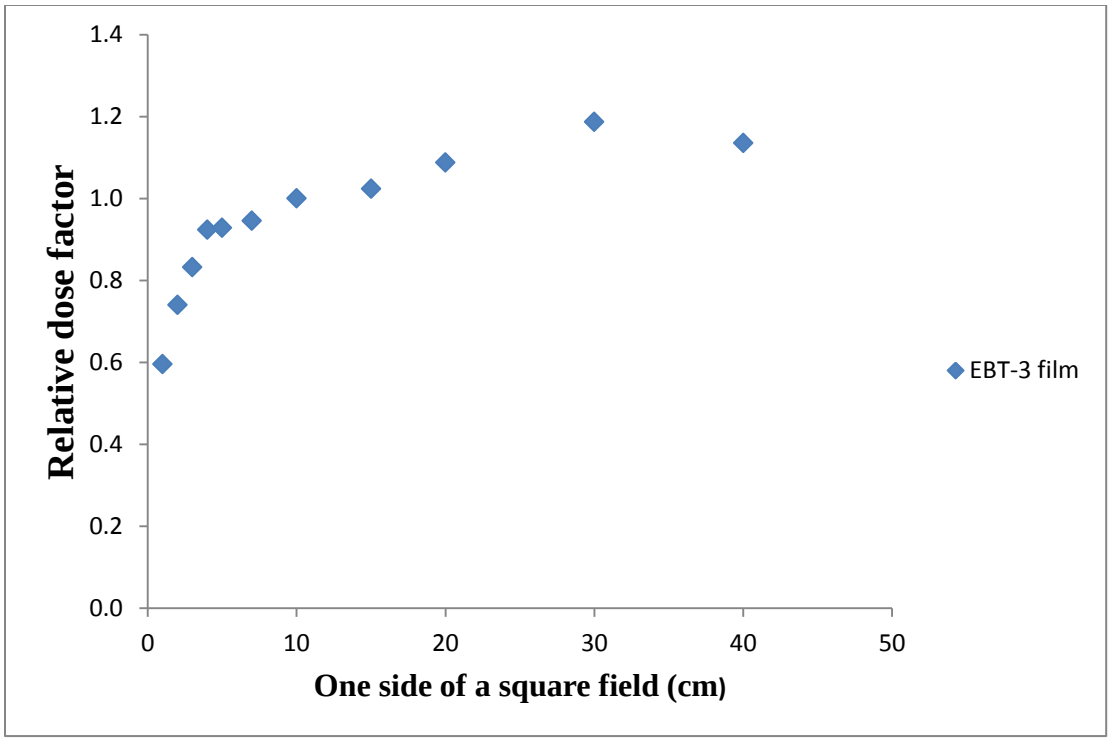

(a)

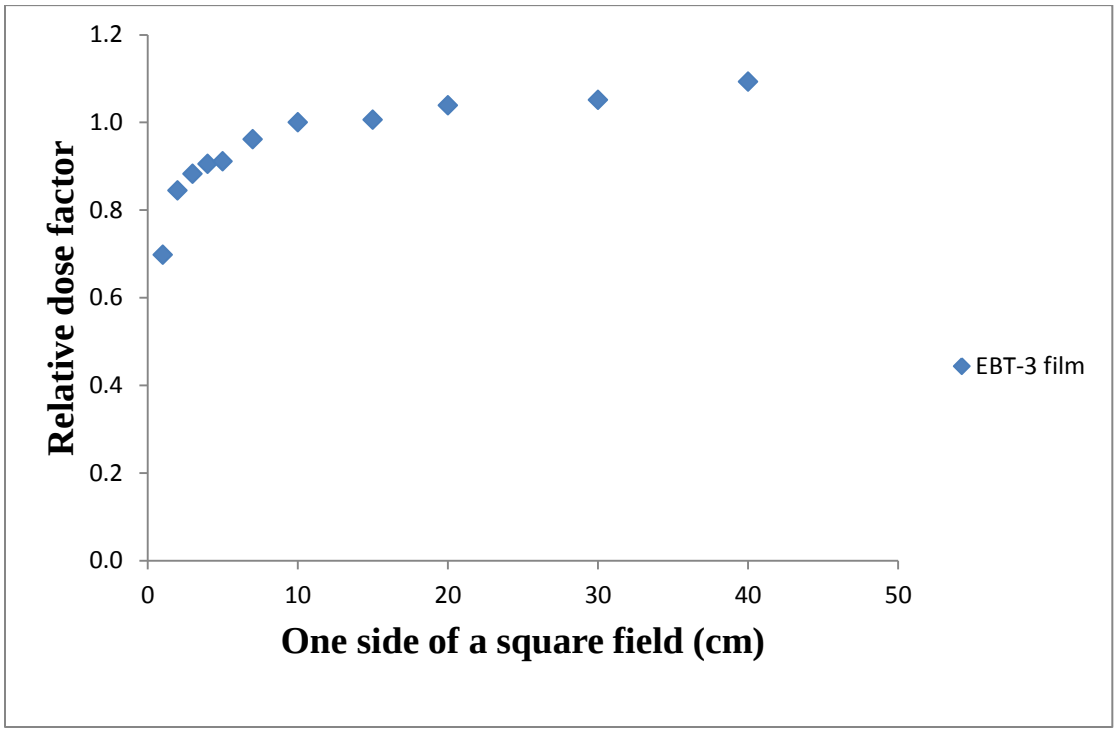

(b)

Figure 4. 8: Relative dose factor measured by using EBT-3 film: (a) at depth of 10.0 cm for SSD = 90.0 cm and (b) at d_{max} for SSD = 100.0 cm

4.7 Assessment of relative dose factors measured by using CC13 ionisation chamber and Gafchromic EBT-3 film

Relative errors calculated between RDFs measured with EBT-3 film and CC13 ionisation chamber were computed by using the equation (4.5) and data obtained presented in Table 4.7. Figure 4.9a and Figure 4.9b represent the comparison of relative dose factors against one side of a square field measured with CC13 chamber and EBT-3 film both at SSDs of 90 cm and 100 cm, at depths of 10 cm and d_{max}, respectively.

$$Percentange\ relative\ error = \frac{RDF_{CC13} - RDF_{EBT3}}{RDF_{CC13}} \times 100 \quad (4.5)$$

Table 4. 7: Relative errors calculated between RDFs measured with CC13 chamber and EBT-3 film

4.7a.			**4.7b.**	
SSD = 90.0 cm, d = 10.0 cm			**SSD = 100.0 cm at d_{max}**	
Field (cm)	Relative error (%) between measured RDFs of $CC13_{IC\ perpen}$ and EBT-3 film	Relative error (%) between measured RDF of $CC13_{IC\ parallel}$ and EBT-3 film	Relative error (%) between measured RDF of $CC13_{IC\ perpen}$ and EBT-3 film	Relative error (%) between measured RDF of $CC13_{IC\ parallel}$ and EBT-3 film
1	-19.679	-2.230	-9.404	0.570
2	5.492	5.972	5.056	5.375
3	0.359	0.478	4.022	4.126
4	-6.207	-6.085	3.415	3.621
5	-3.919	-2.997	4.407	4.407
7	0.316	0.211	1.436	1.436
10	0.000	0.000	0.000	0.000
15	3.214	3.305	2.045	2.045
20	0.731	0.912	0.669	0.574
30	-3.668	-3.397	1.776	1.684
40	3.074	3.322	-1.204	-1.204

Table 4. 8: Difference between relative dose factors measured with CC13 chamber and EBT-3 film

	4.8a.		**4.8b.**	
	SSD = 90.0 cm, d = 10.0 cm		**SSD = 100.0 cm at d_{max}**	
Field (cm)	Difference between measured RDF of $CC13_{IC\ perpen}$ and EBT-3 film	Difference between measured RDF of $CC13_{IC\ parallel}$ and EBT-3 film	Difference between measured RDF of $CC13_{IC\ perpen}$ and EBT-3 film	Difference between measured RDF of $CC13_{IC\ parallel}$ and EBT-3 film
1	-0.098	-0.013	-0.060	0.004
2	0.043	0.047	0.045	0.048
3	0.003	0.004	0.037	0.038
4	-0.054	-0.053	0.032	0.034
5	-0.035	-0.027	0.042	0.042
7	0.003	0.002	0.014	0.014
10	0.000	0.000	0.000	0.000
15	0.034	0.035	0.021	0.021
20	0.008	0.010	0.007	0.006
30	-0.042	-0.039	0.019	0.018
40	0.036	0.039	-0.013	-0.013

From Table 4.8, Fig. 4.9a and Fig. 4.9b it was observed that there is a good agreement on the smaller field size of 1 × 1 cm^2 between relative dose factors measured with CC13 chamber in a parallel direction with respect to the propagation of radiation beam and EBT-3 film. Difference and relative errors found between relative dose factor were -0.013 and 0.004, -2.23% and 0.57% both at SSDs of 90.0 cm and 100.0 cm, respectively.

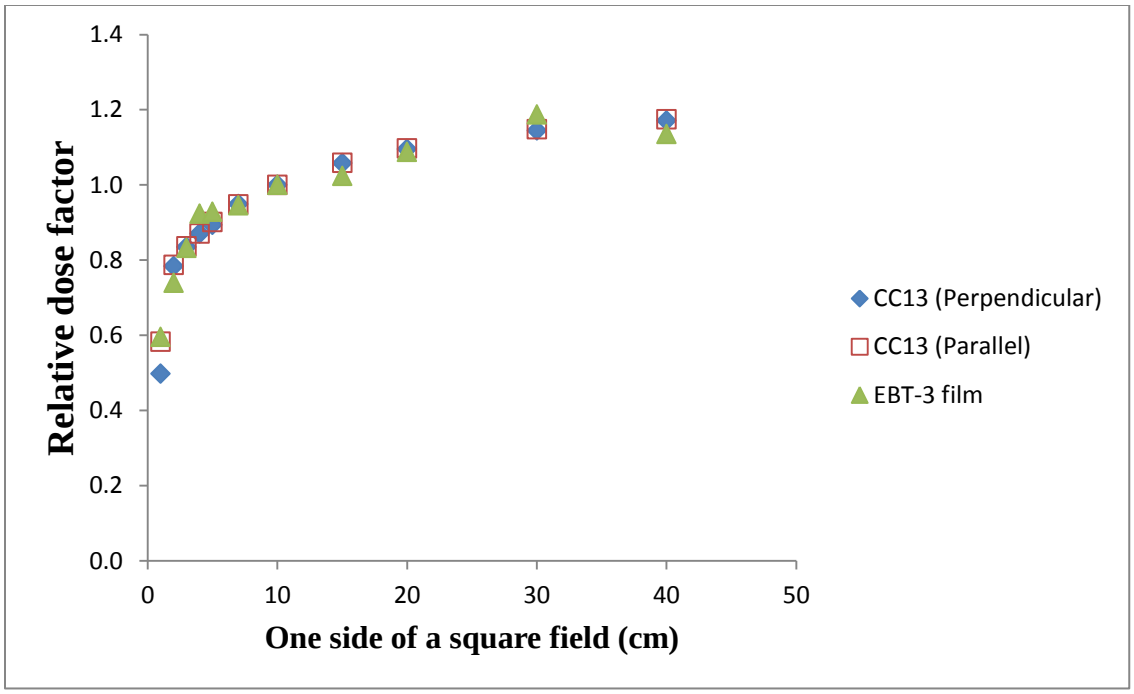

(a)

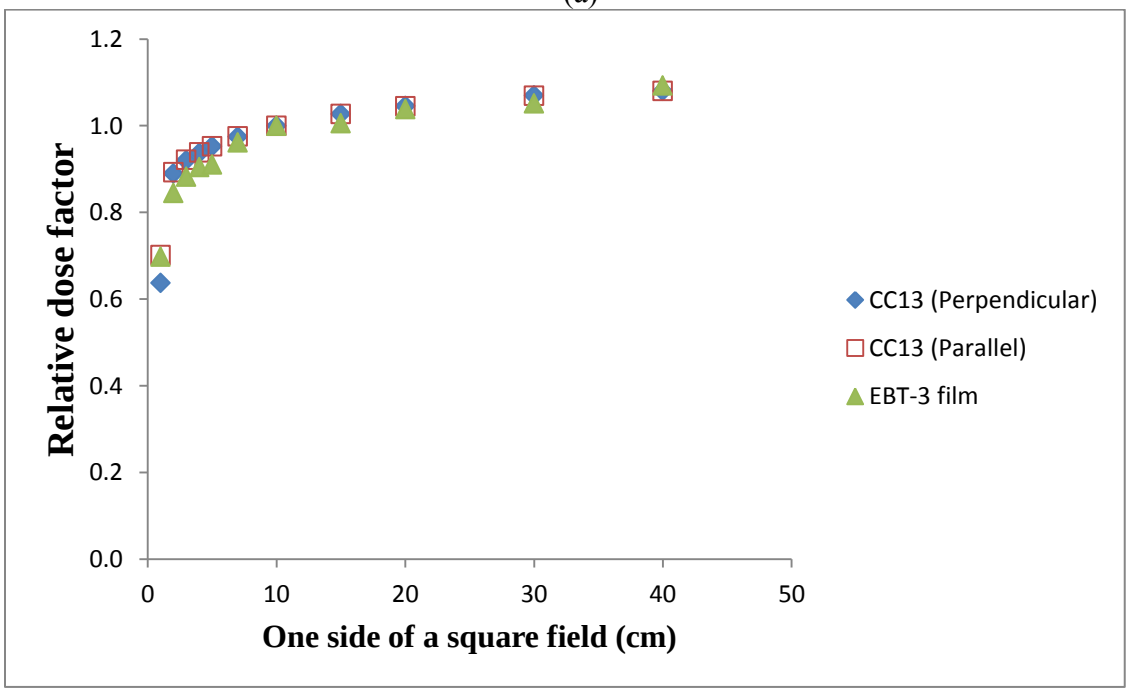

(b)

Figure 4. 9: Relative dose factors measured with CC13 chamber and EBT-3 film: (a) at depth of 10.0 cm for SSD = 90.0 cm at and (b) at d_{max} for SSD = 100.0 cm

4.8 Assessment of relative dose factors measured by using Razor ionisation chamber and Gafchromic EBT-3 film

Relative errors (%) between RDFs measured with EBT-3 film and Razor chamber were calculated by using the equation 4.6 and data obtained are summarized in Table 4.9. Both perpendicular and parallel orientations of Razor chamber relative to radiation propagation were considered in this comparison with EBT-3 film. Figure 4.18 and Figure 4.19 represent the comparison of relative dose factors against one side of a square field measured with CC13 chamber and EBT-3 film both at SSDs of 90 cm and 100 cm, at depths of 10 cm and d_{max}, respectively.

$$Percentange\ relative\ error = \frac{RDF_{razor\ IC} - RDF_{EBT3}}{RDF_{razor\ IC}} \times 100 \qquad (4.6)$$

Table 4. 9: Percentage relative error calculated between RDFs measured with Razor chamber and EBT-3 film

4.9a.			**4.9b.**	
SSD = 90.0 cm, d = 10.0 cm			**SSD = 100.0 cm at d_{max}**	
Field (cm)	Relative error (%) between measured RDF of $razor_{IC\ perpen}$ and EBT-3 film	Relative error (%) between measured RDF of $Razor_{IC\ parallel}$ and EBT-3 film	Relative error (%) between measured RDF of $razor_{IC\ perpen}$ and EBT-3 film	Relative error (%) between measured RDF of $razor_{IC\ parallel}$ and EBT-3 film
1	-3.293	8.449	4.121	12.531
2	5.852	5.612	6.111	5.797
3	-0.362	-0.605	4.126	4.126
4	-7.068	-8.451	3.826	3.518
5	-4.387	-4.153	4.607	4.407
7	-0.212	-1.611	1.839	0.826
10	0.000	0.000	0.000	0.000
15	3.759	3.396	2.425	3.083
20	1.451	1.451	2.166	2.166
30	-0.679	-2.151	4.455	4.018
40	7.119	5.417	3.36	1.885

Table 4. 10: Difference between relative dose factors measured with Razor chamber and EBT-3 film

	4.10a.		**4.10b.**	
	SSD = 90.0 cm, d = 10.0 cm		**SSD = 100.0 cm at d_{max}**	
Field (cm)	Difference between measured RDF of $razor_{IC\ perpen}$ and EBT-3 film	Difference between measured RDF of $razor_{IC\ parallel}$ and EBT-3 film	Difference between measured RDF of $razor_{IC\ perpen}$ and EBT-3 film	Difference between measured RDF of $razor_{IC\ parallel}$ and EBT-3 film
1	-0.019	0.055	0.030	0.100
2	0.046	0.044	0.055	0.052
3	-0.003	-0.005	0.038	0.038
4	-0.061	-0.072	0.036	0.033
5	-0.039	-0.037	0.044	0.042
7	-0.002	-0.015	0.018	0.008
10	0.000	0.000	0.000	0.000
15	0.040	0.036	0.025	0.032
20	0.016	0.016	0.023	0.023
30	-0.008	-0.025	0.049	0.044
40	0.087	0.065	0.038	0.021

From Table 4.10, Fig. 4.10a and 4.10b it was observed that there was a good accordance on the smaller field size of 1 × 1 cm^2 between relative dose factors measured with a Razor chamber in the perpendicular direction with respect to the propagation of radiation beam and EBT-3 film. The difference and relative errors found were -0.019 and 0.030, -3.29% and 4.12% both at depth of 10 cm for SSD = 90 cm and at d_{max} for SSD = 100 cm respectively. It could be understood that the best agreement of two detectors at field size of 1 × 1 cm^2 was found at depth 10.0 cm for SSD of 90.0 cm. From the results obtained it would be better to set the Razor chamber at perpendicular orientation when measuring RDFs for smaller field size dosimetry.

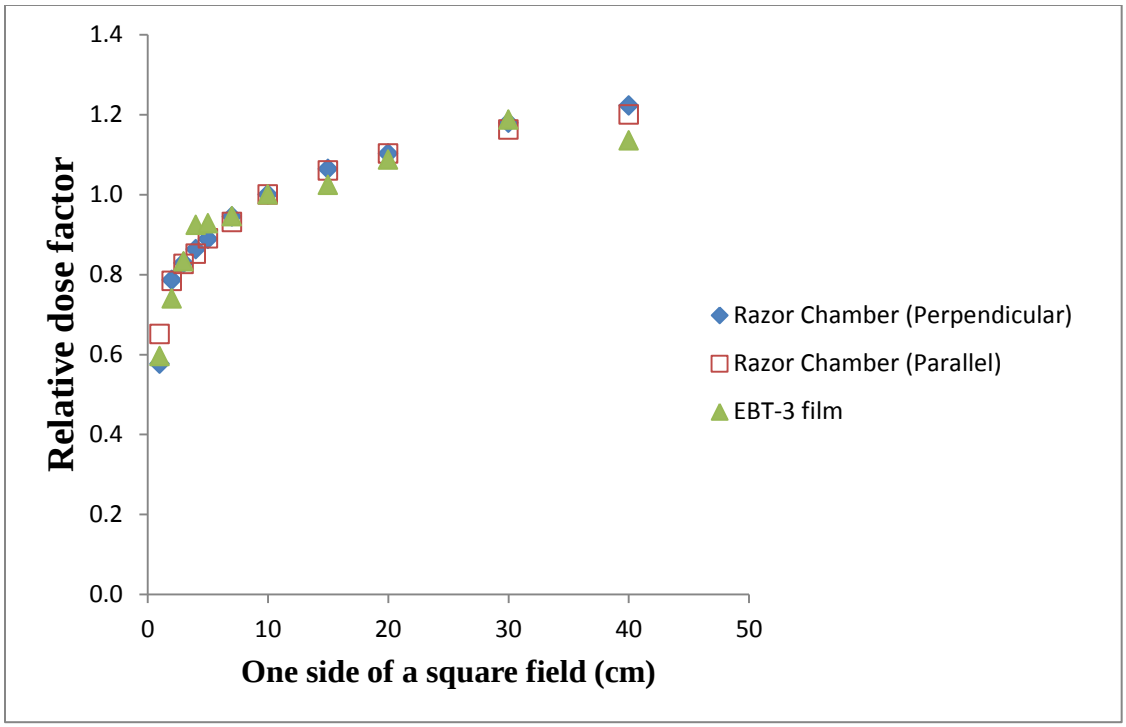

(a)

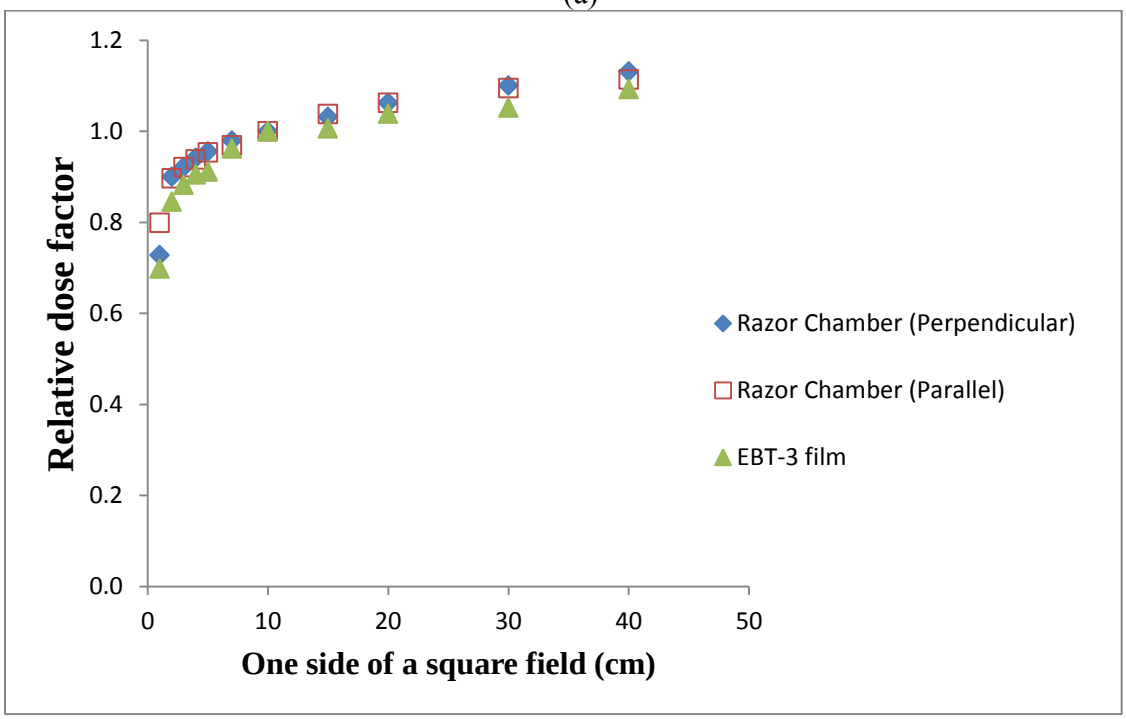

(b)

Figure 4. 10: Relative dose factors measured with Razor chamber and EBT-3 film: (a) at depth of 10.0 cm for SSD = 90.0 cm and (b) at d_{max} for SSD = 100.0 cm

4.9 Assessment of relative dose factors measured by Razor diode and Gafchromic EBT-3 film

Relative errors (%) between RDFs measured with Razor diode and EBT-3 film were calculated from equation (4.7) and summarized in Table 4.11. Figure 4.11a and Figure 4.11b represent the comparison of relative dose factors against one side of a square field measured with Razor diode and EBT-3 film both at SSDs of 90 cm and 100 cm, at depths of 10 cm and d_{max}, respectively.

$$Percentage\ Relative\ Error = \left(\frac{RDF_{Razor\ diode} - RDF_{EBT3\ film}}{RDF_{Razor\ diode}}\right) \times 100 \qquad (4.7)$$

Table 4. 11: Percentage relative errors calculated between RDFs measured with Razor diode and EBT-3 film

4.11a.		**4.12b.**
SSD = 90.0 cm, d = 10.0 cm		**SSD = 100.0 cm at d_{max}**
Field (cm)	Relative error (%) between measured RDF of Razor diode and EBT-3 film	Relative error (%) between measured RDF of Razor diode and EBT-3 film
1	5.696	9.585
2	1.070	4.412
3	-2.463	1.998
4	-8.962	2.688
5	-5.335	3.700
7	-0.961	1.030
10	0.000	0.000
15	5.009	2.614
20	4.313	1.796
30	3.102	3.931
40	11.604	1.973

Table 4. 12: Difference between relative dose factors measured with Razor diode and EBT-3 film

4.12a.		**4.12b.**
SSD = 90.0 cm, d = 10.0 cm		**SSD = 100.0 cm at d_{max}**
Field (cm)	Difference between measured RDFs of Razor diode and EBT-3 film	Difference between measured RDFs of Razor diode and EBT-3 film
1	0.036	0.074
2	0.008	0.039
3	-0.020	0.018
4	-0.076	0.025
5	-0.047	0.035
7	-0.009	0.010
10	0.000	0.000
15	0.054	0.027
20	0.049	0.019
30	0.038	0.043
40	0.149	0.022

From Table 4.11 and Fig.4.11a and Fig.4.11b, the relative errors calculated between RDFs measured with Razor diode and EBT-3 film at field sizes of 1 ×1 cm^2 and 40 × 40 cm^2 were 5.69% and 11. 60%, respectively at SSD of 90.0 cm, depth of 10.0 cm; and 9.58% and 1.97% at d_{max} for SSD = 100 cm, respectively. It was observed that the relative errors calculated at d_{max} for SSD of 100 cm, from 2 × 2 cm^2 to 40 × 40 cm^2 field sizes were less than 4.0% which shows that the RDFs measured with Razor diode and EBT-3 film were in good agreement at this set up.

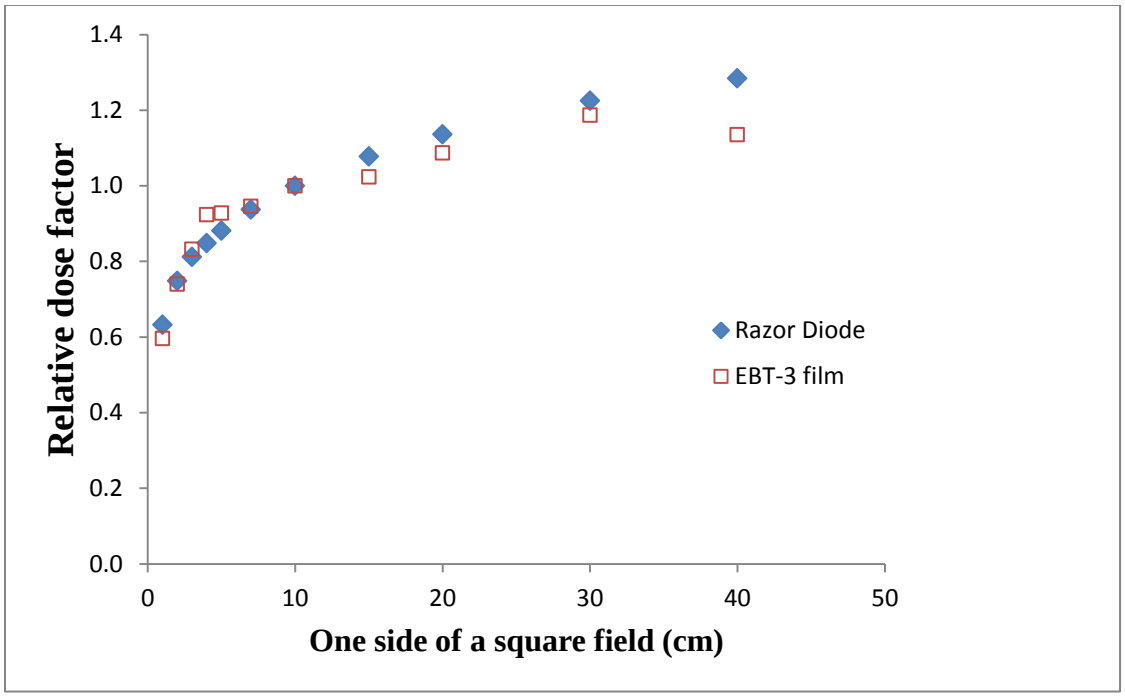

(a)

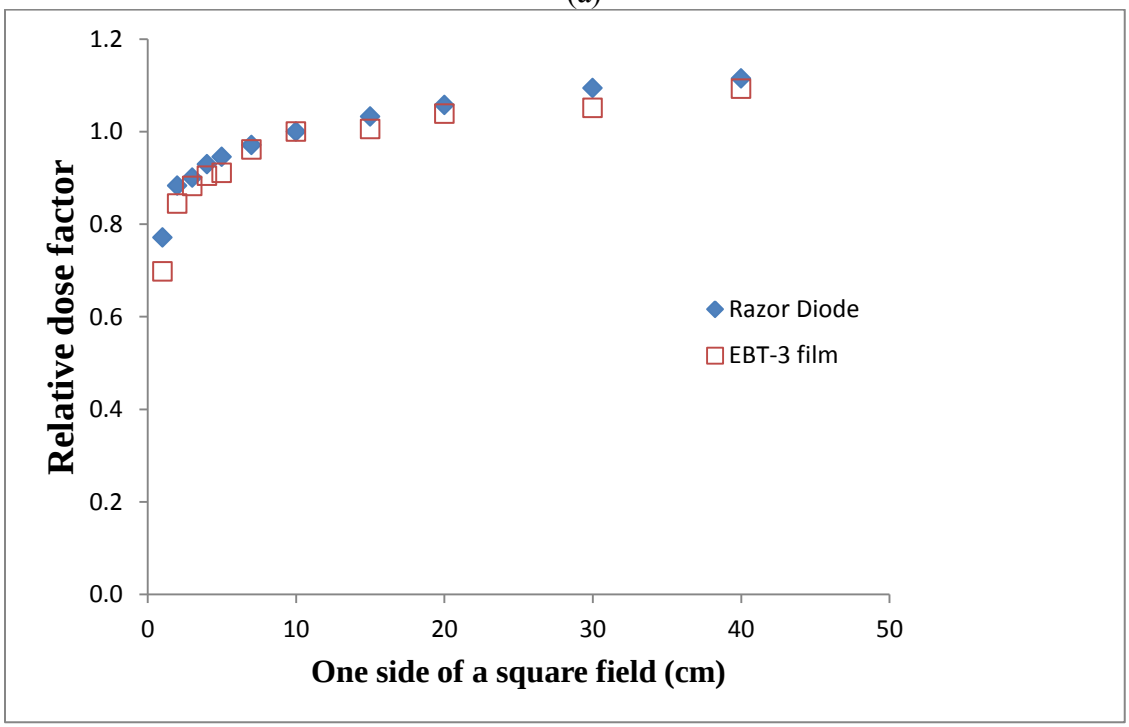

(b)

Figure 4. 11: Relative dose factors measured with Razor diode and EBT-3 film: (a) at depth of 10.0 cm for SSD = 90.0 cm and (b) at d_{max} for SSD = 100.0 cm

CHAPTER FIVE

5.0 CONCLUSIONS AND RECOMMENDATIONS

5.1 CONCLUSIONS

The output factors were measured in blue water phantom[2] by using 0.13 cc chamber, 0.01 cc Razor chamber, the Razor diode detector and Gafchromic EBT-3 film model. During the measurement, each detector was set in perpendicular and parallel orientation with respect to the beam central axis. Measurements were conducted at SSD of 90.0 cm, depth of 10.0 cm and SSD of 100.0 cm, d_{max} of 1.42 cm for field sizes range from 1 × 1 to 40 × 40 cm^2.

The study has shown that 0.13cc chambers would give better readings of output factors for both small and large field sizes when the chamber was positioned parallel with respect to the beam central axis. It was also observed that CC13 ion chamber measured lower dose than Razor chamber at the small field size because of volume averaging effect and lack of electronic equilibrium. The 0.01 cc Razor chamber showed high detection ability in the range of 1 × 1 to 5 × 5 cm^2 field size when it was placed parallel relative to the beam central axis. Razor chamber demonstrated ability to measure output factors for field size ≥ 5 × 5 cm^2 when it was positioned perpendicularly relative to the beam central axis for output factor measurement.

The comparison of relative dose factors measured by CC13 chamber at parallel orientation relative to the direction of propagation and the Gafchromic EBT-3 film showed good agreement by 2.23% and 0.57% of relative error at smaller field size of 1 cm × 1 cm at SSDs of 90 cm and 100 cm, depths of 10 cm and dmax, respectively. Non –

linear characteristic of output factors for small field sizes agrees with further classification of smaller fields.

5.2 RECOMMENDATIONS

i. Further research study on in – air measurements (collimator scatter factor) by using CC13 chamber, Razor chamber, Razor diode and Gafchromic EBT-3 film is recommended.

ii. Further research study is also proposed on correction factors between relative dose factors measured by ionization chambers and Razor diode used in this work.

iii. Further study which would compare output factors measured by both ionization chambers and diode detectors used in this research study with ones obtained from Monte Carlo simulation is recommended.

REFERENCES

[1] Pedro Andreo, "Radiation Dosimetry: Where Do We Stand and Where Do We Go from Here?," in *In: Magjarevic R., Nagel J.H. (eds) World Congress on Medical Physics and Biomedical Engineering 2006. IFMBE Proceedings*, vol. 14, pp 1–7, 2007.

[2] A. Niroomand-Rad, C. R. Blackwell, B. M. Coursey, K. P. G. Soares, J. M. Galvin, W. L. McLaughlin, A. S. Meigooni, R. Nath, J. E. Rodgers, and C. G., "Radiochromic film dosimetry: Report No. 63," *Radiat. Meas.*, vol. 25, no. 63, pp. 2093–2115, 1998.

[3] A. Iftikhar, "Measurements of output factors using different ionization chambers and build up caps," *Iran. J. Radiat. Res.*, vol. 10, no. 2, pp. 95–98, 2012.

[4] R. C. Tailor, D. S. Followill, N. Hernandez, T. S. Zhu, G. S. Ibbott, and U. T. Anderson, "Quality-Assurance Check of Collimator and Phantom- Scatter Factors."pp.1–14, 1998

[5] M. J. Tahmasebi Birgani, N. Chegeni, M. Ali Behrooz, M. Bagheri, A. Danyaei, A. Shamsi, "An Analytical Method to Calculate Phantom Scatter Factor for Photon Beam Accelerators," *Electronic Physician.,* Vol. 9, pp. 3523–3528, 2017

[6] Q. Shamsi, S. A. Buzdar, S. Altaf, A. Atiq, M. Atiq, and K. Iqbal, "Total scatter factor for small fields in radiotherapy : a dosimetric comparison," *Journal of Radiotherapy in Practice*., pp. 1–5, 2017.

[7] E. B. Podgorsak, *Radiation Oncology Physics: A Handbook for Teachers and Students. Chapter 6: External Photon Beams: Physical Aspects.* 2006.

[8] E.B.Podgorsak, "Radiation Oncology Physics: A Handbook for Teachers and

Students," *Int. At. Energy Agency*, vol. 98, p. 1020, 2005.

[9] A. Fogliata, A. Stravato, G. Reggiori, S. Tomatis, J. Würfel, M. Scorsetti, and L. Cozzi, "Collimator scatter factor: Monte Carlo and in-air measurements approaches," *Radiat. Oncol.*, vol. 13, no. 1, pp. 1–10, 2018.

[10] X. A. Li, M. Soubra, J. Szanto, and L. H. Gerig, "Lateral electron equilibrium and electron contamination in measurements of head-scatter factors using miniphantoms and brass caps," *Med. Phys.*, vol. 22, no. 7, pp. 1167–1170, 1995.

[11] P. Cherry and A. Duxbury, *Practical radiotherapy: Physics and Equipment.*, 2nd ed. London: Wiley-Blackwell, 2009.

[12] S. Pai, I. J. Das, J. F. Dempsey, K. L. Lam, T. J. LoSasso, A. J. Olch, J. R. Palta, L. E. Reinstein, D. Ritt, and E. E. Wilcox, "TG-69: Radiographic film for megavoltage beam dosimetry," *Med. Phys.*, vol. 34, no. 6, pp. 2228–2258, 2007.

[13] W. Matthew and P. Metcalfe, "Radiochromic film dosimetry and its applications in radiotherapy," *AIP Conf. Proc.*, vol. 1345, no. 1, pp. 75–99, 2011.

[14] H. Miura, S. Ozawa, F. Hosono, N. Sumida, T. Okazue, K. Yamada, and Y. Nagata, "Gafchromic EBT-XD film: Dosimetry characterization in high-dose, volumetric-modulated arc therapy," *J. Appl. Clin. Med. Phys.*, vol. 17, no. 6, pp. 312–322, 2016.

[15] M. T. Bahreyni Toossi, F. Khorshidi, M. Ghorbani, N. Mohamadian, and D. Davenport, "Comparison of EBT and EBT3 RadioChromic Film Usage in Parotid Cancer Radiotherapy," *Biomed. Phys. Eng.*, vol. 6, no. 1, pp. 145–154, 2016.

[16] S. Devic, N. Tomic, and D. Lewis, "Reference radiochromic film dosimetry: Review of technical aspects," *Phys. Medica*, vol. 32, no. 4, pp. 541–556, 2016.

[17] N. Tomic, C. Quintero, B. R. Whiting, S. Aldelaijan, H. Bekerat, L. Liang, F. Deblois, J. Seuntjens, and S. Devic, "Characterization of calibration curves and energy dependence GafchromicTMXR-QA2 model based radiochromic film dosimetry system," *Med. Phys.*, vol. 41, no. 6, pp. 1–9, 2014.

[18] H. Bekerat, S. Devic, F. Deblois, K. Singh, A. Sarfehnia, J. Seuntjens, S. Shih, X. Yu, and D. Lewis, "Improving the energy response of external beam therapy (EBT) GafChromicTM dosimetry films at low energies (≤100 keV)," *Med. Phys.*, vol. 41, no. 2, pp. 1–14, 2014.

[19] P. Andreo, D. T. Burns, K. Hohlfeld, M. S. Huq, T. Kanai, F. Laitano, V. G. Smythe, and S. Vynckier, *Absorbed Dose Determination in External Beam Radiotherapy: An International Code of Practice for Dosimetry Based on Standards of Absorbed Dose to Water. Technical Reports Series No. 398*. Vienna: International Atomic Energy Agency, pp.1–183, 2000.

[20] P. R. Almond, P. J. Biggs, B. M. Coursey, W. F. Hanson, M. S. Huq, R. Nath, and D. W. O. Rogers, *AAPM's TG-51 protocol for clinical reference dosimetry of high-energy photon and electron beams*, 9th ed., vol. 26, no. 9, pp. 1847–1870. Medical Physics: American Assiciation of Physicists in Medicine, 1999.

[21] C. M. Ma, C. W. Coffey, L. A. DeWerd, C. Liu, R. Nath, S. M. Seltzer, and J. P. Seuntjens, "AAPM protocol for 40-300 kV x-ray beam dosimetry in radiotherapy and radiobiology," *Med. Phys.*, vol. 28, no. 6, pp. 868–893, 2001.

[22] S. Aldelaijan, S. Devic, H. Mohammed, N. Tomic, L. H. Liang, F. DeBlois, and J. Seuntjens, "Evaluation of EBT-2 model gafchromic^{TM} film performance in water," *Med. Phys.*, vol. 37, no. 7, pp. 3687–3693, 2010.

[23] J. P. Gibbons, J. A. Antolak, D. S. Followill, M. S. Huq, E. E. Klein, K. L. Lam, J. R. Palta, D. M. Roback, M. Reid, and F. M. Khan, "Monitor unit calculations for external photon and electron beams: Report of the AAPM Therapy Physics Committee Task Group No. 71," *Med. Phys.*, vol. 41, no. 3, pp. 1–34, 2014.

[24] International Commission on Radiation Units and Measurements, "Determination of Absorbed Dose in a Patient Irradiated by Beams of X or Gamma Rays in Radiotherapy Procedures. ICRU Report No.24," *Med. Phys.*, vol. 4, no. 5, pp. 461–461, 1977.

[25] F. Haristyo and S. A. Pawiro, "Volume averaging correction factor of several detectors in small field radiotherapy dosimetry," *Med. Phys. Biophys.*, vol. 1, no. 1, pp. 16–20, 2014.

[26] M. E. Kabir, H. Singh, R. Lu, B. Olde, L. M. F. Leeb-lundberg, and J. C. Bopassa, "Measurement and Analysis of PDDs Profile and Output Factors for Small Field Sizes by cc13 and Micro-Chamber cc01," *Int. J. Med. Physics, Clin. Eng. Radiat. Oncol.*, pp. 1–11, 2018.

[27] R. J. Underwood, "Small field dose calibrations with gafchromic film," Master Dissertation. Georgia Institute of Technology, pp. 1 – 63, 2013.

[28] IBA-Dosimetry, "Ionization Chambers and Diode Detectors for Relative and Absolute Dosimetry," pp.1-22007.

[29] IBA-Dosimetry, "High Performance Diode Detector for Small Field Dosimetry in Radiotherapy: Razor Detector," 2014. [Online]. Available: https://www.meditron.ch/radiation-therapy/downloads/Razor-Detector-RT-FL-E-

Rev.1-1014.pdf. [Accessed: 09-Jan-2019].

[30] G. Reggiori, P. Mancosu, N. Suchowerska, F. Lobefalo, A. Stravato, S. Tomatis, and M. Scorsetti, "Characterization of a new unshielded diode for small field dosimetry under flattening filter free beams," *Phys. Medica*, vol. 32, no. 2, pp. 408–413, 2016.

[31] D. Lewis, A. Micke, and X. Yu, "An efficient protocol for radiochromic film dosimetry combining calibration and measurement in a single scan," vol. 39, no. 10, pp. 6339–6350, 2012.

[32] Gafchromic™ Dosimetry Media Type EBT3, "Gafchromic™ EBT3 Dosimetry Film." [Online]. Available: http://www.gafchromic.com/documents/EBT3_Specifications.pdf. [Accessed: 15-June-2019]

[33] IBA-Dosimetry, "Commissionning and Annual QA: Blue phantom 2 with omnipro-Accept (V7)," 2015. [Online]. Available: https://www.elsesolutions.com/wp-content/uploads/2015/05/Blue-Phantom2.pdf. [Accessed: 27-Jun-2019].

[34] E. E. Klein, J. Hanley, J. Bayouth, F. F. Yin, W. Simon, S. Dresser, C. Serago, F. Aguirre, L. Ma, B. Arjomandy, C. Liu, C. Sandin, and T. Holmes, "Task group 142 report: Quality assurance of medical accelerators," *Med. Phys.*, vol. 36, no. 9, pp. 4197–4212, 2009.

[35] R. K. Rice, J. J. Hansen, G. K. Svensson, and R. L. Siddon, "Measurements of dose distributions in small beams of 6 MV X-rays," *Phys. Med. Biol.*, vol. 32, no. 9, pp. 1087–1099, 1987.

[36] G. A. Ezzell, J. M. Galvin, D. Low, J. R. Palta, I. Rosen, M. B. Sharpe, P. Xia, Y. Xiao, L. Xing, and C. X. Yu, "Guidance document on delivery, treatment planning, and clinical implementation of IMRT: Report of the IMRT subcommittee of the AAPM radiation therapy committee," *Med. Phys.*, vol. 30, no. 8, pp. 2089–2115, 2003.

[37] M. Westermark, J. Arndt, B. Nilsson, and A. Brahme, "Comparative dosimetry in narrow high-energy photon beams," *October*, vol. 45, pp. 685–702, 2000.

[38] P. Papaconstadopoulos, G. Hegyi, J. Seuntjens, and S. Devic, "A protocol for EBT3 radiochromic film dosimetry using reflection scanning," *Med. Phys.*, vol. 41, no. 12, pp. 1–6, 2014.

[39] E. Y. León Marroquin, J. A. Herrera González, M. A. Camacho López, J. E. Villarreal Barajas, and O. A. García-Garduño, "Evaluation of the uncertainty in an EBT3 film dosimetry system utilizing net optical density," *J. Appl. Clin. Med. Phys.*, vol. 17, no. 5, pp. 466–481, 2016.

[40] I. Das and Y. Akino, "SU-E-T-637: Age and Batch Dependence of Gafchromic EBT Films in Photon and Proton Beam Dosimetry," *Med. Phys.*, vol. 41, no. 6 part 21, pp. 374, 2014.

[41] Wikipedia, "Ionization chamber.", [Online]. Available: https://en.wikipedia.org/wiki/Ionization_chamber [Accessed: 10-May-2019].

[42] Wikipedia, "Scintillation counter." [Online]. Available: (https://en.wikipedia.org/wiki/Scintillation_counter) [Accessed: 15-June-2019].

APPENDIX

The output factors were measured for open fields by using CC13 chamber, Razor chamber, Razor diode and Gafchromic EBT-3 film model. Perpendicular and parallel orientations of ionization chambers with respect to the beam central axis were considered in this research study. All measurements were taken at SSD = 90.0 cm, depth of 10.0 cm and SSD = 100.0 cm at d_{max}. Electrometer readings measured by ionization chambers were corrected for temperature and pressure factor, $K_{T,P}$ from equation (4.1). Electrometer readings measured by 0.13 cc chamber, 0.01 cc chamber, Razor diode and Gafchromic EBT-3 film are summarized in Table A, Table B and Table C respectively.

Table A: Electrometer readings measured by using CC13 ionization chamber corrected for temperature and pressure.

SSD = 90.0 cm at depth = 10.0 cm			**SSD = 100.0 cm at d_{max}**	
Field (cm)	Corrected electrometer readings (nC) (Perpendicular)	Corrected electrometer readings (nC) (Parallel)	Corrected electrometer readings (nC) (Perpendicular)	Corrected electrometer readings (nC) (Parallel)
1	1.503497567	2.399911039	1.745730551	2.627719853
2	2.366409743	3.349114432	2.357040378	3.342435323
3	2.522749125	3.463830992	2.505052376	3.449896088
4	2.629344159	3.527788012	2.609018769	3.513764279
5	2.699392323	3.585653887	2.698320072	3.566480881
7	2.866898805	3.668899532	2.840390328	3.651638469
10	3.021207805	3.763312276	2.995652822	3.743892522
15	3.196835813	3.864831356	3.172225854	3.846284384
20	3.309521991	3.935894712	3.285882059	3.913193917
30	3.458755038	4.027261883	3.439114977	4.003420409
40	3.536924729	4.065839133	3.517253618	4.044985422

Table B: Electrometer readings measured by using 0.01 cc Razor ionization chamber corrected for temperature and pressure.

SSD = 90.0 cm at depth = 10.0 cm			SSD = 100.0 cm at d_{max}	
Field (cm)	Corrected electrometer readings (nC) (Perpendicular)	Corrected electrometer readings (nC) (Parallel)	Corrected electrometer readings (nC) (Perpendicular)	Corrected electrometer readings (nC) (Parallel)
1	0.137066980	0.214251915	0.154742612	0.234881020
2	0.186817218	0.265022512	0.186198487	0.263797258
3	0.196970327	0.271114983	0.196345544	0.270899492
4	0.205092815	0.277207455	0.202433778	0.275972516
5	0.211184681	0.281269102	0.211566129	0.280538238
7	0.224383724	0.288376986	0.221205832	0.285103960
10	0.237582766	0.294469457	0.237559147	0.294235403
15	0.252812431	0.303608165	0.251772088	0.305396056
20	0.261950229	0.312746872	0.261924188	0.312498290
30	0.280225827	0.323916403	0.276137128	0.322137036
40	0.290378936	0.333055110	0.285132289	0.327717363

Table C: Electrometer readings measured by using Razor diode

SSD = 90.0 cm, depth at 10.0 cm			SSD = 100.0 cm at d_{max}	
Field (cm)	Electrometer readings (nC) (Parallel)	Output factor	Electrometer readings (nC) (Parallel)	Output factor
1	8.185333333	0.632072072	12.56333333	0.771703522
2	9.687666667	0.748082368	14.38666667	0.883701884
3	10.51000000	0.811583012	14.66666667	0.900900901
4	10.98333333	0.848133848	15.13666667	0.929770680
5	11.40666667	0.880823681	15.39333333	0.945536446
7	12.13000000	0.936679537	15.81333333	0.971334971
10	12.95000000	1.000000000	16.28000000	1.000000000
15	13.95666667	1.077734878	16.81666667	1.032964783
20	14.71000000	1.135907336	17.22333333	1.057944308
30	15.86666667	1.225225225	17.81333333	1.094185094
40	16.63000000	1.284169884	18.15333333	1.115069615